UNIVERSITY OF MISKOLC
MIKOVINY SAMUEL DOCTORAL SCHOOL OF EARTH SCIENCES

Head of the doctoral school: Prof. Dr. Péter Szűcs

Depositional Sequences and Diagenetic Controls on the Lower Cretaceous Yamama Reservoir, Southern Iraq: Implications for Petroleum Exploration and Basin Evolution

Thesis of the doctoral dissertation (PhD)

Author:

ABBAS KAREEM ABDULSAHIB MOHAMMED

Scientific supervisor:

Dr. habil Velledits Felicitász PhD, DSc

UNIVERSITY OF MISKOLC

FACULTY OF EARTH AND ENVIRONMENTAL SCIENCES AND ENGINEERING

INSTITUTE OF EXPLORATION GEOSCIENCES

2025 Miskolc, Hungary

Recommendation of the Supervisor

The PhD research conducted by **Mr. Abbas Kareem Abdulsahib Mohammed** represents a significant and original contribution to understanding carbonate reservoir development and heterogeneity in the Lower Cretaceous Yamama Formation, southern Iraq. The study integrates advanced sedimentological, petrographic, and geochemical analyses to reconstruct the depositional and diagenetic evolution of this major hydrocarbon-bearing formation.

Carbonate reservoirs are inherently complex due to their variable depositional textures and multi-stage diagenetic overprints. The candidate effectively addressed these challenges using a multidisciplinary approach that combines core description, well-log interpretation, thin-section petrography, SEM-EDS analysis, fluid-inclusion microthermometry, and stable isotope geochemistry ($\delta^{13}C$ and $\delta^{18}O$). This integration enabled him to distinguish between early, burial, and late diagenetic processes and relate them to sequence stratigraphy and reservoir quality.

The thesis clearly defines and achieves its objectives. It identifies key facies associations, sequence boundaries, and maximum flooding surfaces, and links them to reservoir and non-reservoir distribution. The paragenetic and conceptual diagenetic models explain how depositional setting, fluid evolution, and burial history controlled porosity preservation and destruction. These models also serve as valuable analogues for other Cretaceous carbonate reservoirs in the Middle East.

Mr. Abbas demonstrated strong analytical skills, scientific independence, and an exceptional ability to synthesize large datasets into coherent geological interpretations. His conclusions are well supported, providing new insights into the origin, temperature, and chemistry of diagenetic fluids and their influence on reservoir heterogeneity. The thesis is clearly written, well-structured, and supported by high-quality figures and tables.

Throughout his PhD studies, **Mr. Abbas** showed remarkable dedication, creativity, and independence in both laboratory and interpretive work. His research has led to several peer-reviewed publications and conference presentations, confirming the originality and scientific value of his results.

The dissertation was reviewed by two distinguished geoscientists: Professor **Dr. György Less** (Doctor of the Hungarian Academy of Sciences, Professor Emeritus, University of Miskolc) and Professor **Dr. Sadoon Morad** (AdTerra Group, Chemin des Vergers, Geneva, Switzerland). Both reviewers recognized the scientific integrity, depth, and significance of the study, confirming that it meets international PhD standards.

Based on its scientific quality, originality, and contribution, I recommend the thesis for public defense and support the award of the Doctor of Philosophy (PhD) degree to **Mr. Abbas Kareem Abdulsahib Mohammed**.

Dr. habil Felicitász Velledits, DSc
October 2025/Miskolc

Summary

The Lower Cretaceous carbonate reservoir (the Yamama Formation) of southern Iraq represents a critical component of the region's hydrocarbon system, yet their depositional, stratigraphic, and diagenetic complexities pose significant challenges for effective petroleum exploration and development. This study integrates sedimentological, depositional sequences, and diagenetic analyses to elucidate the reservoir characteristics of these carbonate units.

Well logs interpretation, detailed description of about 400 m subsurface drill cores, petrographic analysis of about 170 selected samples, scanning electron microscope (SEM), fluid inclusion microthermometry, and stable isotope ($\delta^{13}C$ and $\delta^{18}O$) geochemistry from different localities from the Yamama Formation, southern Iraq were used to characterize the formation's depositional facies, sequences, and diagenetic alterations.

Detailed facies analysis reveals fourteen distinct facies deposited during Berriasian–early Valanginian in a range of depositional environments from intertidal and restricted lagoons to high-energy shoals and middle-outer ramp, indicative of a homoclinal ramp-type shallow water carbonate platform. The formation is markedly heterogeneous, composed of four reservoir units (YRA-YRD) that mainly consist of shoal grain-supported and Lithocodium-Bacinella reefal facies. These units are separated by four non-reservoir units (B0-B3), which are composed of lagoonal, middle-outer ramp, mud-supported facies.

Diagenetic processes including micritization, cementation, dolomitization, dissolution, and mechanical and chemical compaction have modified the original porosity and permeability of these rocks. Early circumgranular cements and minor scattered equant and syntaxial calcite overgrowths protected grain-supported facies from compaction and preserved good interparticle pores even at depth of about 4100 m. In contrast, extensive equant calcite cementation and pressure dissolution reduced porosity. Micritization induced microporosity in grains, resulting in dual macro- and microporous textures with high porosity but low permeability. Pore-filling kaolinite and Na-rich saponite, mainly in lagoonal facies, further reduced porosity via early and burial-stage authigenesis. Dolomitization, particularly in bioturbated sites, locally enhanced intercrystalline porosity. The calcite micro-overgrowth and compaction reduced the micro-interparticle pores of the matrix in the mud-supported facies. The dissolved calcite by the stylolite pressure dissolution precipitated as blocky calcite in interparticle, moldic and vuggy

pores. These stylolites acted later as barriers prevent vertical fluid flow, resulting in the compartmentalization of the reservoir.

Fluid inclusion microthermometry from blocky calcite in moldic/vuggy pores indicates diagenetic temperatures of 85–140°C (exceeding the maximum burial temperature, ~116°C) and salinities up to 10 wt.% NaCl eq, with $\delta^{18}O\_VSMOW$ values of +4‰ to +8‰. These values, along with depleted $\delta^{18}O\_VPDB$ (-6.9‰ to -5.6‰), suggest precipitation from evolved basinal fluids related to stylolite pressure dissolution. Diagenetic evolution correlates spatially and temporally with the depositional sequence surfaces, emphasizing the role of sea-level fluctuations in porosity modification.

Depositional sequences analysis delineates four third-order cycles, bounded by Type 2 sequence boundaries with episodes of subaerial exposures and marked by transgressive and regressive facies shifts. The reservoir units dominantly correspond to regressive, high-energy shoal facies characterized by grain-supported and Lithocodium-Bacinella with higher interparticle and intraparticle porosity, whereas the intervening non-reservoir units are associated with transgressive, low-energy, mud-supported facies that act as barriers to the fluid flow. Thus, depositional sequence architecture largely coincides with the vertical stacking of reservoir and non-reservoir intervals.

This investigation reveals that reservoir heterogeneity of the formation is attributed to depositional facies, which control the texture of the sediments, and to various types of diagenetic alterations. The close alignment between reservoir units and depositional sequences underscores the value of integrated stratigraphic and diagenetic modeling for accurate prediction of reservoir distribution in ramp-type carbonate systems across the Middle East.

Abbas Kareem Abdulsahib Mohammed

September 2025, Miskolc, Hungary

Table of Contents

List of Figures

List of Tables

Acknowledgments

I would like to express my sincere gratitude to all those who have supported and contributed to the completion of this PhD journey; scientifically, technically, and personally.

On a personal note, I offer heartfelt thanks to my **father and mother**, **brothers**, and **sisters** for their unwavering love and encouragement. To my **friends** and **colleagues**, who have stood by me through every high and low, your support and presence have been invaluable.

I sincerely thank the **Stipendium Hungaricum Scholarship** Program and the **Tempus Public Foundation** for their support, which made it possible for me to pursue my doctoral studies in Hungary through the **Ministry of Higher Education and Scientific Research of Iraq-Scholarships and Cultural Relations Directorate**.

I chose to focus my research on a case study from Iraq with the intent of contributing to the scientific advancement of my country and supporting the long-term interests of the Iraqi petroleum sector. However, obtaining the necessary core samples and subsurface data for this PhD research posed significant challenges. The process of securing approvals and official permissions was complex and time-consuming. Despite these difficulties, I remain grateful to the Iraqi **Oil Exploration Company** and **Basra Oil Company** for providing the essential core samples and data that formed the foundation of this study. I also wish to acknowledge **Missan Oil Company**, my home company, for officially permitting and supporting my academic pursuit. I am grateful to **Mr. Sada Z. Ali**, Geology Department, MOC, for his valuable support.

I am profoundly indebted to my supervisor, **Dr. Felicitász Velledits**, for her exceptional guidance, patience, and encouragement throughout my PhD. Her mentorship has shaped my academic thinking and strengthened my scientific independence. My appreciation extends to the head, **Dr. Mádai Ferenc** and all teaching and technician staff of the Institute of Exploration Geosciences, University of Miskolc, for their academic and logistical support. Their professionalism and assistance were instrumental in completing this research. I extend my thanks to **Dr. Ferenc Kristály** for performing SEM and EDS analyses, which contributed significantly to the diagenetic characterization in this study.

Special appreciation is due to **Dr. Juan Diego Martín Martín** and **Dr. Eloi González-Esvertit** from the University of Barcelona for granting access to the fluid inclusion microthermometry facilities. I am thankful to **Dr. Mohammad Alsuwaidi** (Khalifa University) for his generosity and technical support in fluid inclusion preparation and isotope measurements. Many thanks to **Dr. Daria Ivanova** (Bulgarian Academy of Science, Sofia) for her support in micropaleontology analysis. I also thank **Dr. Axel Munnecke** and the University of Erlangen for providing access to their facilities for thin section scanning. I acknowledge **Dr. Ibrahim Qasim** for his continued scientific support and critical discussions throughout this work.

Sincere thanks are also owed to the reviewers, Prof Dr. György Less and Prof Dr. Sadoon Morad, whose critical reviews and constructive feedback significantly improved the quality and clarity of the dissertation. This work would not have been possible without the collective efforts, contributions, and generosity of all these individuals and institutions. To each of you, I extend my deepest gratitude.

1. Introduction

Nearly 65% of world oil and natural gas production takes place in the Middle East, being hosted mainly by carbonates (Burchette, 2012), such as the Cretaceous Yamama, Thamama Group, Kharaib, Shuaiba, Mauddud, and Mishrif formations. Carbonate reservoirs, which host over 60% of the world's oil and about 40% of the gas reserves (Moore and Wade 2013) globally, are strongly heterogeneous. Despite their economic importance, carbonate reservoirs are notoriously complex due to their strong lateral and vertical heterogeneity. This heterogeneity results from rapid subtle facies and related porosity-permeability changes, sensitivity to diagenetic reactions, and multimodal pore sizes (Lucia 2007; Morad et al. 2018a).

Diagenetic alterations, such as cementation, dissolution, dolomitization, and compaction can overprint depositional porosity-permeability in unpredictable ways, both enhancing and degrading reservoir quality at different times (Lucia 2007; Morad et al. 2019). These diagenetic alterations are often diachronous and varying significantly at a field and basin scales, making it difficult to correlate reservoir characteristics predictively. Furthermore, although certain carbonate strata contain diagnostic biostratigraphic indicators, many lack precise chronostratigraphic markers. Therefore, this limitation necessitates the incorporation of diagenetic alteration into depositional sequence analysis (Morad et al. 2012, 2013; Seibel and James 2017).

Mechanical compaction reduces porosity by causing closer grain packing and pseudoplastic deformation of ductile peloids and thus reduce pore space. Cementation, most commonly by calcite and dolomite, can reduce porosity, while dissolution, driven by changes in fluid chemistry, may enhance porosity. Micritization, the process by which fine-grained micrite forms from the breakdown of larger grains particles, contributes to the rock's texture and can therefore, affect porosity and permeability (Flügel 2010; Morad et al. 2018a). Diagenetic alterations are influenced by burial depth, fluid composition, and depositional environment, resulting in the reservoir heterogeneity and are crucial for understanding the reservoir characteristics of carbonate rocks (Morad et al. 2019; Bahrehvar et al. 2021; Khalil et al. 2024; Mohammed and Velledits 2024a). This heterogeneity imposes challenges for acquiring accurate reservoir characterization for efficient hydrocarbon production and recovery operations and optimization of the field developments plans and management (Burchette 2012).

The Yamama Formation is a prolific hydrocarbon-bearing unit in southern Iraq and across parts of the Arabian Gulf region. However, its reservoir characteristics remain poorly understood due to the complex interplay between depositional heterogeneity and post-depositional diagenetic alteration. Furthermore, the formation exhibits variable reservoir quality across different oilfields, ranging from dry zones in some localities to productive intervals with successful hydrocarbon flow in other places. Moreover, in southern Iraq, the Yamama is deeply buried, reaching up to 4100 m, which rises significant challenges for acquiring essential subsurface data such as the core samples and well logs. Although several local studies have addressed its petrophysical properties and general depositional setting (Saleh 2014; Al Mafraji and Al-Zaidy 2019; Handhal et al. 2020; Idan et al. 2020; Al-Iessa and Zhang 2023; Li et al. 2024), Limited studies have specifically addressed the controls of facies/microfacies and diagenetic alterations on reservoir evolution across spatial and stratigraphic units at the field and regional scales.

There is a lack of detailed integration between facies/microfacies analysis, petrographic diagenetic alteration, fluid inclusion thermometry, and stable isotopic signatures, which are critical to reconstruct the diagenetic history and to constrain the thermal and geochemical conditions under which reservoir properties evolved. Furthermore, the spatial variability of porosity-reducing versus porosity-enhancing diagenetic processes across the carbonate ramp and their depositional sequences context remain unclear.

1.1 Objectives of the Study

This study aims to address these gaps through a comprehensive sedimentologic, petrographic and geochemical investigation of the Lower Cretaceous Yamama Formation in southern Iraq. This study is based on cores, borehole and geological data from numerous oilfields in the Mesopotamian Foreland Basin in southern Iraq (Fig. 1), The main objectives are to:

- Synthesize current knowledge on sedimentological, and diagenetic factors influencing reservoir quality and heterogeneity of the Yamama Formation (the focus of this study) in Iraq and Middle East. Thorough critical review to enhance the understanding of the Lower Cretaceous reservoirs and the implications for hydrocarbon exploration and production.
- Evaluate the petrophysical properties (porosity, permeability, volume of shale, and fluid saturation) to identify the reservoir and non-reservoir units.

- Analyze and interpret the sedimentary depositional facies/microfacies of the formation and establish their spatial and stratigraphic distribution.
- Identify and characterize the diagenetic processes (e.g., cementation, dissolution, dolomitization, micritization) that have affected the reservoir quality.
- Assess the impact of facies and diagenetic processes on the petrophysical properties of the reservoir.
- Constrain the timing, temperature, and geochemical conditions of diagenetic fluid events using integration of petrographic, scanning electron microscopy, fluid inclusion microthermometry and stable isotopes ($\delta^{13}C$ and $\delta^{18}O$) analysis.
- Integrate diagenetic evolution into depositional sequence framework to provide new insights into how sea-level fluctuations controlled fluid flow patterns and drove the diagenetic alteration of reservoir porosity.

2. Literature Review

2.1 Introduction

The Cretaceous was marked by intense seafloor spreading, the opening of the Atlantic Ocean, and the continued breakup of Pangaea, These tectonic events lead to eustatic sea level rise and, consequently, to the establishment of extensive shallow-water marine shelves near the equator (Bice et al., 2003; Jenkyns, 2010). These conditions favored the deposition of marine carbonate successions across the region (Ziegler, 2001). Moreover, the period encountered an increase in oceanic anoxic events (OAEs), leading to the accumulation of highly organic-rich sediments that formed the source rocks of hydrocarbon (Lawa et al., 2023). Carbonate reservoirs are considered to be challenging because of their strong lateral and vertical heterogeneity, which is caused by rapid facies and related porosity-permeability changes, sensitivity to diagenetic reactions with most fluids, and their multimodal pore sizes (Lucia, 2007).

The Yamama Formation (the focus of this study) extends from the Mesopotamian Foreland Basin (MFB) in southern Iraq and across parts of the Arabian Plate (Fig. 1). In southern Iraq, the formation grades from the shallow-water carbonates to mixed carbonates-siliciclastics of the Zangura and Garagu formations in central and northern Iraq, to the hemipelagic facies of the Sarmord Formation in Kirkuk and western Kurdistan region, to the deep-water carbonates of the Lower Balambo, and the Upper Chia Gara Formation in NE Kurdistan region (Van Bellen et al., 1959; Sadooni, 1993). The formation has regional equivalents, including the Minagish Formation in Kuwait (Al-Helal et al., 2023), the Lower Fahliyan Formation in the Persian Gulf of Iran (Valinasab et al., 2023; Hosseiny and Mohseni, 2023), Habshan Formation of the Thamama Group in Abu Dhabi, and Rayda Formation in Oman (Aziz and El-Sattar, 1997; Ziegler, 2001). The Yamama Formation is absent in western Iraq due to the non-deposition event after the tectonic uplift of the Rutbah High (Al Naqib, 1967) (Fig. 1a).

This chapter aims to synthesize current knowledge on the sedimentological, and diagenetic factors influencing reservoir quality and heterogeneity of the Yamama Formation (the focus of this study) in Iraq and Middle East. Thorough critical review enhances the understanding of the Lower Cretaceous reservoirs and the implications for hydrocarbon exploration and production.

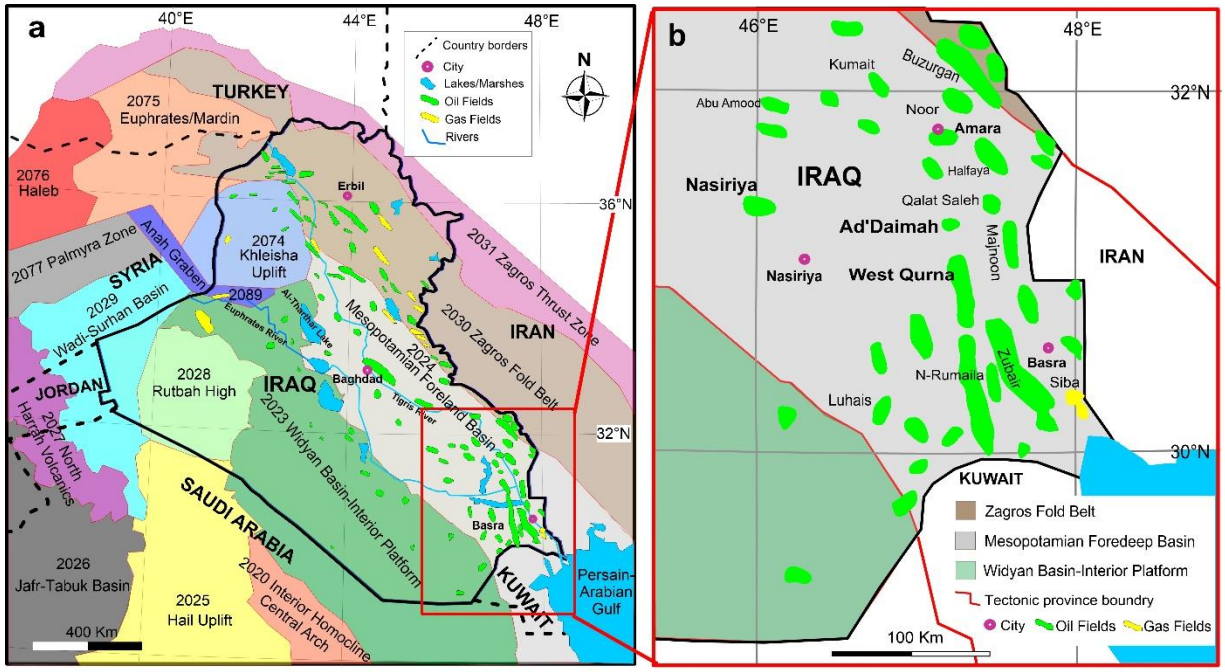

Figure 1. *(**a**) Tectonic map of Iraq and surrounding countries showing location of most of Iraqi oilfields within the Mesopotamian Foreland Basin, which is situated between the Zagros Fold Belt and the Widyan Basin. Modified from Mohammed and Velledits (2024a). (**b**) Close up map showing location of the studied oilfields in southern Iraq. The Nasiriya, Ah'Dimah, and West Qurna oilfields (highlighted in bold) were used in this study, from which core data were collected. (author's own edit).*

2.2 Geological Setting

2.2.1 Tectonic Framework of Iraq During Early Cretaceous

The northeastern margin of the Arabian Plate in the Late Triassic to Early Cretaceous was dominated by passive-margin with broad warm shallow-water seas, which facilitated the formation of carbonate platforms (Phillips et al., 2013). From the Late Jurassic to Early Cretaceous, periodic uplift and eastward tilting of the Arabian Plate margin occurred and was driven by the early stages of rifting and seafloor spreading in the Indian Ocean.

These processes ultimately contributed to the continental separation of the African-Arabian and Indian plates by the end of the Jurassic (Ziegler, 2001). The Late Jurassic was marked by a regional unconformity across the Arabian Plate (149 Ma, Sharland et al., 2004), resulting from tectonic uplift and erosion. This unconformity caused a stratigraphic gap separating the Jurassic sequences from overlying Cretaceous deposits and thereby influencing the reservoir distribution in the region (Pitman et al., 2004). It also marked the cessation of uppermost Jurassic evaporite deposition and the accumulation of Cretaceous carbonate deposits (Droste, 2013).

During the Early Cretaceous, the sediments accumulated on open carbonate platforms and within intrashelf basins of the Arabian Plate, which was bordered by passive margins bounded by the Neo-Tethys Ocean to the north, east, and south. The opening of the Neo-Tethys contributed to the creation of accommodation that enabled the deposition of significant hydrocarbon-bearing carbonates, including the Yamama Formation and the organic-rich source rocks in the intrashelf basins (Ziegler, 2001).

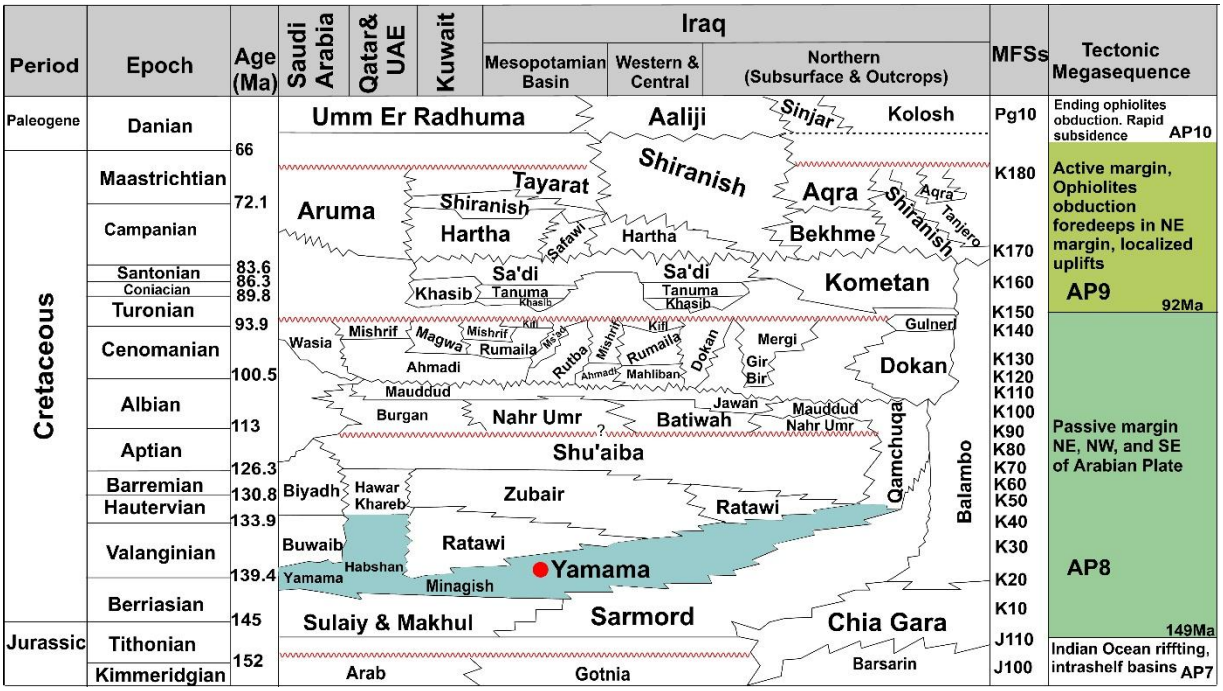

Figure 2. *Chronostratigraphic chart of the Cretaceous period in Iraq and adjacent regions. Compiled from Ziegler (2001), Sharland et al. (2004), and Mohammed (2018). The ages are correlated to Haq (2014). The red lines represent unconformities within the AP8 and AP9* (*author's own edit*).

The obduction of Oman ophiolites onto the eastern and northeastern margins of the Arabian Plate during the Turonian (Fig. 2) led to the formation of the Mesopotamian Foreland Basin, which was filled with Upper Cretaceous and Paleogene deposits. The Cretaceous Mesopotamian sedimentary successions underwent further deformations through thrusting and folding during the Zagros orogeny, which played a key role in the formation of most of the structural hydrocarbon traps in the region (Glennie et al., 1973; Phillips et al., 2013). As the convergence between the Arabian and Eurasian plates intensified, compressional forces began to reshape the region, resulting in the development of the Zagros Fold-thrust Belt.

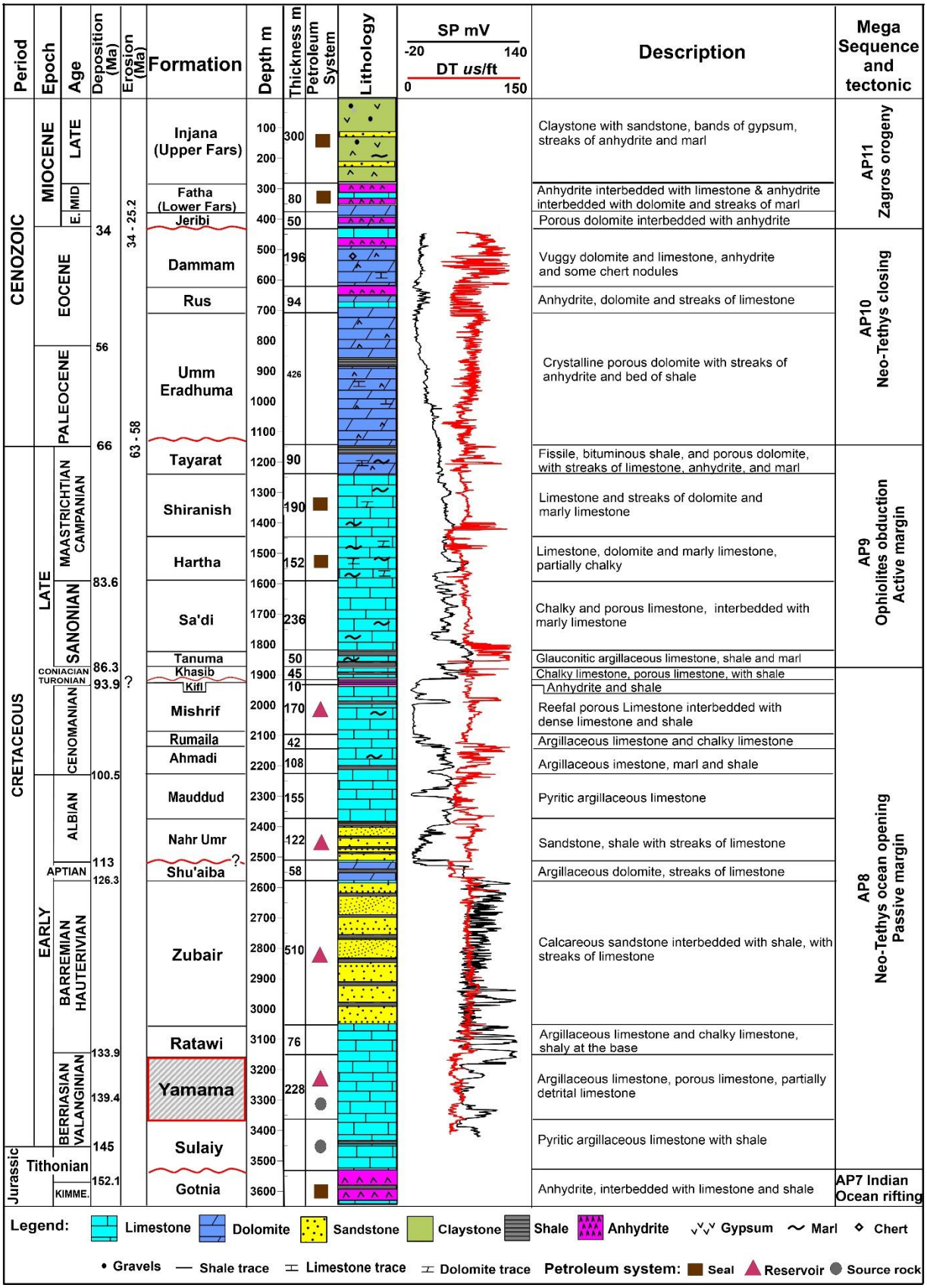
Period
Epoch
Age
Deposition (Ma)
Erosion (Ma)
Formation
Depth m
Thickness m
Petroleum System
Lithology
SP mV
-20
140
DT us/ft
0
150
Description
Mega Sequence and tectonic
CENOZOIC
MIOCENE
LATE
E. MID
EOCENE
PALEOCENE
CRETACEOUS
LATE
MAASTRICHTIAN
CAMPANIAN
SANONIAN
CONIACIAN
TURONIAN
CENOMANIAN
EARLY
ALBIAN
APTIAN
BARREMIAN
HAUTERIVIAN
BERRIASIAN
VALANGINIAN
Jurassic
Tithonian
KIMME.
34
56
66
83.6
86.3
93.9
100.5
113
126.3
133.9
139.4
145
152.1
34 - 25.2
63 - 58
?
Injana (Upper Fars)
Fatha (Lower Fars)
Jeribi
Dammam
Rus
Umm Eradhuma
Tayarat
Shiranish
Hartha
Sa'di
Tanuma
Khasib
Kifl
Mishrif
Rumaila
Ahmadi
Mauddud
Nahr Umr
Shu'aiba
Zubair
Ratawi
Yamama
Sulaiy
Gotnia
100
200
300
400
500
600
700
800
900
1000
1100
1200
1300
1400
1500
1600
1700
1800
1900
2000
2100
2200
2300
2400
2500
2600
2700
2800
2900
3000
3100
3200
3300
3400
3500
3600
300
80
50
196
94
426
90
190
152
236
50
45
10
170
42
108
155
122
58
510
76
228
Claystone with sandstone, bands of gypsum, streaks of anhydrite and marl
Anhydrite interbedded with limestone & anhydrite interbedded with dolomite and streaks of marl
Porous dolomite interbedded with anhydrite
Vuggy dolomite and limestone, anhydrite and some chert nodules
Anhydrite, dolomite and streaks of limestone
Crystalline porous dolomite with streaks of anhydrite and bed of shale
Fissile, bituminous shale, and porous dolomite, with streaks of limestone, anhydrite, and marl
Limestone and streaks of dolomite and marly limestone
Limestone, dolomite and marly limestone, partially chalky
Chalky and porous limestone, interbedded with marly limestone
Glauconitic argillaceous limestone, shale and marl
Chalky limestone, porous limestone, with shale
Anhydrite and shale
Reefal porous Limestone interbedded with dense limestone and shale
Argillaceous limestone and chalky limestone
Argillaceous imestone, marl and shale
Pyritic argillaceous limestone
Sandstone, shale with streaks of limestone
Argillaceous dolomite, streaks of limestone
Calcareous sandstone interbedded with shale, with streaks of limestone
Argillaceous limestone and chalky limestone, shaly at the base
Argillaceous limestone, porous limestone, partially detrital limestone
Pyritic argillaceous limestone with shale
Anhydrite, interbedded with limestone and shale
AP11 Zagros orogeny
AP10 Neo-Tethys closing
AP9 Ophiolites obduction Active margin
AP8 Neo-Tethys ocean opening Passive margin
AP7 Indian Ocean rifting
Legend:
Limestone
Dolomite
Sandstone
Claystone
Shale
Anhydrite
Gypsum
Marl
Chert
Gravels
Shale trace
Limestone trace
Dolomite trace
Petroleum system:
Seal
Reservoir
Source rock

Figure 3. *General stratigraphic column of southern Iraq showing the lithological variation and formations description, mega-sequences and tectonic setting. The Yamama Formation is highlighted, representing a key Lower Cretaceous carbonate reservoir deposited during the Berriasian–Valanginian* (*author's own edit*).

This tectonic evolution gave rise to structural traps, fault-bounded reservoirs, and folded anticlines, all of which are crucial for hydrocarbon accumulation in Iraq (Pitman et al. 2004). The structural features, shaped by earlier tectonic events and punctuated by the regional unconformity, are fundamental to Iraq's current petroleum system (Ziegler, 2001; Alavi, 2004). The Yamama Formation in the Mesopotamian Foreland Basin (MFB) is tectonically bounded by the Widyan Basin-Interior Platform to the west (Fig. 1a), while its eastern section aligns with the Zagros Fold Belt, an active tectonic region influenced by compression and folding due to the convergence of the Arabian and Eurasian plates.

2.2.2 Stratigraphy of the Yamama Formation

The deposition of the evaporitic Gotnia Formation to the north and northeast of the Arabian Plate during the Late Jurassic ended abruptly followed by the deposition of the fine-grained limestones of Sulaiy Formation (Fig. 2 and 3). The contact between the Kimmeridgian Gotnia and the Tithonian-Berriasian Sulaiy represented by the regional unconformity at the end of the Jurassic. This unconformity corresponds to the contact between mega-sequences AP7 and AP8 of Sharland et al. (2004). The Yamama Formation conformably lies over the Sulaiy Formation and underlies the silty limestones of Ratawi Formation (Van Bellen et al., 1959). The Sulaiy, Yamama, and Ratawi formations represent the lower/first cycle of the mega-sequence AP8 (Sadooni and Aqrawi, 2000) (Fig. 2 and 3). The carbonates of the Yamama Formation are overlain by the silty to argillaceous limestone interbeds of the lower Ratawi Formation. while, in some areas, the siliciclastic Zubair Formation directly lies unconformably on the Yamama Formation. These transitional layers grade upward into the sandstones and shales of the Zubair Formation. These lithological transitions reflect changes in depositional environments and basin dynamics, primarily the influx of siliciclastic sediments derived from erosion of the uplifted Arabian Shield (Ziegler 2001).

2.2.3 Distribution of the Yamama Formation in Southern Iraq

The Yamama Formation exhibits considerable thickness variations in Iraq and other parts of the Arabian Plate due to differences in the tectonic subsidence rates (Khalil et al., 2024). The formation is deepening towards northeast and southeast near the Iraqi Iranian border (Fig. 4a).

While the thickness varies considerably from 80 m in the eastern part (Noor oilfield) to over 350 m in West Qurna, Zubair and Faihaa oilfields (Fig. 4b), with localized thickening in structural lows towards the east, where subsidence was more active (Mohammed and Velledits, 2024a).

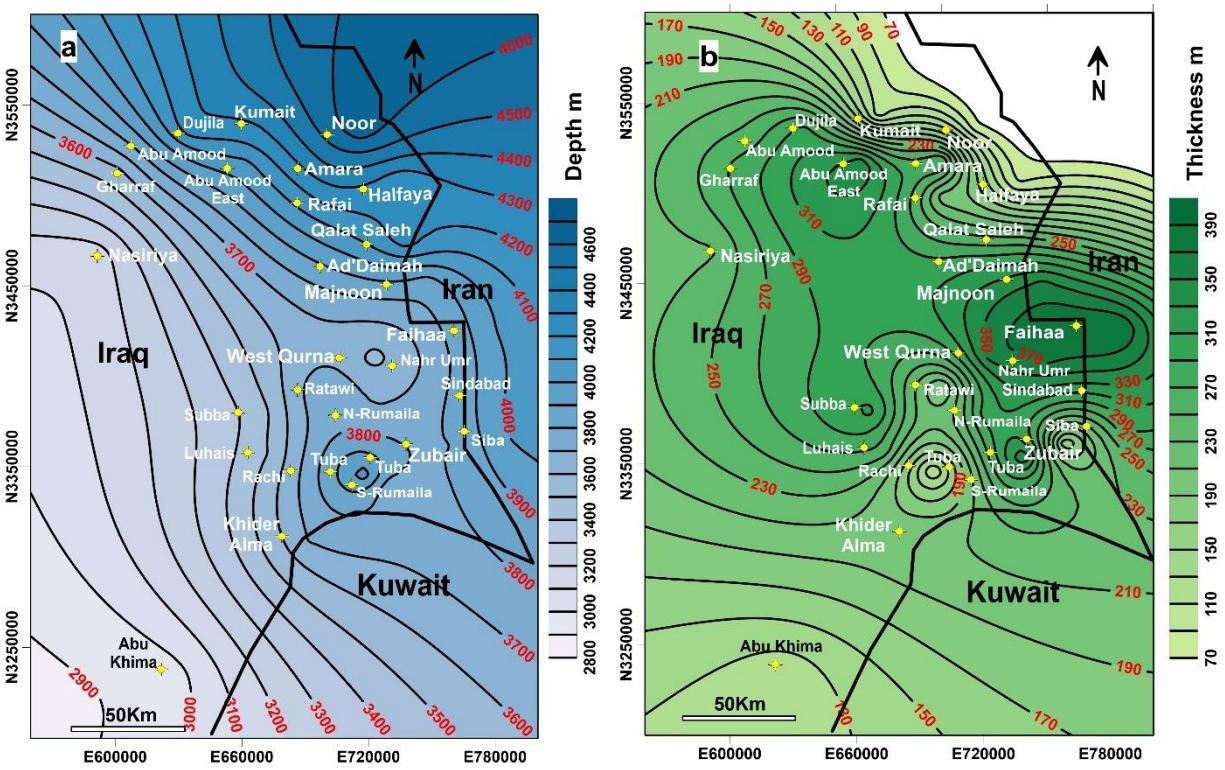

Figure 4. *(**a**) Top contour map, (**b**) isopachous map of the Yamama Formation in southern Iraq, showing increasing depth toward the east and northeast and thickness variation, with an overall decreasing trend in thickness in northeast direction* (*author's own edit*).

2.3 Paleontology and Biostratigraphy of the Yamama Formation

The challenge of achieving a detailed high-resolution biozonation for the Lower Cretaceous Yamama Formation and its equivalents in the Arabian Plate remains a subject of debate. The scarcity of reliable biostratigraphic markers and the absence of isotope dating efforts reduce chronological precision. However, paleontological studies have attempted to identify the age of the Yamama Formation in south of Iraq based on benthic foraminifera and algae. The *Charentia cuvillieri* and *Psudochrysalidina infracretacea* (Berriasian age), *Pseudocyclammina Lituus* (Valanginian age), *Nezzazata Perforata* with *Choffatella* (Berriasian-Valanginian age), Desycladales green algae *Cylindroporella* (Berriasian age), and *Salpingoporella cf. circassa* (Valanginian age) (Al-Hassani and Al-Dulaimi, 2021). Whereas, the *Psudochrysalidina*

infracretacea and *Pseudocyclammina Lituus* were identified as Berriasian and Valanginian age, respectively (Khazaal and Shakir, 2022). Aziz and El-Sattar (1997) identified the Valanginian of Habshan Formation in Abu Dhabi from the occurrence of the Dasycladales *Salpingoporella.* They stated that the appearance of the *Lenticulina* encountering of *Lithocodium aggregatum* correspond to Hauterivian age that represented by the Zakum Formation (which is equivalent of Ratawi Formation in south of Iraq). Nagm et al. (2018) confirmed the age of the Yamama Formation as early Valanginian based on sequence stratigraphy, correlating it with the global sequence framework of Haq (2014) and the European stratigraphic sequences of Hardenbol et al. (1999). The *Trocholina elongata*, *Pseudocyclammina lituus*, and *Nautiloculina oolithica*, suggest Berriasian- Valanginian age, while *Salpingoporella annulata* is frequently associated with the top of the Manifa Member and suggests Berriasian age in the Persian Gulf of Iran (Bahrehvar et al., 2021).

2.4 Lithology, sedimentology and reservoir quality of the Yamama Formation

2.4.1 Lithological characteristics

Core examination and well logs interpretation showed that the Yamama Formation varies in composition from pure limestones, argillaceous limestones, dolomitic limestones, marly limestones, to dolomitic limestones. These compositional variations of the limestones affect the overall heterogeneity of the formation in southern Iraq (Mohammed and Velledits, 2024a, b). To the east and southeast (e.g., in Kumait, Noor, and Halfaya oilfields; Fig. 1b), the formation consists of marly and pyritic limestone and interbedded shales. In Qalat Saleh Oilfield (north of Majnoon Oilfield; Fig. 1b), the formation showed thin layers of fine-grained sandstones interbedded with chalky and marly limestones and, less commonly, shales. In Kifl Oilfiel, the formation consists of limestones, dolostones, shales and anhydrites (Alobaidy and Al-Banna 2021).

2.4.2 Facies Associations in the Yamama Formation

The Yamama Formation exhibits facies associations with distinct textural, compositional, and skeletal grains contents (e.g. foraminifera and mollusks) across shallow-water marine ramp. The shoal grain-supported facies in the Nasiriya Oilfield (Fig. 1b; Mohammed and Velledits, 2024b), and the Lithocodium-Bacinella floatstones/boundstones, forming reefal patches and barrier in the Ah'Dimah and West Quran oilfields (Fig. 1b) are characterized by good reservoir quality (Mohammed and Velledits, 2024a). These facies transitions reflect changes the depositional

conditions (e.g. water energy, sediment supply, and biological activities) (Esrafili-Dizaji et al., 2020; Bahrehvar et al. 2021; Khalil et al. 2024).

The facies distribution within the Yamama Formation shows considerable lateral and vertical variations at basin and fields scales: (a) grain-supported limestones are characterized by a high abundance of non-skeletal grains that deposited in the shoal, (b) the Lithocodium-Bacinella floatstones/boundstones and the reefal skeletal facies forming barriers in the back and foreshoal, (c) mud-supported mudstones and wackestones typically occurring in relatively deep water settings, in lagoonal settings and below the fair weather wave base (middle and outer ramp) (Sadooni, 1993; Mohammed and Velledits, 2024b). Dolomitization has affected the shallow-water marine facies (Bahrehvar et al., 2021). Patchy dolomitization is commonly associated with bioturbation sites. The presence of anhydrite suggests that dolomitization occurred by seepage reflux of hypersaline brines (cf. Morad et al., 2023). The distribution of these facies varies throughout the region due to variations in paleogeography, changes in sea level, and rates of sediment supply. Paleogeographic variations influenced accommodation space and water circulation patterns, affecting carbonate production and facies heterogeneity. Transgressive events favoring open marine settings and regressive promoting restricted conditions conducive to dolomitization (Ziegler, 2001; Pitman et al., 2004).

2.4.3 Depositional Environments

The significant vertical and lateral facies variations are attributed to substantial changes in the depositional conditions across the marine ramp being influenced by interplay between relative sea-level changes, regional tectonics, and rates of sediment supply (Pitman et al. 2004). The formation and its regional equivalents manifest the depositional evolution of the Arabian carbonate platforms and its intrashelf basins (Fig. 5). The depositional environments ranging from inner to outer-ramp platform settings is recorded by intertidal and shoal facies. The middle to outer-ramp environments were characterized by the deposition of bioclastic packstones, bioclastic wackestones, and mudstones (e.g., Sulaiy and Rayda formations in Saudi Arabia and Oman) (Nagm et al. 2018; Fallatah et al. 2024). Mixed carbonate and siliciclastic were deposited to the north and northeast of Yamama (e.g., Zangura and Garagu formations). Wackestones and mudstones accumulated in offshore environment below the storm wave base in intrashelf basins

including the Chia Gara, Balambo and Lower Sarmord formations in the eastern and northeast parts of the Arabian Plate (Fig. 5).

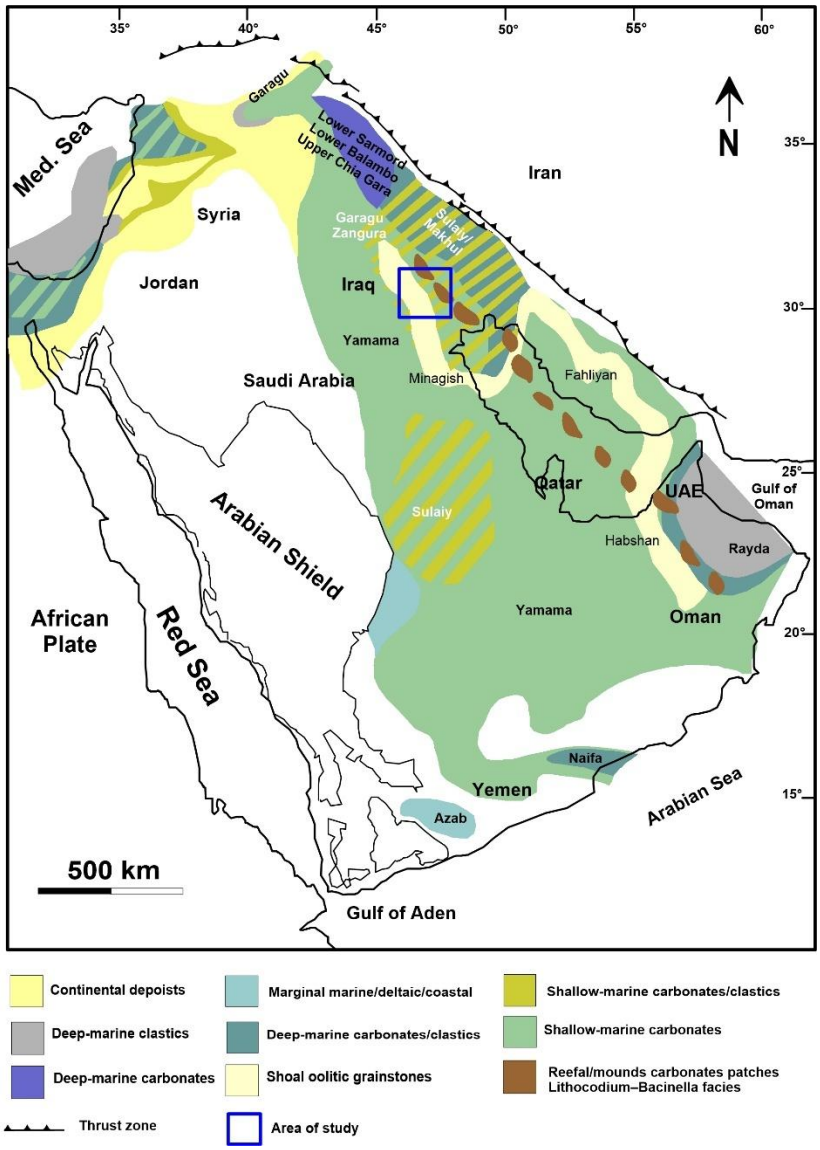

Figure 5. *The lowermost Cretaceous paleofacies (Berriasian-Valanginian, 144-132 Ma), covering the Yamama Formation and its regional equivalents including Chia Gara, Lower Sarmord, Minagish, Habshan, and Rayda formations (MFS: K20, K30 and K40), reveal relatively continuous sedimentation in Oman. These sediments accumulated on open platforms and in intrashelf basins across the Arabian Plate. Adapted from Ziegler (2001) and Fallatah et al. (2024). The lithocodium reefal facies are illustrated as reported by Mohammed and Velledits (2024a), Bahrehvar et al. (2021), Valinasab et al. (2023), Esrafili Dizaji et al. (2020), and Jeong et al. (2017). (author's own edit).*

In southern Iraq, the facies distribution (Fig. 6) varies from high-energy shoals to the west, characterized by ooidal grainstones, to lagoonal and backshoal algal skeletal wackestones and

packstones deposited in more restricted, lower-energy settings. These deposits grades to the middle and outer ramp environments to the east, where finer grained limestones accumulated (Fig. 6). The interplay between changes in the relative sea level and rates of sediment supply (i.e. carbonate production) exerted considerable impact on reservoir quality of the Yamama Formation and its equivalents formations in oilfields across the region. The presence of porous-permeable grainstones, along with early diagenetic modifications, such as dolomitization and dissolution, have enhanced reservoir quality, making the Lower Cretaceous carbonates primary exploration targets in Iraq, Iran, Kuwait, Saudi Arabia, and the UAE. These depositional patterns are crucial for understanding reservoir distribution, connectivity, and potential hydrocarbon accumulation zones.

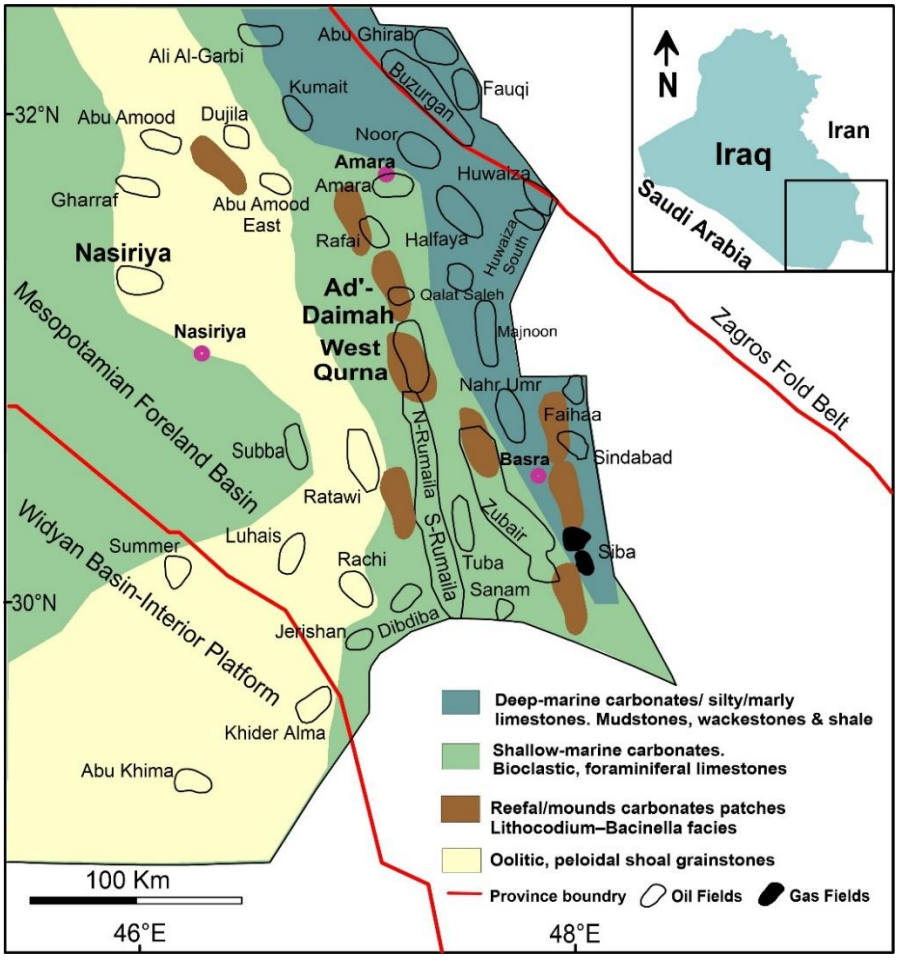

Figure 6. *Paleofacies map of the Yamama Formation in south and southeast Iraq, showing facies transition from shallow-marine and shoal facies in the west to deep-marine facies in the east, with reefal patches along the platform margin* (*author's own edit*).

2.5 Petroleum System of the Yamama Formation

The Yamama Formation and its equivalent formations (Fig. 2 and 3) host substantial hydrocarbon reserves deposited in shallow-water marine environments along the eastern part of the Arabian Plate (Fig. 5), particularly in southern Iraq, Saudi Arabia, Iran, Kuwait, UAE and Oman. The shoal facies, including the grain-supported limestones and the reefal (mounds/patches) Lithocodium–Bacinella and algal facies, exhibit favorable porosity and permeability (cf. Jeong et al., 2017; Bahrehvar et al., 2021). These facies-controlled reservoir properties originated from the highly well-connected primary/depositional interparticle and intraparticle macroporosity. Porosity was further improved by the presence of secondary moldic and vuggy pores.

The main source rocks for hydrocarbons in the Yamama Formation include the underlying Jurassic and lower Cretaceous sections primarily the Sulaiy Formation (Abeed et al., 2011). Although most organic maturity data indicate that peak oil generation has not yet been reached (Abeed et al., 2011), Al-Ameri and Al-Ibrahim (2015) reported that the Yamama Formation functions both as a reservoir and a source rock. The crude oils are characterized by low Pr/Ph ratios, an even-over-odd carbon number predominance, and front-end biased n-alkane distributions, indicating a marine carbonate source rock containing Type II-S kerogen (Abeed et al. 2012).

The eastern stratigraphic equivalents of the Yamama Formation reflect a transition into formations deposited in deeper marine intrashelf basins, including the Lower Sarmord, Upper Chia Gara, and Lower Balambo formations (Fig. 5). The Chia Gara includes deep-water ammonitic radiolarian spiculitic limestones and shales (Ahmed and Al-Hameedy, 2023), with only its upper part overlapping in age with the Yamama. The Lower Balambo, radiolarian planktonic limestones deposited in outer shelf–deep water bathyal environment (Sarraj and Mohialdeen, 2020). The Balambo Formation contains mixed organic matter (Type II), including small amounts of continental plant remains, pollen, and spores with a total organic carbon range of 0.14–8.85% (Al-Habba and Abdullah, 1989). The potential of the Yamama and Sulaiy formations as source rocks could be influenced by two key factors, including: (i) The eastern part of the basin along the northeastern part of the Neo-Tethys Ocean contains deep-water marine intrashelf carbonate facies (see Fig. 5) with high TOC contents (Wang et al., 2025). (ii) The tectonic compression resulting from the collision between the Arabian and Eurasian plates

may have led to deeper burial, potentially increasing thermal maturity. These factors could contribute to the Yamama and Sulaiy formations serving as source rocks for the adjacent reservoirs.

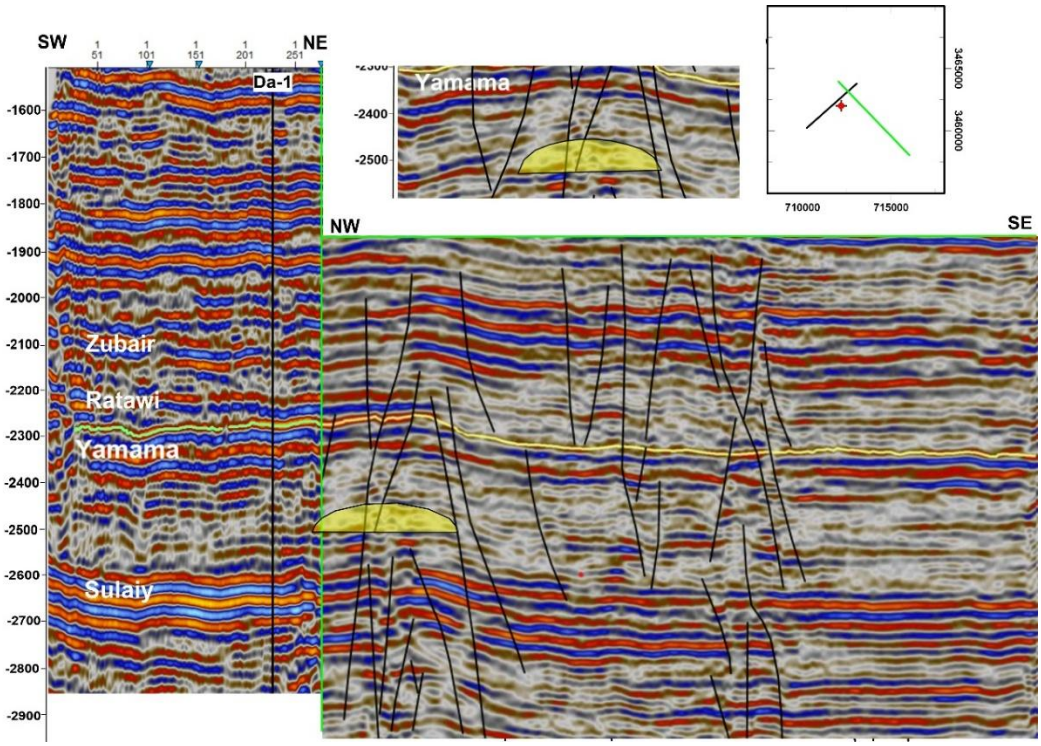

Figure 7. *Interpreted seismic sections (SW–NE and NW–SE) across the Ah'Dimah Oilfield, South of Iraq illustrating the structural and stratigraphic framework of the Lower Cretaceous interval. The highlighted Yamama Formation exhibits lateral facies variations and is intersected by multiple fault systems. The yellow lens indicates a possible direct hydrocarbon indicator (DHI), suggesting hydrocarbon accumulations. Faulting is extensive and appears to influence both structural compartmentalization and potential hydrocarbon migration pathways. Note that some fault systems penetrate from below the Sulaiy Formation upwards into the Yamama and overlying units* (*author's own edit*).

3-D modeling indicates that hydrocarbon generation and expulsion from the matured Jurassic source rocks of the intrashelf basins into the upper-lying Cretaceous reservoirs (including Yamama) began during the Late Cretaceous and Early Miocene (Pitman et al. 2004), with vertical migration dominating due to direct contact between the source and overlying Lower Cretaceous reservoirs. The fault systems served as vertical pathways of the hydrocarbon from the Upper Jurassic and Lower Cretaceous source rocks into the upper-lying reservoirs (Fadhel and Al-Rahim 2019; Fig. 7). Trap formation is primarily associated with the reactivation of deep-seated Precambrian faults and synorogenic faulting during the Mesozoic, promoting the diapiric rise of Precambrian salt (e.g., Hormuz) and the development of large drape folds over

basement fault blocks, leading to petroleum accumulation mainly within fault-block anticlines above evaporites (Pitman et al. 2004). The lower part, shaly, argillaceous limestones of the Ratawi Formation (thickness varies) seal the top of the Yamama Formation, while the Lower Cretaceous fine-grained, pyritic Sulaiy limestones (around 170m thick) locally, and the Upper Jurassic evaporitic Gotnia (around 120 m thick) regionally, seal the Yamama from the bottom. Regionally, the shaly, thinly bedded limestones of the Lower Sarmord, Lower Balambo, Sulaiy/Makhul and Upper Chia Gara prevent the lateral hydrocarbon migration of the Yamama Formation.

The timing of hydrocarbon migration is closely tied to the tectonic and stratigraphic development of the Arabian Plate including the obduction of ophiolites and the Zagros orogeny. Moreover, the migration timing corresponds with the structural (anticlines and fault closures) and stratigraphic trap (lateral facies changes) development in the Yamama Formation. The presence of two types of organic matter coupled with variation in crude oil specific gravity within the Yamama Formation (Table 1) suggests contributions from two distinct source rocks during separate hydrocarbon migration phases. The first phase likely occurred after the obduction of ophiolites, with hydrocarbons sourced from Jurassic formations. The second migration phase, from the Upper Jurassic and Lower Cretaceous source rocks, took place due to the reactivation of hydrocarbon maturation and generation associated with the Zagros orogen and continued into the Early Miocene and later (Fox and Ahlbrandt 2002).

The burial-thermal history of the Yamama Formation in the southern Mesopotamian Basin reflects the impact of multiple tectonic events that shaped its geothermal gradient and, consequently, influenced the hydrocarbon generation, migration, and accumulation (Fig. 8). The region underwent the opening of the Neo-Tethys Ocean along the northern margin of the Arabian Plate during the Late Jurassic to Early Cretaceous. This event resulted in the formation of a passive-margin setting conducive to the deposition of thick shallow-water marine carbonates, including the Yamama Formation (Ziegler, 2001). By the Late Cretaceous, tectonic activity intensified as the Neo-Tethys began to close, causing compressional forces that led to the obduction of the Oman-UAE ophiolites onto the Arabian Plate. This tectonic shift included the formation of a foreland basin, which promoted further burial of the Yamama Formation, and thereby accelerated thermal maturation of organic matter and hydrocarbon generation (Glennie et al., 1973; Phillips et al., 2013). During the Middle Eocene, as the collision between the

Arabian and Eurasian plates intensified due to Zagros orogeny, significant subsidence within the foreland basin commenced. This subsidence contributed to forming the hydrocarbon structural traps in the area (Pitman et al., 2004).

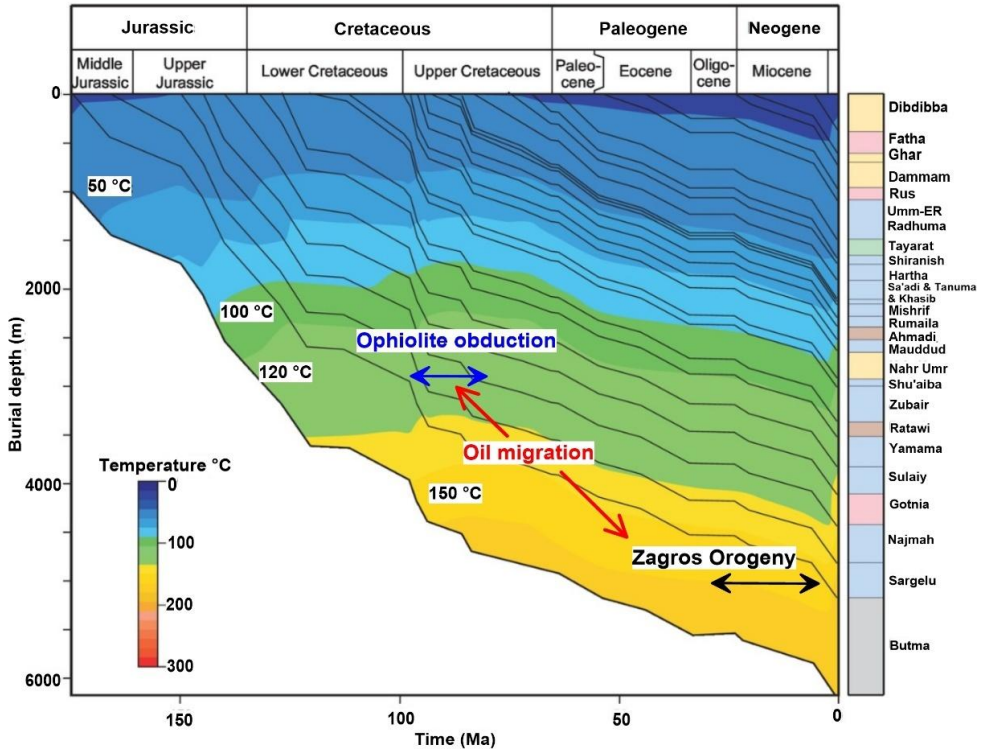

Figure 8. *Burial-thermal history plot in south of Iraq (adapted from Abeed et al. 2013) on which the timing of the obduction of ophiolites and Zagros orogeny and their impact on hydrocarbon migration are indicated.*

Crude oil analysis from the Yamama Formation indicates that the reservoir contains medium to light, non-biodegraded oils with notably high sulfur content (Pitman et al. 2004; Abeed et al. 2012; Al-Ameri and Al-Ibrahim 2015). The API gravity values vary significantly across different oilfields and reservoir units of the same fields. These variations do not display a straightforward regional trend, suggesting that depositional facies, burial depth, and diagenetic processes influenced the oil quality. Additionally, thermal maturity gradients related to differential burial and basin subsidence may enhance secondary cracking of hydrocarbons in deeper zones (Peters et al., 2004). Medium-light gravity, high sulfur crude oils are typically derived from carbonate source rocks containing type IIS kerogen (Pitman et al. 2004). During diagenesis, sulfur is preferentially incorporated into the organic matter (kerogen), particularly in anoxic to dysoxic marine environments where sulfate-reducing bacteria facilitate sulfur incorporation. This leads to the generation of high sulfur oils, especially in settings with limited

iron (Fe) availability, which prevents the absorption of hydrogen sulfide (H_2S) as pyrite (Berner 1984; Ahmad 2016). This process is especially pronounced in units formed within restricted platform environments, where limited water circulation and high organic productivity foster reducing conditions that promote sulfur enrichment.

Table 1. *The production rates, API, Sulfur contents and hydrogen sulfide concentration in the different reservoir units of the Yamama Formation across different oilfields in Iraq (Burgan is from Kuwait), (- = no data)* (*author's own edit*)

Field	Formation top depth m	Unit	Production rate BPD	API°	Sulphur %	H_2S ppm
Abu Amood	4073	YRA	1970	39.6	1.07	4.1
		YRB	4500	39.5	1.24	-
		YRC	-	36.5	1.56	-
Garraf	3600	YRA	5500	36.4	1.6	-
		YRB	5100	34.5	1.75	-
Halfaya	4195	YRA	5500	-	1.49	-
Nahr Umr	3740	YRC	4990	41.2	-	0.86
Nasiriya	3157	YRA	3000	-	-	-
		YRB	2150	-	-	-
		YRC	1250	-	-	-
		YRD	7730	28	-	1.75
Zubair	3800	YRA	-	40	-	-
		YRB	4690	37.2	-	0.76
West Qurna	3570	YRA	2000	34	0.1	450
		YRB	-	36.4	-	-
Burgan	-	-	-	20-31	-	-
Ratawi	3806	YRA	3660	43	1.37	-
		YRB	6400	41	1.15	-
Subba	3446	-	-	35.9	1.96	-
Luhais	3507	-	-	25.9	5.38	-
Ah'Dimah	3955	YRD	Oil flows	31.5	2.23	-
Rumaila North	3715	-	-	-	2.4	-
Rumalia South	3732	-	-	-	2	-
Majnoon	3850	YRA	Oil flows	31	-	-
		YRB	2280	38	-	-
		YRC	2100	36	-	-
Sindbad	4020	YRA	3370	42	-	48.2
		YRB	5125	44.5	-	67
		YRC	7133	44.4	-	50.8
Tuba	3800	-	325	34.4	2.27	-

2.6 Challenges in Exploration and Development

The exploration and development of the Yamama Formation face significant technical challenges, particularly due to reservoir heterogeneity imposed by vertical and lateral facies changes as well as the diagenetic alterations. The complex depositional environments of the Yamama Formation led to substantial variability in primary porosity and permeability across the reservoirs, making it difficult to predict flow characteristics and optimize recovery strategies. Additionally, diagenetic alterations, such as dolomitization, compaction and cementation, have altered primary pore geometry, which impacted the effective porosity and permeability negatively. This variability requires detailed facies and microfacies analysis to identify high-quality zones and understand reservoir connectivity. Special attention can be paid to the lateral and vertical distribution and correlation of the grain-supported and reefal facies, which exhibit good reservoir properties (Nazemi et al. 2024).

Enhanced oil recovery from the Yamama Formation will likely depend on integrating advanced geological modeling techniques and modern recovery methods. 3D seismic imaging and improved logging tools (e.g., image logs) may aid in identifying high-potential zones and better characterizing reservoir heterogeneity. Additionally, the application of targeted enhanced oil recovery (EOR) techniques, such as gas or water flooding and matrix acidizing tailored to Yamama reservoir, could help improve production efficiency (Almalichy et al., 2024, 2025). Long-term production strategies may also consider CO_2 injection as a potential EOR method, in the Yamama reservoir units where it can improve sweep efficiency. Advanced reservoir simulation, combined with innovative drilling practices, could further increase recovery rates and optimize development strategies across the heterogeneous Yamama reservoir.

2.7 Advances in the Study of the Yamama Formation and Regional Equivalents

Studies conducted on the Lower Cretaceous Yamama Formation and its regional equivalents including the Minagish Formation in Kuwait, Habshan in the UAE, and Fahliyan in Iran, have yielded new insights into depositional environments, diagenetic processes, and reservoir characteristics. The grain-supported oolitic and peloidal grain-supported limestone facies of the Minagish Formation in Kuwait, developed within the shoal area of a shallow carbonate ramp, exhibit the best reservoir quality. However, extensive cementation and compaction reduced the porosity and permeability (Gezeeri et al. 2007; Datta et al. 2013; Singh et al. 2017). The variation n in oil specific gravity (API) observed in the Minagish Formation in its different

reservoir units suggests multiple oil emplacements during reservoir charging (Gezeeri et al. 2007).

The Habshan Formation in the UAE has been studied through sequence stratigraphy using sedimentological and well logs data (Aziz and El-Sattar 1997). They found that relative sea-level changes critically influence the continuity and quality of reservoir intervals. A recent study on the Lower Fahliyan Formation in the Dorood Oilfield in Iran has detailed the depositional facies and diagenetic alterations (cementation and compaction) that have exerted a profound impact on reservoir quality (Nazemi et al., 2024). The depositional environments of the Yamama Formation in Saudi Arabia range from lagoonal to outer ramp settings, while the diagenetic alterations are controlled by changes in the sea level during the Berriasian-Valanginian (Nagm et al. 2018; Khalil et al. 2024).

Based on the seismic cross section through Ah'Dimah Oilfield in southern Iraq (Fig. 7), there are subtle seismic facies changes, particularly in the NW-SE section, which is interpreted to indicate lateral facies variations within the Yamama Formation. While high amplitude reflections typically associated with carbonate build-ups are not clearly observed in the section. However, the absence of such amplitude does not eliminate the possibility of finding carbonate build-ups in the area. These faults could not only contribute to structural compartmentalization and hydrocarbon migration but also have acted as conduits for the flow of hydrothermal fluids. These fluids could significantly influence the extent of diagenetic alterations and thus the reservoir quality of the Yamama Formation. Further seismic analysis, like acoustic impedance inversion, could help identify lateral lithological changes. Additionally, a potential direct hydrocarbon indicator (DHI) feature, such as a flat spot, may indicate gas presence, but more detailed seismic and log data would be necessary for confirmation. It is concluded that Lithocodium–Bacinella formed build-ups and reefal patches within the formation, and they are of interests for field development plans and strategies (Valinasab et al., 2023). Meanwhile, the seismic stratigraphy approach has been used to model hydrocarbon potential in the Al-Fao area, near Basra City, south of Iraq, to identify reservoir intervals with higher hydrocarbon-bearing potential (Abd and Abd, 2024). This modelling approach has confirmed the presence of carbonate build-ups within the Yamama Formation and specific reservoir units exhibited favorable characteristics for hydrocarbon storage, potentially aiding in future development planning and production strategies.

Recent technological advancements in seismic interpretation, reservoir modeling, and geophysical tools have significantly enhanced the precision of analyses conducted the Yamama Formation and its equivalents. Seismic stratigraphy interpretations and approaches have enabled the identification of different seismic stratigraphic traps within the Yamama Formation in southern Iraq (Abd and Abd 2024; Khadhaier and Ali, 2024). Petrophysical studies combined with facies modeling have allowed for more precise prediction of reservoir quality, enabling enhanced planning for hydrocarbon production (Khalil et al. 2024). Integrates seismic attributes and well data of the Yamama Formation were used to differentiate reservoir and non-reservoir units in the Nasiriya Oilfield. P-impedance volume and neural network analysis were used to model and estimate reservoir properties, ultimately confirming significant hydrocarbon accumulation within the reservoir (Khorshid et al. 2021). The facies types within the Yamama Formation in the Ratawi Oilfield have been modeled to better understand depositional environments and reservoir heterogeneity (Al-Iessa and Zhang, 2023). However, petrophysical properties like porosity and permeability were not integrated into the various facies, highlighting the need for future studies to enhance reservoir characterization by combining facies and petrophysical data. The integrated depositional facies and diagenetic models aid to evaluate the reservoir complexity in heterogeneous carbonate systems (Datta et al., 2013). Using advanced petrophysical models can account for the complexities within carbonate reservoirs, especially in semi-restricted depositional environments (Li et al., 2024).

Future research directions for the Yamama and its equivalent formations should include improving reservoir simulation, enhancing oil recovery techniques, and more precise biostratigraphic correlation. Reservoir simulation is particularly important given the high degree of heterogeneity within the formation. There is a need for high-resolution models that can better capture the variability within the reservoir which is a key factor for optimizing recovery strategies. Moreover, enhanced recovery techniques such as CO_2 injection, water flooding and matrix acidizing can significantly improve extraction efficiency, particularly in the naturally low permeability reservoir units. Additionally, biostratigraphic correlation of the Berriasian–Valanginian successions is necessary for establishing more accurate regional frameworks through the integration of microfossil assemblages such as calcareous nannofossils, planktonic and benthic foraminifera. These biostratigraphic markers allow more precise age determination and correlation across distant fields/regions within the Arabian Plate. This is especially critical

in carbonate-dominated systems like the Yamama Formation, where lithostratigraphic correlation alone may be challenging due to facies variability and diachronism (Alavi, 2004). The isotopic stratigraphy approach may improve the correlation of the Lower Cretaceous strata across the region (Nagm et al., 2018).

Therefore, correlating the Berriasian–Valanginian biostratigraphy with sequence stratigraphy can provide useful insights into sedimentary cycles, depositional environments, and reservoir quality on a regional scale. This integration offers a valuable framework for understanding how regional and global sea-level fluctuations influenced the sedimentary facies development of the Yamama and its equivalents in the Middle East. For instance, aligning biostratigraphic markers with transgressive-regressive cycles can improve predictions of reservoir distribution and continuity within each sequence. The use of biostratigraphic data to calibrate sequence boundaries allows obtaining a more refined chronostratigraphic framework, which helps in mapping depositional trends, identifying high-porosity zones, and precisely distinguishing reservoir from non-reservoir units. This approach can further assist in reconstructing paleo-environments in the regional correlation of the reservoirs to anticipate lateral facies changes and diagenetic variations that impact reservoir quality across the region.

3. Materials and Methods

Borehole data, geological reports, seismic sections, and well log sets of the Yamama Formation from several oil fields from south of Iraq (Fig. 1b) were collected. Core intervals of about 400 m from three different oilfields (Nasiriya, Ah'Dimah, and West Qurna) were employed for the purpose of this study. These cored intervals cover most parts of the formation.

Gamma-ray, density, neutron, sonic and resistivity logs were used to empirically calculate properties such as total porosity $PHIT$, effective porosity $PHIE$, sonic-derived porosity $PHIS$, volume of shale (Vsh), and water saturation (Sw) following the approach in Mohammed et al. (2022). These calculations were integrated with porosity and permeability measurements and petrography analysis. Well logs are widely used effective tools for accurately estimating petrophysical properties such as porosity, shale volume, and water saturation in subsurface formations.

To evaluate the formation and differentiate between reservoir and non-reservoir zones, the total porosity ($PHIT$), the effective porosity ($PHIE$), and the sonic-derived porosity ($PHIS$) are calculated from the density-neutron, and sonic logs. These calculations are reliable and widely used in reservoir characterization and typically have a precision of ±1-3% when cross-calibrated with core data (Crain 1986; Rider 1996).

$$PHIT = \frac{PHIN + PHID}{2} \qquad (1)$$

$PHIN$ refers to the porosity obtained directly from the neutron porosity log, while $PHID$ indicates the porosity derived from density log. The formula for calculating $PHID$ is provided below (Asquith et al. 2004)

$$PHID = \frac{\rho ma - \rho b}{\rho ma - \rho fl} \qquad (2)$$

ρma represents the matrix density, which is assumed to be 2.71 g/cm³ (density of calcite), given that the Yamama Formation is primarily limestone. ρb is the density directly derived from the density log reading, and ρf denotes the fluid density, assumed to be 0.9 g/cm³, which is the density of oil.

To quantify the influence of non-reservoir components and refine effective porosity calculations, effective porosity $PHIE$ derived by correcting the total porosity for shale volume, representing interconnected pore space as follows (Schlumberger 1974):

$$PHIE = PHIT * (1 - Vsh) \quad (3)$$

The volume of shale (Vsh) was determined using Larionov's equation (1969), which is commonly applied in formations with low to moderate shale content. This method provides reliable results with an accuracy of approximately ±2% in such carbonate reservoirs (Rider 1996).

$$Vsh = 0.33 * (2^{2*GRI} - 1) \quad (4)$$

GRI is the gamma-ray index that can be represented by the following equation.

$$GRI = \frac{GRlog - GRlow}{GRhigh - GRlow} \quad (5)$$

$GRlog$ represents the direct gamma-ray log reading, $GRhigh$ and $GRlow$ represent the highest and lowest gamma-ray readings respectively for a certain interval.

Porosity-derived sonic is calculated from sonic log using Wyllie's equation (Wyllie et al. 1958), to detect the effects of diagenetic processes on the overall porosity. The $PHIE$ represents the overall porosity, the primary porosity that formed during the deposition and the secondary porosity that formed after deposition due to the diagenetic alterations. Conversely, $PHIS$ mainly represents the primary porosity. Therefore, the difference between the $PHIE$ and $PHIS$ can refer to the secondary porosity (Asquith et al. 2004).

$$PHIS = \frac{\Delta T - \Delta Tma}{\Delta Tfl - \Delta Tma} \quad (6)$$

ΔT represents the acoustic transit time obtained directly from the sonic log, ΔTma is the acoustic transit time for the matrix, assumed to be 47 µs/ft for calcite, and ΔTfl denotes the fluid's acoustic transit time, assumed to be 188 µs/ft.

The porosity-derived sonic is then empirically corrected to account the shale and oil effects (Schlumberger 1974).

$$PHISc = PHIS * (1 - Vsh) * 0.9 \quad (7)$$

Variations in water saturation, along with changes in the resistivity of pore-filling fluids, generate distinct resistivity patterns in well logs. These patterns are instrumental in identifying hydrocarbon-bearing formations (Tiab and Donaldson 2016). To determine the fluid content within the reservoir, critical for identifying hydrocarbon-bearing zones, Archie's equation (Archie 1942) used to calculated the water saturation. The precision of Archie's equation depends on the input values of formation water resistivity (Rw), cementation exponent (m), and saturation exponent (n). The method typically has an uncertainty range of ±5–10% due to the sensitivity of these parameters (Schlumberger 1974).

$$Sw = \left(\frac{a*Rw}{PHIE^{m}*Rt}\right)^{1/n} \quad (8)$$

$PHIE$ represents the effective porosity, Rw is the formation water resistivity, Rt represents the resistivity obtained from the true resistivity log. a, m and n are the tortuosity factor, cementation factor, and the saturation exponent, assumed for carbonate rocks 1, 2, and 2, respectively. The formation divided into reservoir and non-reservoir units based on the effective porosity with consideration to the water saturation values. Zones with averaged effective porosity <5% are non-reservoir zones, with averaged effective porosity 5-10% are poor reservoirs, with averaged effective porosity 10-15% are fair reservoirs, and with averaged effective porosity ≥15% are good reservoirs. The water saturation cut-off value was 40%, higher than this value are non-reservoirs zones, less than 40% considered reservoirs.

The lithofacies of the formation were identified using integration of borehole data (final geological reports) and core data. These were calibrated with well logs to reveal the type of lithofacies (limestone, dolomite, dolomitic limestone, argillaceous limestone…etc.).

The electrofacies were identified from well logs (Ye and Rabiller 2000; Kadkhodaie-Ilkhchi et al. 2013; Davis 2018) to cover and evaluate the entire formation (including the non-cored intervals) using the supervised dynamic clustering technique available in Geolog7 software. Each electrofacies exhibits a distinct response pattern across the different well logs. Dynamic clustering method divided the data set into a number of predesignated groups. Each group has similar logs response ranges. The different electrofacies in the Yamama Formation were distinguished, classified and named from the clustering results and through the integration of the well logs supported by the available cores and petrography data.

The depositional facies were analyzed in a total of 400 m cored intervals that cover most of the Yamama Formation parts from different localities, based on the sediment textures, sedimentary structures, lithology, and fossils contents. One hundred-seventy representative samples were cleaned from oil residues before vacuum impregnation with blue-resin before thin sections preparation. The samples selection aimed to represent the entire formation. Samples were chosen to cover various zones and to capture diversity in color, sedimentary structures, and other observable properties such as visible porosity, density variations, and oil show zones, allowing for a thorough assessment of lithological and sedimentologic characteristics within the formation. The thin sections were analyzed and described petrographically in terms of sediment texture, pore types, and the diagenetic alterations.

The samples were classified based on the texture classification of Dunham (1962), the modification introduced by Embry and Klovan (1971) and the standard microfacies classification (RMFs) of Flügel (2010) (Fig. 9 and 10). Gamma-ray logs were calibrated with core data to ensure accurate depth alignment. Key lithological markers and horizons observed in both datasets were matched, and any depth discrepancies were corrected to achieve precise integration of petrophysical and core data.

The assessment of microfacies involved a detailed examination of textural attributes, such as grain size, packing density, and the presence of skeletal and non-skeletal components, along with sedimentary structures identified within the thin sections under a polarized microscope. This approach facilitated a systematic differentiation of microfacies types, thereby enabling a comprehensive identification of the primary facies/microfacies categories present within the formation. Microfossil analysis was employed to document the abundance, diversity, distribution of benthic foraminifera within Yamama Formation, and identify their stratigraphic ranges/ages.

Backscattered Electron (BSE) imaging and Energy Dispersive Spectroscopy (EDS) were conducted using a scanning electron microscope (SEM) in the XRD lab at the Institute of Exploration Geosciences, University of Miskolc, Hungary to investigate the mineralogical composition and elemental distribution of diagenetic phases. BSE images provided high-resolution contrast based on atomic number, allowing the identification of mineral textures and pore-filling phases. EDS elemental mapping and point analyses were employed to determine the

chemical composition of selected areas, aiding in the identification of authigenic minerals. These analyses were performed on polished samples that were coated with carbon to ensure conductivity.

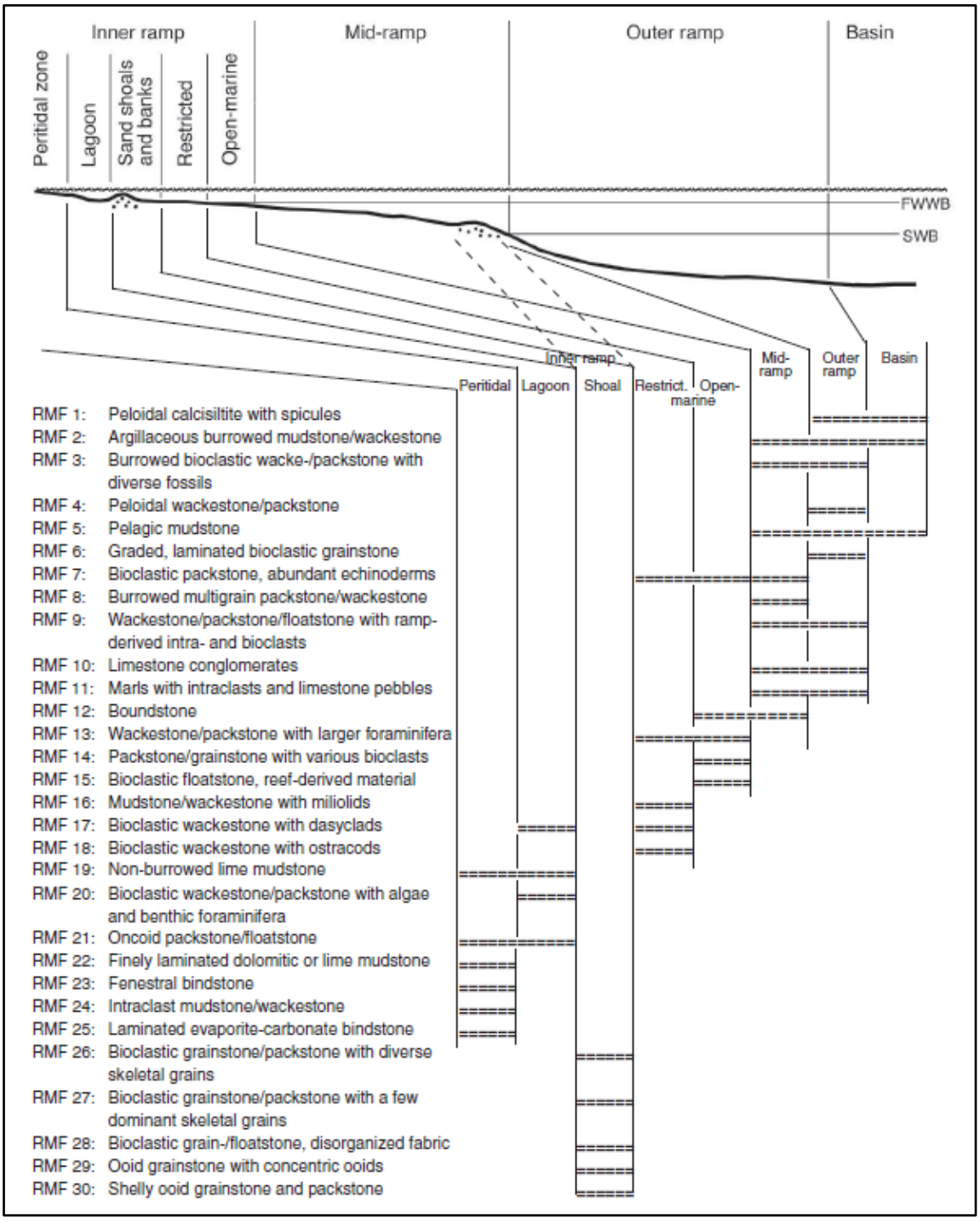

Figure 9. *Generalized facies/microfacies distribution in different environments of a homoclinal carbonate ramp (Flügel 2010).*

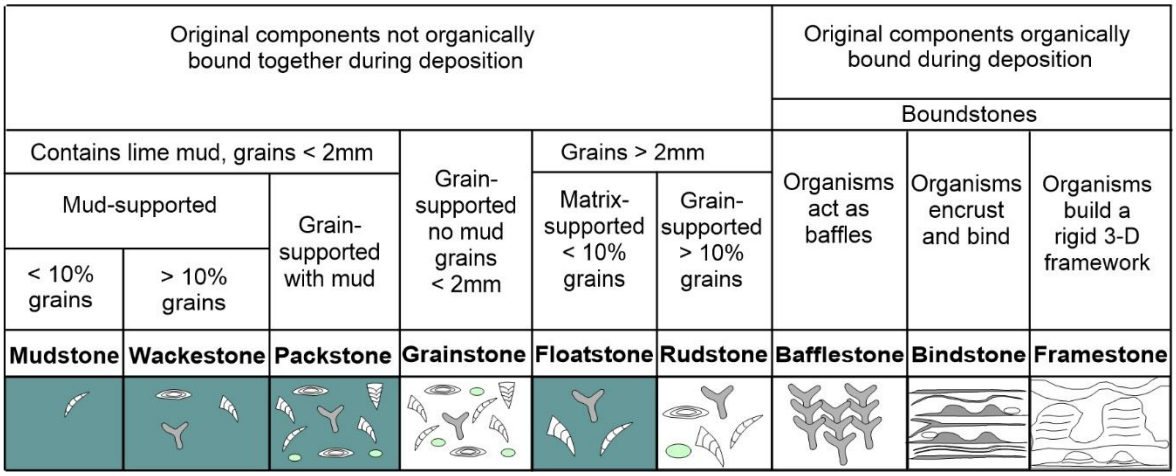

Figure 10. *Limestone's classification scheme. After Dunham (1962) and Embry and Klovan (1971).*

To analyze the visible porosity in thin sections, the porosity was classified petrographically based on Choquette and Pray (1970), categorized into interparticle, intraparticle, vuggy, channel and moldic porosity (Fig. 11).

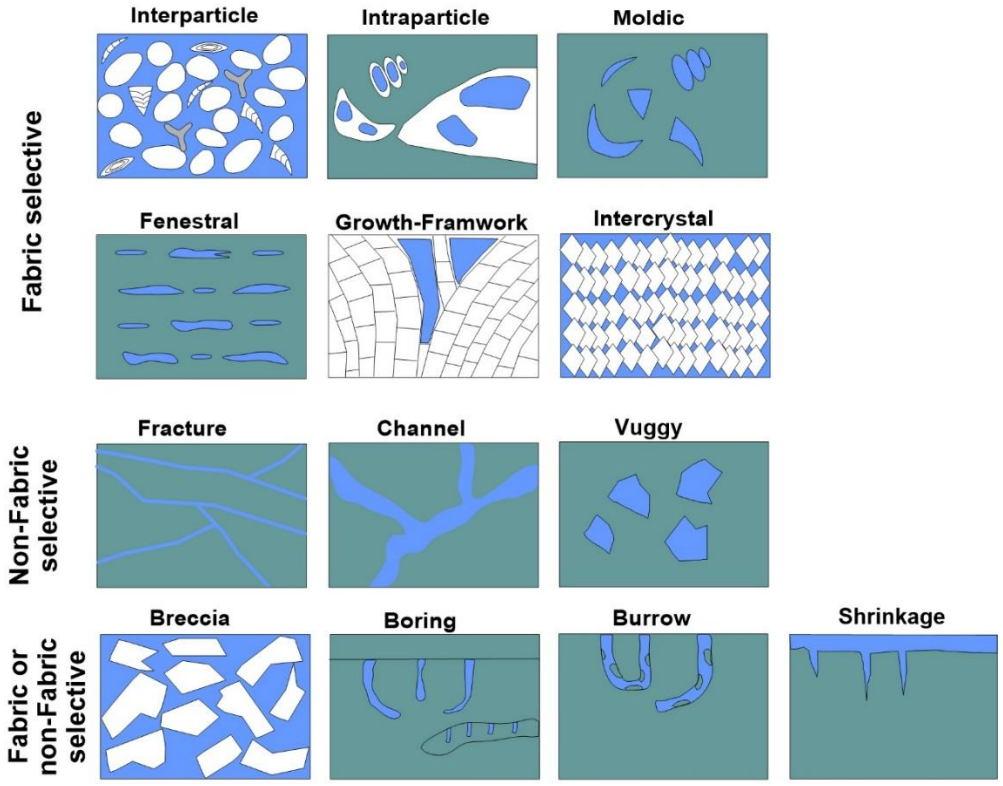

Figure 11. *Porosity classification in carbonate rocks. After Choquette and Pray (1970).*

Stable carbon ($\delta^{13}C$) and oxygen ($\delta^{18}O$) isotope analyses were conducted at the Ján Veizer Stable Isotope Laboratory (formerly the G.G. Hatch Stable Isotope Laboratory), University of Ottawa,

Canada to assess the geochemical conditions of the Yamama Formation. Twenty-four samples were selected to represent various facies and carbonate components. Powdered carbonate material was extracted using a microdrill and weighed into exetainers, and 0.1 mL of orthophosphoric acid (specific gravity 1.91) was added to the inside lip. The exetainers were sealed and helium-flushed while horizontal, then reacted upright at 25.0 °C for 24 hours (calcite) and 50.0 °C for 24 hours (dolomite) to release CO_2. The gas was extracted in a continuous helium flow via a Gas Bench II (Thermo Finnigan) connected to a Conflo IV interface and analyzed using a Delta XP isotope ratio mass spectrometer. Six replicate peaks were measured per sample and then averaged. Isotopic values are reported in per mil (‰) relative to the Vienna Pee Dee Belemnite (VPDB) standard, with an analytical precision of ±0.1‰ (2σ).

Fluid inclusion petrography in calcite cement helps identify inclusion types, origins, and entrapment sequences, offering vital context for interpreting fluid evolution and diagenetic processes. Microthermometry was carried out at Department of Mineralogy, Petrology and Applied Geology, University of Barcelona, Spain on calcite in limestones of the Yamama Formation using a LinkamTHMS600G heating–freezing stage, coupled with an Olympus BX60 transmitted light microscope. Homogenization temperatures (minimum fluid entrapment temperatures; T_h) and final ice melting temperatures (Tmice) were measured. The latter, which reflects fluid salinity (wt% NaCl eq.; Bodnar (1993); Goldstein and Reynolds (1994)), is the temperature at which the last ice crystal melts in an aqueous fluid inclusion. Nitrogen was used to cool the stage. Synthetic pure water and CO_2 inclusions were used to calibrate the stage thermocouple.

Critical features such as the Yamama Formation tops and bottoms, sequence boundaries (SBs), maximum flooding surfaces (MFSs), and reservoir units have been identified using an integrated approach including borehole well reports, well logs, core samples, petrographic data, regional correlations, and previously published studies for the Yamama Formation in Iraq and Middle East. This approach provided a better understanding of reservoir distribution in relation to sequence stratigraphy. The sequence stratigraphy of the Yamama Formation was built based on the approach of Catuneanu (2022). The depositional sequences have been identified based on facies/microfacies.

4. Results

4.1 Lithofacies distribution of the Yamama Formation

The integration of borehole data, core intervals, and well log interpretations, reveals that the Yamama Formation consists of six distinct lithofacies. These are characterized by unique sedimentological features, porosity, and shale content. These lithofacies include:

- Marly limestones: Porosity ≤5% with a relatively high shale volume.
- Argillaceous limestones: Porosity between 5–10% with a high shale volume.
- Limestones (pure limestones): Porosity ≥10% with a low shale volume.
- Dolomitic limestones: Porosity ≤10%, containing dolomite.
- Bioturbated dolomitic limestones: Porosity ranging from 0–10%, with a moderate shale volume and dolomite concentrated within burrows.
- Chalky limestones: Porosity reaching 10%, a low shale volume, and high water content.

4.2 Density-Neutron cross plots

The density-neutron cross-plot analysis (Fig. 12) was conducted to assess lithology, porosity variations, and fluid distribution within the Yamama Formation in the three different localities. This can enable differentiation between lithofacies (limestones, dolomitic limestone, and marly limestones), providing insights into reservoir quality and heterogeneity. Furthermore, it helps to validate well log data reliability by identifying potential inconsistencies or anomalies in porosity and density measurements. The cross-plot analysis confirms that the Yamama Formation within the studied wells is dominantly composed of limestone, with varying degrees of dolomitization. The identified lithofacies include marly limestones, argillaceous limestones, limestones, dolomitic limestones, and bioturbated dolomitic limestones.

In the cross-plots, marly limestones are positioned towards higher neutron porosity values due to clay-bound water and slightly lower density. Argillaceous limestones plot slightly lower in porosity but still exhibit elevated neutron response. Pure limestones align along the limestone trend line, exhibiting moderate porosity values. Dolomitic limestones shift towards higher density and lower neutron porosity, trending closer to the dolomite line. Bioturbated dolomitic limestones display increased scatter due to heterogeneity, plotting around the dolomite trend but with a broader range of porosity values.

The porosity distribution highlights reservoir heterogeneity, with evidence suggesting secondary porosity development and potential hydrocarbon presence. Well-to-well variability indicates differing degrees of diagenetic alteration and porosity evolution, necessitating further integration of core data and resistivity logs to refine reservoir characterization and examine the reliability of well log data. The cross plots reveal that the Yamama porosity ranges from 0 - 25%.

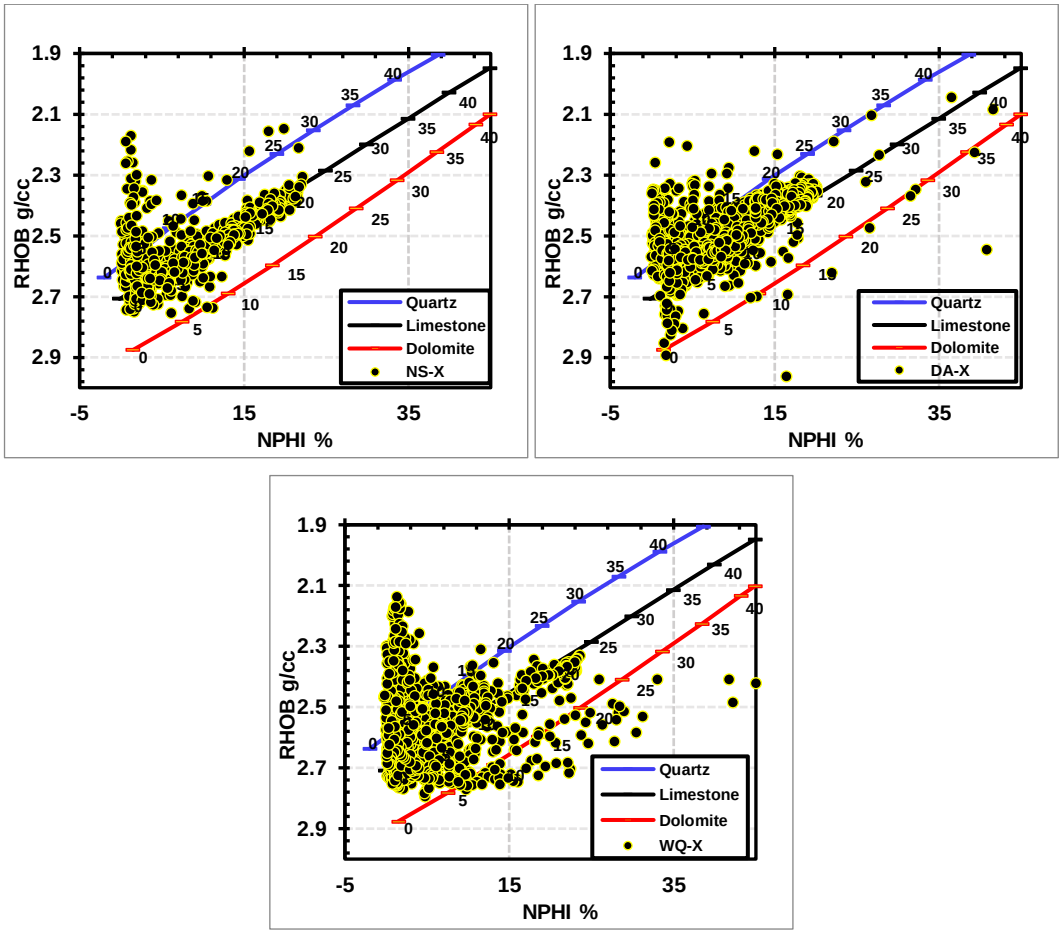

Figure 12. *Density-Neutron cross plots in the Nasiriya (NS-X), Ah'Dimah (DA-X), and West Qurna (WQ-X) showing that the formation porosity ranges between 0-25%, some data points are filling on the quartz and dolomite lines* (*author's own edit*).

4.3 Electrofacies distribution of the Yamama Formation

The clustering analysis of well logs identified five distinct electrofacies, each varying in depth across different reservoir and non-reservoir units. These electrofacies were classified based on reservoir properties, including well log signals, effective porosity, shale volume, and water saturation (Table 2). They are as follows:

Table 2. *Summaries electrofacies petrophysical properties from the Nasiriya Oilfield (NS-X), Ah'Dimah (DA-X), and West Qurna (WQ-X), and the average of the three wells. It shows percentage (%) and thickness (m) of each electrofacies. Average results of gamma-ray, density (RHOB), deep resistivity (RT), sonic (DT), and neutron (NPHI) logs. It shows the average of effective porosity (PHIE), volume of shale (Vsh), and water saturation (Sw) for each electrofacies* (*author's own edit*)

Field/Well	Electro-facies codes	Description	Percentage %	Thickness (m)	GR API	RHOB g/cc	RT ohm.m	DT *us*/ft	NPHI %	PHIE %	Vsh %	Sw %
NS-X	EF-1	Marly limestone	13.1	30	33	2.67	35	53	5.2	2.6	16.3	76.7
	EF-2	Dense limestone	26.2	60	23	2.6	39	53.4	4.3	5.4	8.8	73.4
	EF-3	Moderate porous limestone	36.7	84	20	2.5	8.5	60.3	10.8	9.9	6.9	59.4
	EF-4	Porous limestone	20.5	47	16	2.42	4	67	17.2	16.2	5.1	37.3
	EF-5	Vuggy limestone	3.5	8	25	2.3	74	52.5	5.9	20.7	10.6	46.5
DA-X	EF-1	Marly limestone	3	9	34	2.83	52	60.5	6.0	5.5	40.6	67.8
	EF-2	Dense limestone	26.6	82.5	20	2.57	121	55.5	2.9	3.9	17.9	54.0
	EF-3	Moderate porous limestone	40.3	125	16	2.5	31	62.5	8.9	8.4	13.0	42.1
	EF-4	Porous limestone	29.9	93	13	2.4	16	70	15.8	13.8	8.9	39.2
	EF-5	Vuggy limestone	0.2	0.62	26	2.2	122	55	4.9	16.0	25.0	10.4
WQ-X	EF-1	Marly limestone	17.5	60.5	39	2.67	224	54	6.4	2.1	23.7	60.8
	EF-2	Dense limestone	57.4	199	19	2.62	203	52.7	2.4	4.9	7.0	62.5
	EF-3	Moderate porous limestone	14.3	49.5	23	2.52	88	59	8.0	9.7	9.5	35.2
	EF-4	Porous limestone	4.8	17	26	2.37	46	77.5	2.6	17.0	13.3	23.9
	EF-5	Vuggy limestone	5.9	20	22	2.28	297	51.3	5.5	22.8	9.4	17.2
Average 3	EF-1	Marly limestone	11.3	100	37	2.69	151	54.5	6.0	2.6	23.3	66.1
	EF-2	Dense limestone	38.7	342	20	2.6	154	53.5	2.9	4.7	10.0	62.4
	EF-3	Moderate porous limestone	29.1	257	19	2.51	35	61	9.3	9.2	10.3	46.3
	EF-4	Porous limestone	17.6	156	15	2.4	16	70	16.9	15	8.3	36.9
	EF-5	Vuggy limestone	3.3	29	23	2.29	220	52	5.6	21.7	10.1	37.5

- Marly limestone (EF-1): Low porosity (<5%), high shale volume (>15%), and high water saturation (>60%) (non-reservoir electrofacies).
- Dense limestone (EF-2): Low porosity (<5%), relatively lower shale volume (<15%), and high water saturation (>50%) (non-reservoir electrofacies).
- Moderately porous limestone (EF-3): Porosity ranging from 5-10%, low shale volume (<15%), and water saturation between 35–60% (fair reservoir electrofacies).
- Porous limestone (EF-4): High porosity (14-17%), shale volume between 5–13%, and water saturation of 24-40% (Good reservoir electrofacies).

- Vuggy limestone (EF-5): High porosity (16-22.8%), with shale volume and water saturation varying across different oilfields (Good porosity, low water in Ah'Dimah and West Qurna but water bearing in some intervals in Nasiriya Oilfield).

Electrofacies EF-1 and EF-2 represent non-reservoir facies, while EF-3 corresponds to moderate reservoir facies. EF-4 is classified as a good reservoir facies. The characteristics of EF-5 vary by location. In the Nasiriya and West Qurna oilfields, its shale volume remains below 10%, whereas in the Ah'Dimah Oilfield, it reaches up to 25%. However, it records less than one meter thick in Ah'Dimah. Similarly, EF-5's water saturation varies, with values of 46.5% in Nasiriya, 10% in Ah'Dimah, and 17% in West Qurna. As a result, EF-5 is a water-bearing facies in some intervals in Nasiriya but functions as a reservoir facies in West Qurna.

4.4 Distribution of reservoir vs non-reservoir units in the Yamama Formation

The formation is divided into four reservoir units; Yamama Reservoir A (YRA), Yamama Reservoir B (YRB), Yamama Reservoir C (YRC), and Yamama Reservoir D (YRD), which are characterized by high effective porosity and low water saturation. These are separated by four non-reservoir units; Barrier 0 (B0), Barrier 1 (B1), Barrier 2 (B2), and Barrier 3 (B3), which are characterized by low effective porosity and higher-water saturation. The YRA, YRC, and YRD units are further subdivided into two reservoir subunits each, named as YRA1, YRA2, YRC1, YRC2, YRD1, and YRD2. These are separated by thin non-reservoir beds. Intervals with porosity range 0-5% and high-water saturation are considered impervious (non-reservoir) (Table 3). The reservoir units are composed limestones that are interbedded with argillaceous limestones in some intervals whereas the non-reservoir units are composed of argillaceous limestones interbedded with marly and dolomitic bioturbated limestones. The B0 unit acts as a seal for the formation and separates the Yamama and the overlying Ratawi Formation. The results show that the reservoir properties for the same layer/zone (reservoir or non-reservoir) considerably vary in the different oilfields.

4.4.1 Nasiriya Oilfield (NS-X)

The Yamama Formation in the Nasiriya Oilfield (NS-X) (Fig. 1 and 6) exhibits a vertically heterogeneous reservoir system, with distinct variations in petrophysical properties across the different reservoir and non-reservoir units (Fig. 13). The reservoir units consist of mainly

limestones with some presence of argillaceous limestones, while the non-reservoir units consist of argillaceous, marly, dolomitic, and bioturbated dolomitic limestones.

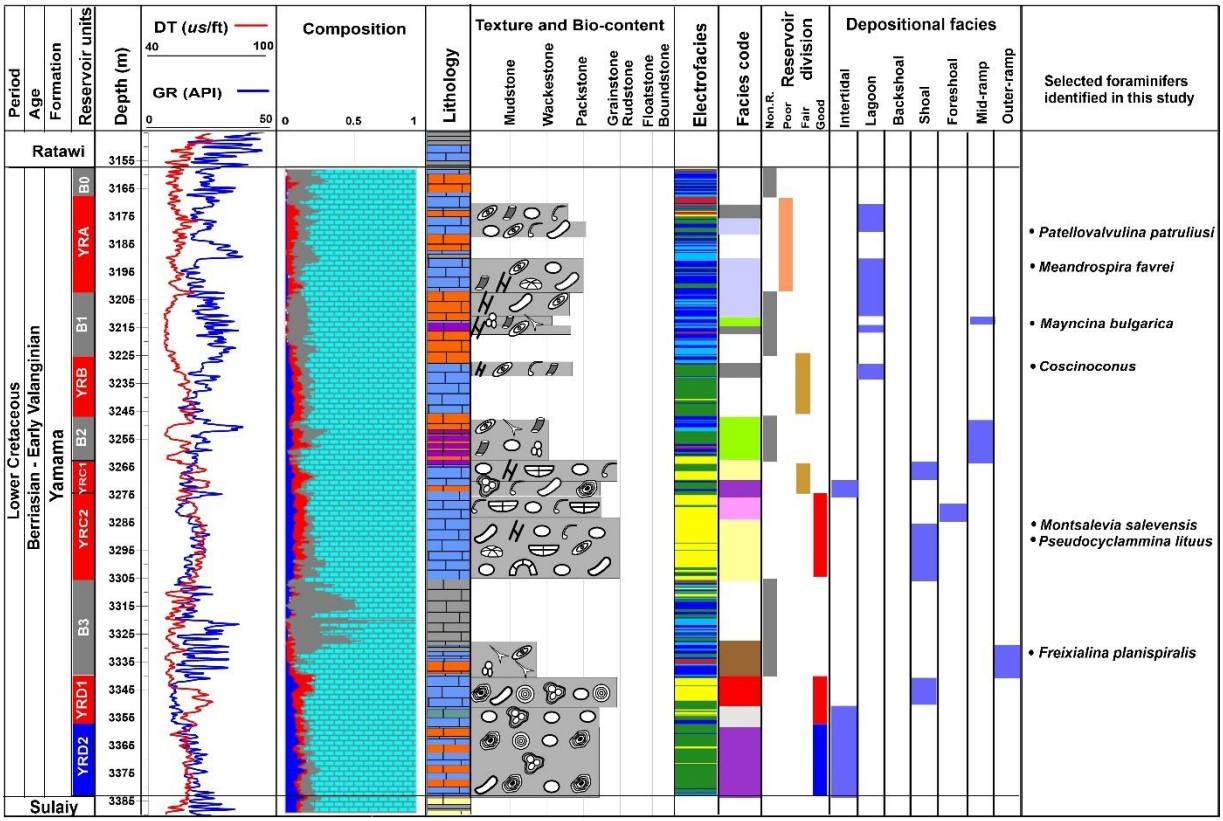

Figure 13. *Detailed graphic and wireline logs of the Yamama Formation in the Nasiriya Oilfield, showing that the formation is heterogenous and consists of five different lithology types, nine facies vary with depth, effective and sonic porosity (PHIE and PHIS), percentage of porosity filled with hydrocarbon and with water, gamma ray and sonic logs, depositional environments of each facies. Refer to Figure 14 for legend* (*author's own edit*).

The B0 unit, at the top of the formation, is classified as a non-reservoir (sealing) unit with an effective porosity (PHIE) of 7%, sonic-derived porosity (PHIS) of 3%, a volume of shale (Vsh) of 13%, and a high water saturation of about 67% (Table 3). The thickness of this unit is 15 m and dominated by EF-2 with some occurrence of EF-1 and characterized by the argillaceous limestones confirming its poor reservoir properties.

The YRA unit is 33 m thick and identified as a poor- fair reservoir unit that is dominated by EF-5 and EF-4 at the upper part of the unit and characterized by the presence of EF-1 and EF-2 at the lower part (Fig. 13). This unit is exhibiting a PHIE of 8%, PHIS of 4%, Vsh of 9%, and Sw of 31% (Table 3). The upper part is consisting of limestones interbedded with argillaceous limestones, while the lower part characterized by the limestones lithofacies.

The non-reservoir unit B1 has 24 m thick with low porosity (PHIE 4%, PHIS 2%), a moderate shale content (Vsh 14%), and a high water saturation of 84%. This unit is dominated by EF-1 and EF-2 electrofacies and defined by the argillaceous limestones with occurrence of bioturbated dolomitic limestones bed.

The YRB unit is 19 m thick and classified as a fair reservoir unit that characterized by the limestones and dominated by the EF-3. This unit shows PHIE of 10%, PHIS of 7%, Vsh of 7%, and Sw of 53%.

The B2 unit is a non-reservoir with 6 m thick and shows low porosity values (PHIE 4%, PHIS 2%), a shale content of 14%, and full of water (Sw is about 98%; Table 3). This unit is defined by EF-1, EF-2 and EF-3 and dominated by of the bioturbated dolomitic limestones that interbedded with argillaceous limestones (Fig. 13).

The YRC unit is a good-quality reservoir in Nasiriya Oilfield. The unit is 55 m thick and dominated by the pure limestones. The upper part is characterized by the presence of EF-4 that interbedded with EF-3, whereas the lower part is mainly EF-4. This unit displays higher porosity values (PHIE 14%, PHIS 9%), a relatively low Vsh of 6%, Sw of 48%.

The non-reservoir unit B3 is 35 m thick and dominated by the marly limestones and characterized by the presence of the EF-1, EF-2 with some occurrence of EF-3. This unit is defined by PHIE of 7%, PHIS of 3%, Vsh of 8%, and Sw of about 90%.

The YRD1 unit is 15 m thick and classified as a good reservoir. It is dominated by the pure limestones lithofacies and defined by the EF-5 with some occurrence of dolomitic limestone at the base (Fig. 13). This unit exhibits PHIE of 15%, PHIS of 11%, Vsh of 2%, Sw of 27% (Table 3).

The YRD2 unit is 28 m thick and consisting of limestones interbedded with argillaceous limestones and dominated by EF-3. This unit shows PHIE of 11%, PHIS of 7%, Vsh of 7%, and a high Sw of 85%, indicating its significant water content.

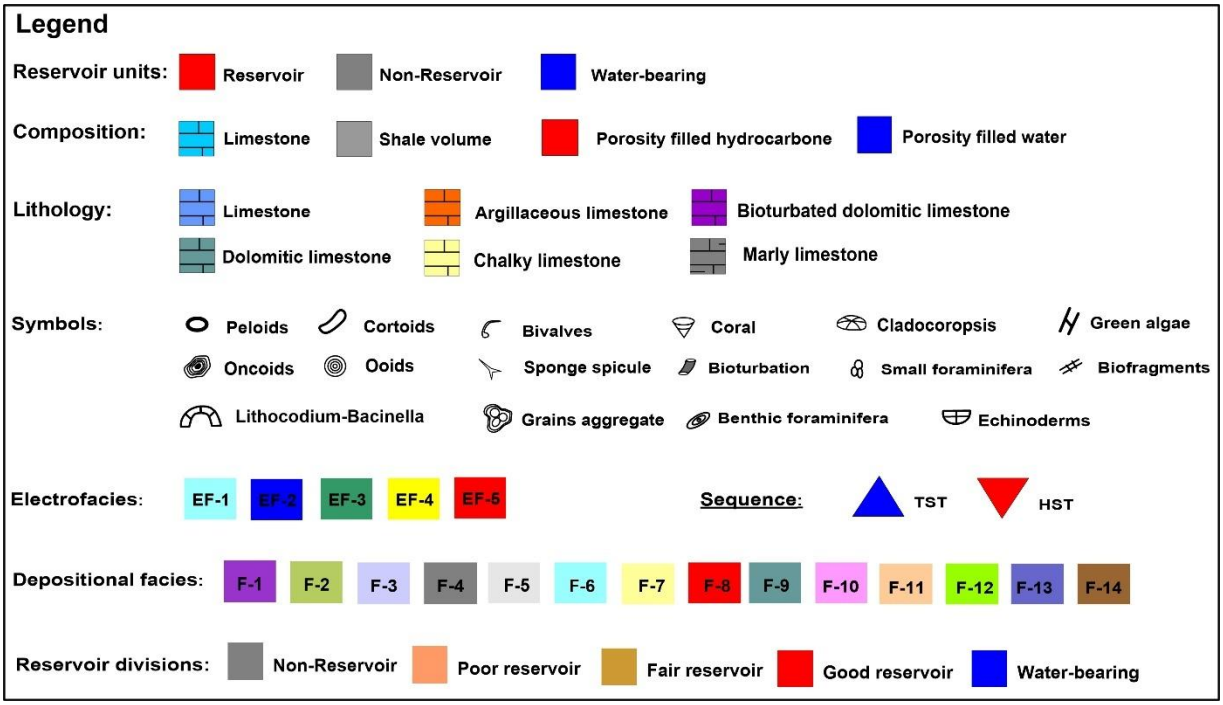

Figure 14. *Unified legend for this study illustrating the codes color used for reservoir units, lithological compositions, symbols of grains used in the sedimentological and depositional models of the Yamama Formation. The legend also includes standardized electrofacies (EF-1 to EF-5), depositional facies (F-1 to F-14), and sequence surfaces, transgressive system tracts (TST) and highstand system tract (HST)* (*author's own edit*).

4.4.2 Ah'Dimah Oilfield (DA-X)

The Yamama Formation in the Ah'Dimah Oilfield (DA-X) (Fig. 1 and 6) follows a similar vertical facies distribution when compared to Nasiriya Oilfield, but with some variations in petrophysical characteristics. The results show that the Yamama Formation in Ah'Dimah Oilfield is heterogenous and overall consists of limestone and argillaceous limestone with some appearance of chalky, marly and dolomitic, and bioturbated dolomitic limestones in trace amount (Fig. 15). The non-reservoir units B1, B2, and B3 split the YRA, YRB, YRC and YRD reservoir units. Whereas B0 represent seal of the formation.

The non-reservoir unit B0 is 20 m thick that consists of mainly argillaceous limestones with the occurrence of marly and bioturbated dolomitic limestones (Fig. 15). It is dominated by the presence of EF-2 with the presence of EF-1 and EF-3. This unit exhibits a PHIE of 6%, PHIS of 4%, a high shale volume (Vsh) of 27%, and Sw of 35% (Table 3).

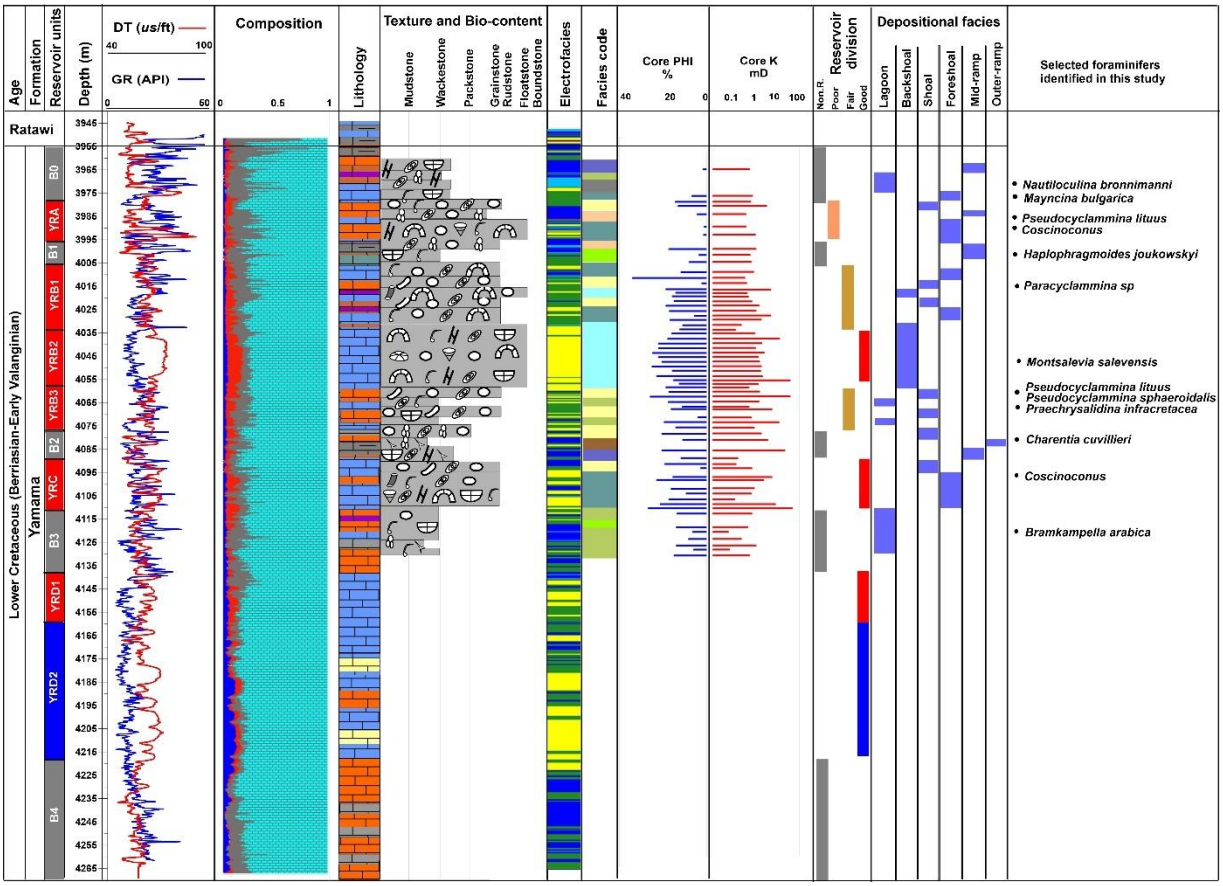

Figure 15. *Detailed graphic and wireline logs of the Yamama Formation in Ah'Dimah Oilfield, showing that the formation is heterogenous and consists of six different lithology types, seven facies vary with depth, effective and sonic porosity (PHIE and PHIS), percentage of porosity filled with hydrocarbon and with water, gamma ray and sonic logs, core porosity (PHI) and permeability (K), depositional environments of each facies and distribution of foraminifers* (*author's own edit*).

The YRA unit is about 21 m and identified as a poor reservoir. It is consisting of pure limestones interbedded with argillaceous limestones and dominated by the EF-3 at the upper part, while the lower part is characterized by the EF-2 with some occurrence of thin beds of EF-4 (Fig. 15). This unit displays a PHIE of 8%, PHIS of 7%, Vsh of 20%, and Sw of 24% (Table 3).

The non-reservoir unit B1 is about 6 m of marly limestones and dolomitic limestones and dominated by EF-1 and EF-2. This unit is characterized by PHIE of 4%, PHIS of 4%, a high Vsh of 25%, and Sw of 33% (Table 3).

In contrast, the YRB unit exhibits good reservoir characteristics, with PHIE of 12%, PHIS of 10%, Vsh of 14%, and Sw of 25%. This unit is 77 m thick and divided into three subunits (YRB1, YRB2, and YRB3). The YRB1 contains pure limestones interbedded with argillaceous

and bioturbated dolomitic limestones and defined by EF-3 that interbedded with EF-4. The YRB2 comprises of mainly pure limestones and dominated by the EF-4 (Fig. 15). While the YRB3 is distinguished by interbedding limestones and argillaceous limestones and characterized by the EF-4 that interbedded with EF-2 and EF-3.

The B2 unit is 12 m of marly and argillaceous limestones and dominated by EF-2 (Fig. 15). This unit has PHIE of 7%, PHIS of 5%, Vsh of 13%, and Sw of 27% (Table 3).

The YRC unit displays 20 m thick of pure limestones that interbedded with argillaceous limestones and defined by the presence of EF-4 that interbedded with EF-2 (Fig. 15). This unit records PHIE of 12%, PHIS of 10%, Vsh of 13%, and Sw of 27%.

The non-reservoir unit B3 is about of 27 m of argillaceous limestones with the occurrence of dolomitic and bioturbated dolomitic limestones. This unit has PHIE of 6%, PHIS of 6%, Vsh of 16%, Sw of 55%, and dominated by EF-2 with occurrence of EF-3 in thin beds.

The YRD1 unit is 20 m of limestones that is defined by the EF-4 with the presence of EF-3 (Fig. 15). It has PHIE of 11%, PHIS of 9%, Vsh of 7%, and Sw of 43%. At the base of the formation, the YRD2 unit is about 59 m thick and characterized by the pure limestones with the occurrence of argillaceous and chalky limestones. This unit is defined by the presence of EF-4 and EF-3 and exhibiting PHIE of 12%, PHIS of 10%, Vsh of 6%, and a high Sw that reaches average of about 66% representing water-bearing unit (Table 3).

4.4.3 West Qurna Oilfield (WQ-X)

The Yamama Formation in the West Qurna Oilfield (WQ-X) (Fig. 1 and 6) displays notable variability in reservoir quality in the different reservoir and non-reservoir units (Fig. 16). based on the date availability, the overall evaluation of the Yamama Formation shows that the formation has poorer reservoir properties in West Qurna when compared to the Nasiriya and Ah'Dimah oilfields.

The non-reservoir unit B0 (the seal layer) consists argillaceous and marly limestones and characterized by the presence of the EF-1 and EF-2 (Fig. 16). This unit displays very low PHIE (3%), PHIS of 5%, and relatively high shale content (Vsh 16%), and Sw of 58% with 35 m thick (Table 3).

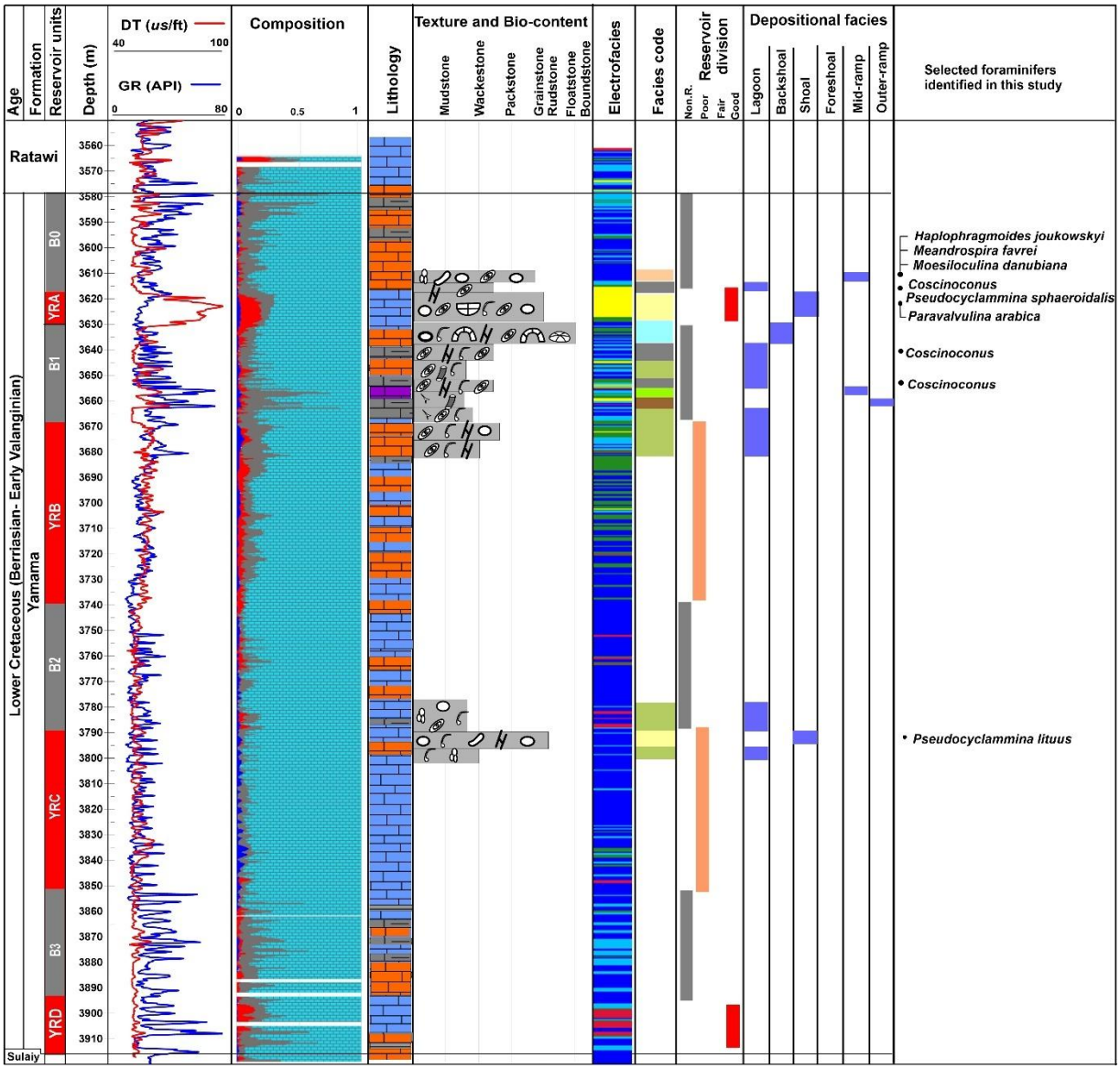

Figure 16. *Detailed graphic and wireline logs of the Yamama Formation in West Qurna Oilfield, showing that the formation is heterogenous and consists of six different lithology types, seven facies vary with depth, effective and sonic porosity (PHIE and PHIS), percentage of porosity filled with hydrocarbon and with water, gamma ray and sonic logs, depositional environments of each facies and distribution of foraminifers* (*author's own edit*).

The YRA unit forms 14 m thickness and represents a good-quality reservoir, consisting of pure limestones and dominated by the EF-4 (Fig. 16). This unit exhibits significantly higher porosity (PHIE 17%, PHIS 20%), a relatively low Vsh of 8%, and Sw of 17%, confirming its favorable reservoir characteristics (Table 3).

The non-reservoir unit B1 is 37 m thick and characterized by the marly limestones that interbedded with argillaceous limestones with the occurrence of the bioturbated dolomitic

limestones. The EF-1 and EF-2 are dominated with some presence of the EF-3. This unit records PHIE of 5%, PHIS of 6%, Vsh of 17%, and Sw of 44%.

Table 3. *Summarizes the average petrophysical properties (derived from well logs) including the effective porosity (PHIE), sonic derived porosity (PHIS), volume of shale (Vsh), water saturation (Sw), thickness, the type of depositional facies and electrofacies in each reservoir and non-reservoir unit, porosity types, and sequence tracts in the Yamama Formation, Nasiriya Oilfield (NS-X), Ah'Dimah (DA-X), and West Qurna (WQ-X) (author's own edit)*

Unit	Field/well	PHIE %	PHIS %	Vsh %	Sw %	Thickness m	Depositional facies type	Electrofacies type	Porosity type	Sequence	Description
B0	NS-X	7	3	13	67	15	-	EF-1 & EF-2	Minor interparticle, isolated molds	TST4	Poor to non-reservoir (seal)
	DA-X	6	4	27	35	20	F-2, F-4 & F-13	EF-1, EF-2 & EF-3			
	WQ-X	3	5	16	58	35	F-4 & F-11	EF-1 & EF-2			
YRA	NS-X	8	4	9	31	33	F-3 & F-4	EF-1 to EF-4 & trace EF-5	Interparticle, intraparticle, dissolved grains	HST3	Poor reservoir
	DA-X	8	7	20	24	21	F-7, F-9 & F-11	EF-2, EF-3 & EF-4			
	WQ-X	17	20	8	17	14	F-6 & F-7	EF-4			Good reservoir
B1	NS-X	4	2	14	84	24	F-3, F-4 & F-12	EF-1 & EF-2	Moldic & minor interparticle		Non-reservoir
	DA-X	4	4	25	33	6	F-11 & F-12	EF-2			
	WQ-X	5	6	17	44	37	F-2, F-4 & F-12	EF-1, EF-2 & EF-3		TST3	
YRB	NS-X	10	7	7	53	19	-	EF-3	Interparticle, intraparticle, vuggy	HST3	Fair reservoir
	DA-X	12	10	14	25	77	F-6, F-7 & F-9	EF-3 & EF-4			
	WQ-X	6	9	9	36	72	F-2	EF-2 & EF-3		TST3	Poor reservoir
B2	NS-X	4	2	14	98	6	F-12	EF-1, EF-2 & EF-3	Isolated molds	TST3	Non-reservoir
	DA-X	5	4	13	27	12	F-13 & F-14	EF-2			
	WQ-X	4	3	6	72	49	F-2	EF-2 & trace EF-5			
YRC	NS-X	15	9	6	48	55	F-1, F-7 & F-10	EF-3 & EF-4	Interparticle, intraparticle, dissolved non-skeletal grains	HST2	Good reservoir
	DA-X	12	10	13	27	20	F-7 & F-9	EF-2 & EF-3			Fair reservoir
	WQ-X	4	4	5	94	57	F-2 & F-7	EF-2			Poor reservoir
B3	NS-X	7	3	8	90	35	F-14	EF-1 & EF-2	Isolated molds	TST2	Poor to non-reservoir
	DA-X	6	6	16	55	27	F-2 & F-12	EF-2 & EF-3			
	WQ-X	4	3	13	40	45	-	EF-1 & EF-2			
YRD1	NS-X	15	11	2	27	15	F-5 & F-8	EF-3 & EF-4	Interparticle, partially & completely dissolved non-skeletal grains	HST1	Good reservoir
	DA-X	11	9	7	43	20	-	EF-3 & EF-4			Fair reservoir
	WQ-X	11	2	13	8	22	-	EF-5			
YRD2	NS-X	11	7	7	85	28	F-1	EF-3	Interparticle, minor channels	HST1	Water-bearing
	DA-X	12	10	6	66	59	-	EF-3 & EF-4			
	WQ-X	-	-	-	-	-	-	-		-	Absent

The reservoir unit YRB is classified as a poor reservoir unit. This unit characterized by pure limestones interbedded with argillaceous limestones. The EF-2 is dominated with some occurrence of EF-3 in streaks amount. This unit comprises 72 m and exhibits PHIE of 6%, PHIS of 9%, Vsh of 9%, and Sw of 36% (Table 3).

The non-reservoir unit B2 consists of argillaceous limestones with the presence of marly limestones and dominated by EF-2. It has thickness of about 49 m and displaying PHIE of 4%, PHIS of 3%, a low Vsh of 6%, and Sw of 72% (Table 3).

The YRC unit is classified as a poor reservoir consisting of pure limestones and dominated by EF-2 (Fig. 16). This has thickness of about 57 m and demonstrates low porosity values (PHIE 4%, PHIS 4%), a Vsh of 5%, and Sw of 94%.

The non-reservoir unit B3 comprises 45 m of argillaceous limestones interbedded with marly limestones (Fig. 16). It is defined by the presence of the EF-1 and EF-2 and has PHIE of 4%, PHIS of 3%, Vsh of 13%, and Sw of 40% (Table 3).

The YRD unit (stratigraphically equivalent to YRD1 in Nasiriya and Ah'Dimah oilfields) is classified as a good reservoir, comprises of about 22 m of pure limestones that dominated by EF-5. It displays PHIE of 11%, PHIS of 2%, Vsh of 13%, and a remarkably low Sw of about 8%, suggesting favorable reservoir potential. The YRD2 unit is absent in this studied well.

4.5 Porosity vs Permeability Relationship

No distinct overall relationship observed between porosity and permeability measurements within the Yamama Formation across the various reservoir and non-reservoir units with depth (Fig. 17a). This is typical for porosity and permeability relationship in carbonate rocks (Lucia 2007). The core porosity measurements tended to exhibit somewhat higher values when compared to the porosity values derived from logs. The overall exponential correlation between porosity and permeability measurements yielded a coefficient of determination (R^2) of approximately 0.25. However, observable trends and relationships emerged when the formation was divided into the various reservoir and non-reservoir units (Fig. 17b). YRA, YRB1, and YRB2 show limited porosity and permeability relationships. Whereas notable relationships were observed in B1, YRB3, YRC, and B3. The overall Grain-supported, Lithocodium–Bacinella and reefal facies tend to have higher poro-perm values comparing to the mud-supported facies (Fig. 17c). Divide the formation into hydraulic flow units and reservoir rock

types based on porosity-permeability measurements is a valuable method. However, this approach was not utilized in this study due to the limited porosity-permeability lab measurements but is recommended for future research to enhance the understanding of the Yamama Formation's reservoir characteristics.

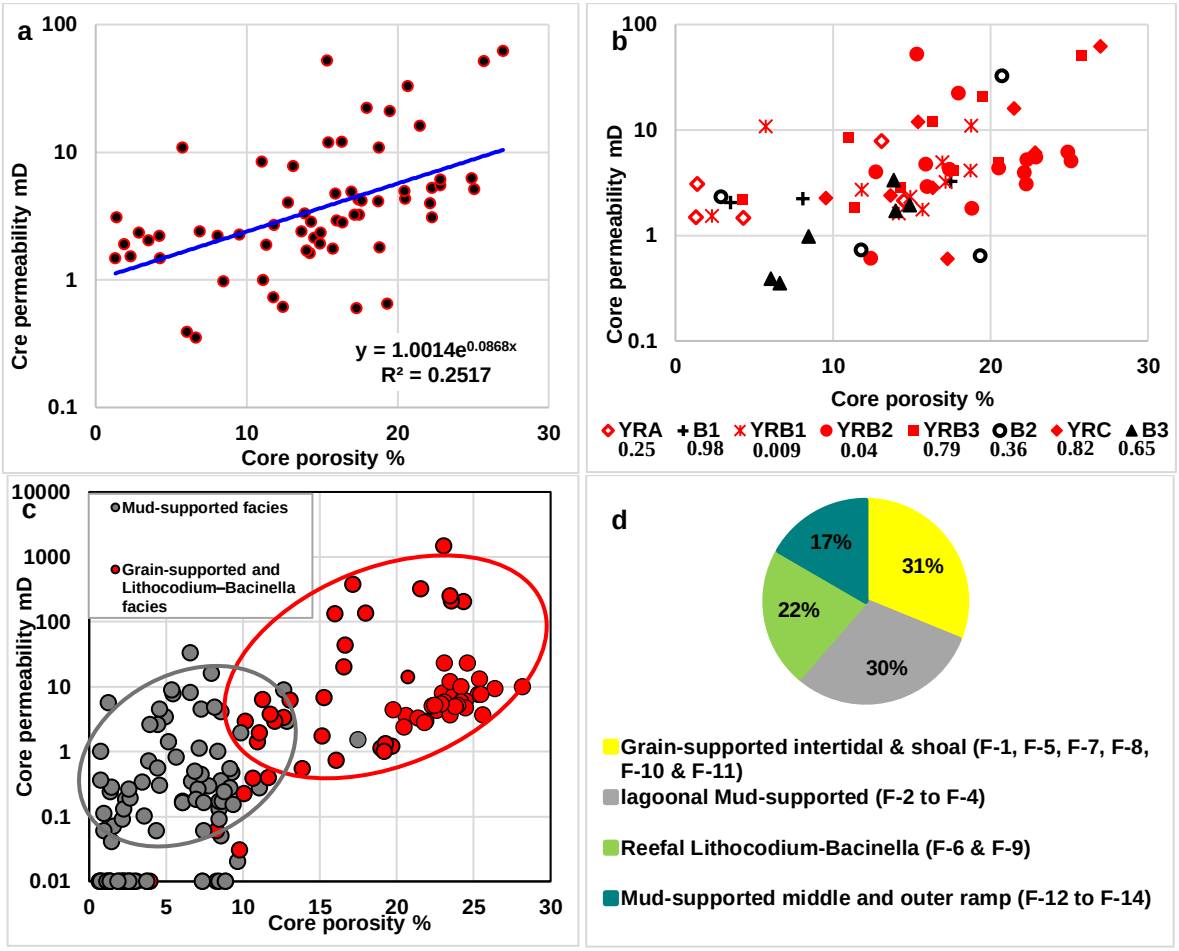

Figure 17. a) *Porosity-permeability (obtained from lab measurements) cross plot of the Yamama Formation in Ah'Dimah Oilfield.* ***b)*** *Porosity-permeability cross plots for each different reservoir and non-reservoir unit. Coefficient of determination (R^2) are shown for each unit.* ***c)*** *Cross plot of core plug porosity vs permeability of the mud and grain-supported facies in the Yamama Formation (data are from the different selected oilfields).* ***d)*** *pie chart shows the facies percentage recognized in this study from the three oilfields. Grain-supported, Lithocodium–Bacinella and reefal facies mainly deposited in the inner ramp shoal environments during HST, while mud-supported facies deposited in lagoonal, middle, and outer ramp during TST* (*author's own edit*).

4.6 Facies analysis

In this chapter, the terms facies and microfacies will be used. The term facies describes the overall characteristics of a sedimentary unit that observed on the core/slabbed samples which

reflect its depositional environment, while microfacies focuses on the microscopic features observed through thin sections analysis, including texture, fabric, and specific mineral and fossil components (Reading 2009; Flügel 2010).

4.6.1 The Underlying Sulaiy Formation

Petrographic analysis of the top of the underlying Sulaiy Formation revealed that the formation is composed of micritic limestones in mud-supported fabric. The matrix is typically fine-grained and homogeneous, with irregularly distributed patches of micritized grains (Fig. 18a and b).

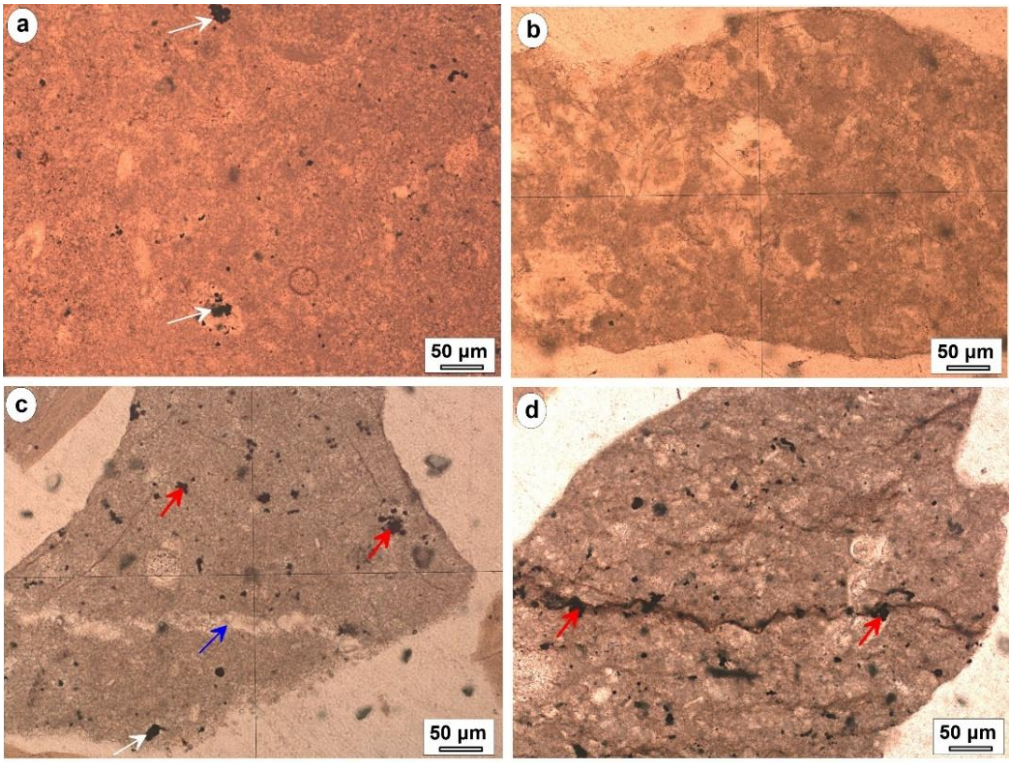

Figure 18. *Photomicrographic images showing features observed within the Sulaiy Formation.* ***a****) Pyritization in micritized texture (white arrows refer to pyrite).* ***b****) Cementation in micritized texture.* ***c****) microfracture filled sparry calcite cement (blue arrow), organic matters-bitumen (red arrows), pyrites (white arrows).* ***d****) Insoluble residues of organic matters-bitumen along stylolite* (*author's own edit*).

This texture reflects differential micritization of originally skeletal or fine-grained carbonate material during early marine or shallow burial diagenesis. Grain boundaries are typically indistinct, and interparticle porosity is absent, consistent with pervasive compacted micritic texture. The formation exhibits abundance of organic matters/bitumen and pyrite (Fig. 18c and d). Microfractures are observed but totally cemented by sparry calcite (Fig. 18c). The insoluble residues of the organic matters and/or bitumen are observed along the stylolite (Fig. 18d).

4.6.2 The Overlying Ratawi Formation

Thin section analysis across the Yamama–Ratawi boundary reveals distinct facies changes. The upper part of Yamama Formation consists of mud- wackestones containing planktic foraminifera (Fig. 19a and b).

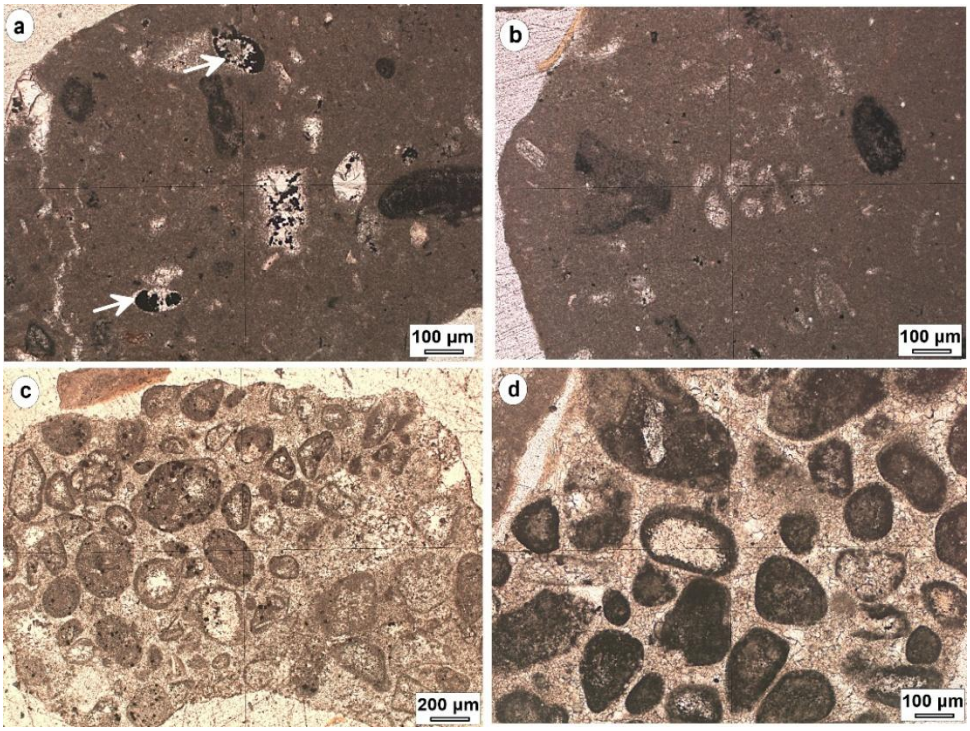

Figure 19. *Photomicrographic images illustrating the facies transition across the Yamama–Ratawi contact.* ***a)*** *Fossil chambers and skeletal grains filled with pyrite or organic residues (white arrows) in mud-supported texture (lower Yamama Formation).* ***b)*** *Outer ramp dominated mud- wackestone with benthic foraminifera from the upper Yamama Formation (B0).* ***c*** *and* ***d)*** *Grain-supported limestones with coated grains, oncoids and peloids from the lower Ratawi Formation* (*author's own edit*).

The lower part of Ratawi Formation is composed of grain-supported packstones to grainstones, containing oncoids, peloids, and coated grains that are sparry calcite cemented (Fig. 19c and d). Many of the grains exhibit micritic envelopes and varying degrees of micritization. Drusy sparite cement is filling interparticle pore spaces and coating grain surfaces. The lower Ratawi Formation shows poor reservoir quality.

4.6.3 Facies Analysis of the Yamama Formation

The cores and thin sections examinations revealed that the Yamama Formation consists of fourteen distinct microfacies (Fig. 20 and Table 4). These microfacies deposited in the inner

ramp, middle ramp, and outer ramp (Fig. 35 and 36). They can be grouped according to their similar sedimentary environments into seven facies association (A1-A7) as follows:

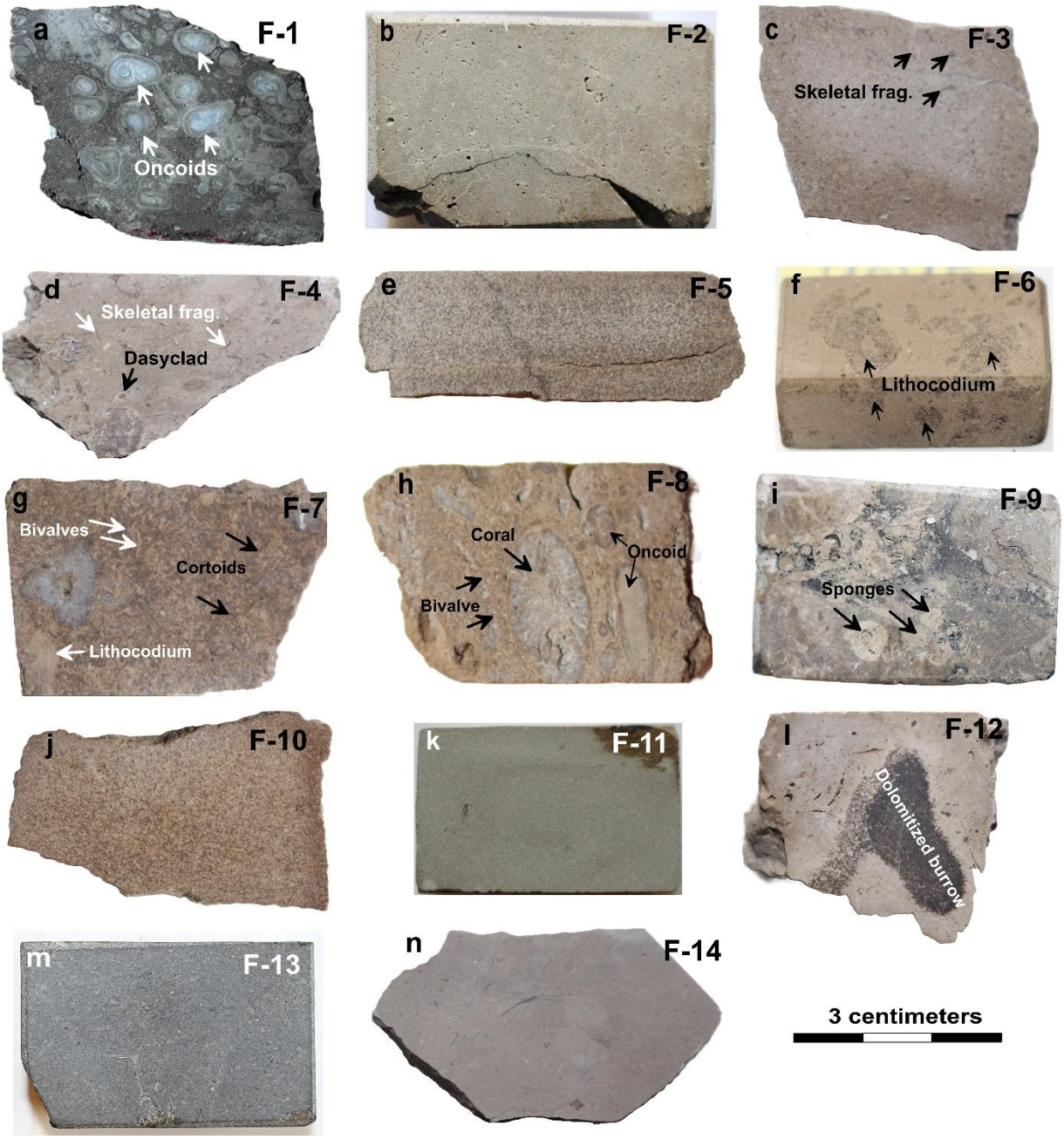

Figure 20. *Core slabbed from the different microfacies in Yamama Formation from the different oilfields.* ***a****) Peloidal oncoidal grainstones-to rudstones (F-1),* ***b****) bioclastic mud- to wackestones (F-2),* ***c****) bioclastic cortoidal wacke- to packstones (F-3),* ***d****) bioclastic dasyclads wacke- to packstones (F-4),* ***e****) Pelletal peloidal pack- to grainstones (F-5),* ***f****) Lithocodium-Bacinella float- to boundstones (F-6),* ***g****) peloidal grainstones (F-7),* ***h****) ooidal peloidal grain- to rudstones (F-8),* ***i****) reef debris float- to rudstones (F-9),* ***j****) bioclastic grainstones (F-10),* ***k****) miliolidal pack-*

to grainstones (F-11), ***l****) bioturbated dolomitic wackestones (F-12),* ***m****) bioclastic foraminiferal wackestones (F-13), and* ***n****) spiculitic skeletal mud- to wackestones (F-14).* (*author's own edit*).

The proximal inner-ramp (intertidal) facies association (A1) is represented by:

- Peloidal oncoidal float- to rudstones (F-1; Fig. 21).

The proximal lagoonal inner-ramp facies association (A2) is represented by:

- Bioclastic mud- to wackestones (F-2; Fig. 22).
- Bioclastic cortoidal wacke- to packstones (F-3; Fig. 23).
- Bioclastic dasycladalean wacke- to packstones (F-4; Fig. 24).

The shoal facies associations can be further subdivided into three categories, including the proximal shoal (backshoal) facies association (A3), the middle shoal (shoal crest) facies association (A4), and the distal shoal (foreshoal) facies association (A5).

Table 4. *Summary of microfacies types, composition/description, energy level, facies association, thickness, percentage, and average petrophysical properties values (derived from well logs) including effective porosity (PHIE), sonic-derived porosity (PHIS), volume of shale (Vsh), and water saturation (Sw) in each different facies* (*author's own edit*)

Facies/microfacies	Description, composition, and diagenetic features	Energy level	Facies association	Reservoir quality	Thickness m Percentage %	Average			
						PHIE %	PHIS %	Vsh %	Sw %
F-1 Peloidal oncoidal grain- to rudstones	Oncoids, peloids, ooids, grain aggregates. Interparticle and channel pores. Equant cement.	High	Intertidal	Water-bearing	25.5 6.9	11	7	7	86
F-2 Bioclastic mud- to wackestones	Thick shells and bivalve fragments, intermittent sponge spicules, minor peloids and echinoderms, stylolite.	Moderate - low	Lagoonal	Poor to non–reservoir	60.8 16	6	4	14	55
F-3 bioclastic cortoidal wacke- to packstones	Cortoids, peloids, skeletal fragments. Minor moldic pores. Micritization. Equant calcite filling interparticle pores, stylolite.				26.5 7	4	3	12	67
F-4 bioclastic dasycladalean wacke- to packstones	Dasycladaleae algae, skeletal fragments, bivalves, large and small foraminifera, minor peloids. Minor moldic pores. Equant calcite filling moldic pores. Micritization, stylolite.				27.8 7.3	5	4	11	45

Facies/microfacies	Description, composition, and diagenetic features	Energy level	Facies	Reservoir quality	Thickness m Percentage %	Average			
						PHIE %	PHIS %	Vsh %	Sw %
F-5 Pelletal peloidal pack- to grainstones	Fine laminated, pellets, occasionally dolomitic, few ooids. Interparticle and channel pores. Circumgranular cement. Dolomitization.	Moderate	Backshoal	Fair	6.5 1.7	11	7	3	43
F-6: Lithocodium-Bacinella float- to boundstones	Lithocodium-Bacinella, shell fragments, echinoderms, and coral debris. Occasionally peloids and intraclasts occurred. Dolomitization.			Good	46.6 12.2	15	14	10	19
F-7 Peloidal grainstones	Peloids, cortoids, large foraminifera, bivalves, echinoderms. Interparticle, vugs, molds and channels. Circumgranular and extensive syntaxial overgrowth calcite cement.	High	Shoal	Fair-good	67.3 17.7	12	10	10	38
F-8 Ooidal peloidal grain- to rudstones	Intermittent crossbedding, peloids, ooids, oncoids, cortoids, large foraminifera, bivalves and echinoderms. Interparticle and moldic pores. Circumgranular and dogtooth cement, grains dissolution grains.	High		Good	9.9 2.6	16	12	2	23
F-9: Reef debris float- to rudstones	Lithocodium-Bacinella, coral, Caldocoropsis, large foraminifera, gastropods, echinoderms, also peloids and intraclasts occasionally occurred, vuggy.	Moderate - high	Foreshoal	Fair-good	37.2 9.8	12	9	15	27
F-10 Bioclastic grainstones	Intermittent cross bedding, peloids, echinoderms and bivalves' fragments, and few small foraminifera. Interparticle pores. Syntaxial overgrowth cement, dissolution of grains.			Good	5.0 1.3	17	12	4	39
F-11: Miliolidal pack- to grainstones	Well sorted, fine peloids and cortoids with abundance of the small size foraminiferas.	Low	Middle ramp	Non-reservoir	4.7 1.2	4	3	19	29
F-12 Bioturbated dolomitic wackestones	Skeletal fragments, sponge spicules, small foraminifera, few benthic foraminifera, dolomitic burrows patches, bioturbation. Moldic pores. Equant/blocky calcite cement, stylolite.				19.5 5.1	5	4	12	58
F-13: Bioclastic foraminiferal wackestones	Bioclasts, large and small foraminifera, echinoderms, sponge spicules, stylolite.				25.0 6.6	4	4	22	26
F-14 Spiculitic skeletal mud- to wackestones	Skeletal fragments, sponge spicules, small foraminifera. Moldic pores. Equant/blocky calcite cement, stylolite.		Outer ramp		19 5	4	3	11	56

The proximal shoal (backshoal) facies association (A3) is represented by:

- Pelletal peloidal pack- to grainstones (F-5; Fig. 25)
- Lithocodium-Bacinella float- to boundstones (F-6; Fig. 26)

The middle shoal (shoal crest) facies association (A4) is represented by:

- Peloidal grainstones (F-7; Fig. 27)
- Ooidal peloidal grain- to rudstones (F-8; Fig. 28)

The distal shoal (foreshoal) facies association (A5) is represented by:

- Reef debris float- to rudstones (F-9; Fig. 29)
- Skeletal grainstones (F-10; Fig. 30)

The middle-ramp facies association (A6) is represented by:

- Miliolidal pack- to grainstones (F-11; Fig. 31)
- Bioturbated dolomitic wackestones (F-12; Fig. 32)
- Foraminiferal wackestones (F-13; Fig. 33)

The outer-ramp facies association (A7) is represented by:

- Spiculitic skeletal mud- to wackestones (F-14; Fig. 34)

The skeletal components include large benthic foraminifera (Miliolids, *Pseudochrysalidina*, *Pseudocyclammina littus*, *Trocholina sp*., and *Lenticulina*), echinoderms, bivalves, coral, green-algae and rare red algae. Planktonic foraminifera and sponge spicules occur in small amounts. Most facies are dominated by non-skeletal grains such as peloids, ooids, pisoids, oncoids, cortoids, and grain aggregates that form grain-supported limestone facies.

4.6.4 Facies Associations

The main facies associations are divided into three main categories; inner ramp (FA1), middle-ramp (FA2), and outer-ramp facies associations (FA3).

Inner-ramp Facies Associations (FA1)

Three facies associations are recognized within the inner ramp including:

- Proximal intertidal (A1)
- Proximal lagoonal (A2)
- Distal shoal (A3)

The A1 and A3 are dominated by coated grains include oncoids, peloids/pellets, ooids, and intraclasts, with in subordinate amounts of bivalves, benthic foraminifera, echinoderms. While

A2 is dominated by bioclasts, Dasycladaleae algae, cortoids, benthic foraminifera and minor amount of sponge spicules and planktic foraminifera.

Proximal Intertidal Facies Association (A1)

This facies association is represented by the peloidal oncoidal grainstones to rudstones.

Peloidal oncoidal grain- to rudstones microfacies (F-1)

This microfacies appears in the lower most part of the Yamama Formation, in Nasiriya Oilfield (Fig. 13), and is absent in Ah'Dimah and West Qurna cored intervals. This microfacies exhibits a thickness of 26 m, forming 7% of the cored intervals. The core samples are beige to grey in color and show interbedding of grain-supported facies, grainstones and rudstones, with some floatstone. It also shows some appearance of the floatstone texture in some intervals (Fig. 20a and 21).

The grains include mostly poorly sorted peloids (0.05-0.1 mm), oncoids, cortoids, and intraclasts. The ooids are less frequent. The oncoids are distinctive for this facies and generally larger than 0.2 mm to even ≥ 1cm and have irregular to subrounded shapes (Fig. 21a-d). The oncoids consist of micritic cortices around distinct nuclei, are mostly skeletal fragments such as foraminifera (Fig. 21e), echinoderms, algae, and bivalves. The nuclei can be grains aggregates. Some of the oncoids are completely micritized (Fig. 21f-h). The intraclasts consist of peloids or other skeletal fragments that are cemented together, hence forming grapestone like.

The cortoids (> 0.1 mm) are elongated to subrounded covered by micritic envelop. Well preserved skeletal grains are absent. Interparticle and channels porosity dominates, whereas vuggy pores are less abundant (Fig. 21g and h). The average effective porosity is about 11% that ranges from ranging from 3 to 14% while the sonic porosity is around 7% (Table 4). It shows low volume of shale that reaches an average of about 7%. However, the water saturation is high and reaches 85%. Blocky calcite cement is observed filling pore spaces.

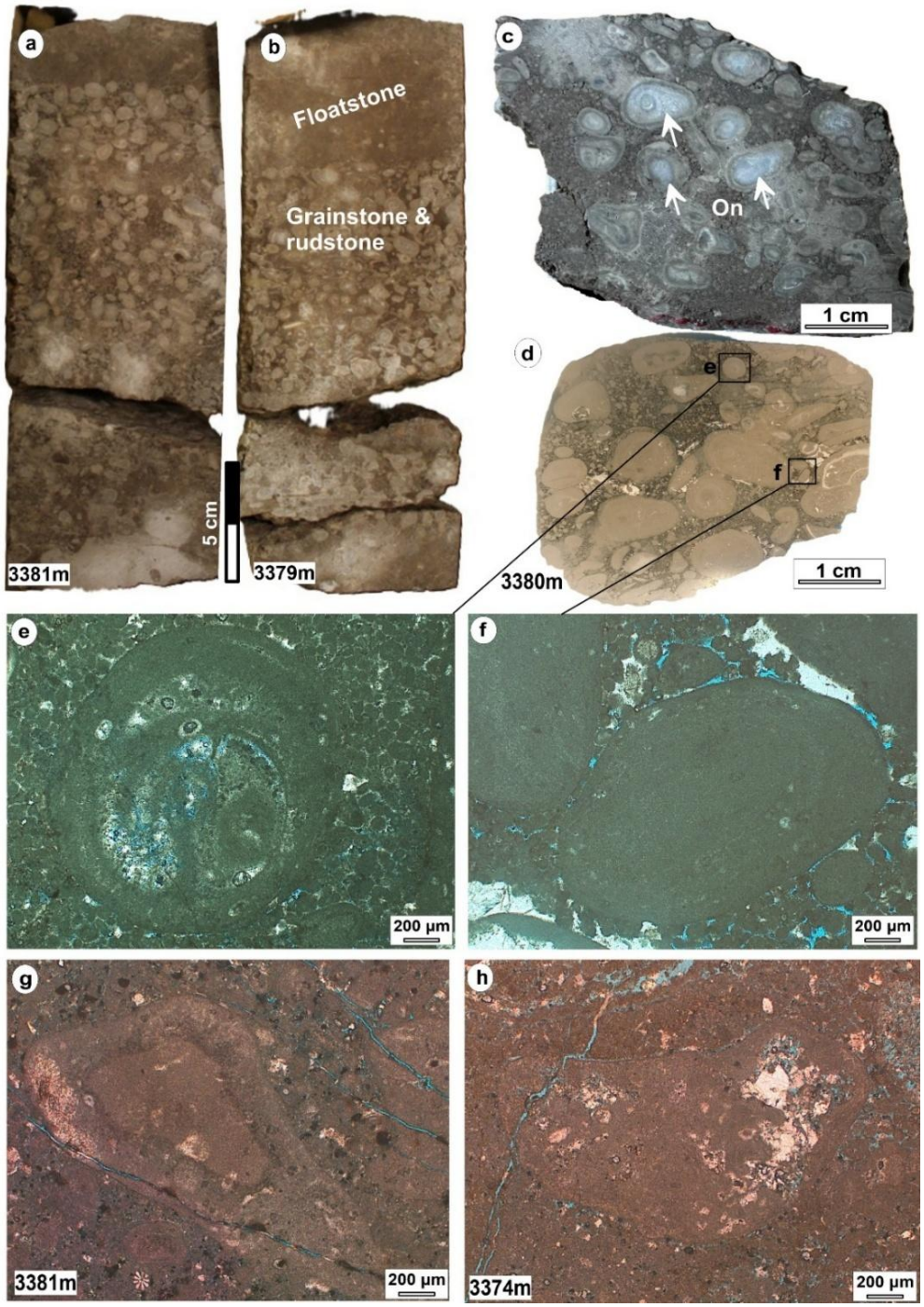

Figure 21. Peloidal oncoidal grain- to rudstones microfacies (F-1). ***a*** *and* ***b****) core photos showing oncoids in grainstone and floatstone texture, from the lower part of the Yamama in Nasiriya Oilfield.* ***c*** *and* ***d****) scanned images showing the peloidal oncoidal grain- to rudstones. On = oncoids.* ***e****) oncoid, the core is foraminifera in grain- to rudstones texture.* ***f****) completely micritized oncoid.* ***g*** *and* ***h****) oncoids with channel pores. Depths are shown in the bottom left corner* (*author's own edit*).

Lagoonal Facies Association (A2)

Three different microfacies are recognized within the lagoonal facies association:

1. Bioclastic mud- to wackestones (F-2)
2. Bioclastic cortoids wacke- to packstones (F-3)
3. Bioclastic dasycladalean wacke- to packstones (F-4)

1- Bioclastic mud- to wackestones microfacies (F-2)

This particular microfacies is observed at the lowermost part of the cored interval within the Yamama Formation in Ah'Dimah Oilfield (Fig 15), and the middle and upper parts of West Qurna Oilfield (Fig. 16). It is characterized by grey color and the presence of an abundance of thick shells and bivalve fragments, as well as skeletal grains (Fig. 20b and 22). This microfacies comprises up to 85% of the mud-matrix. Furthermore, a certain proportion of argillaceous limestone is notable, with intermittent occurrences of sponge spicules in some intervals.

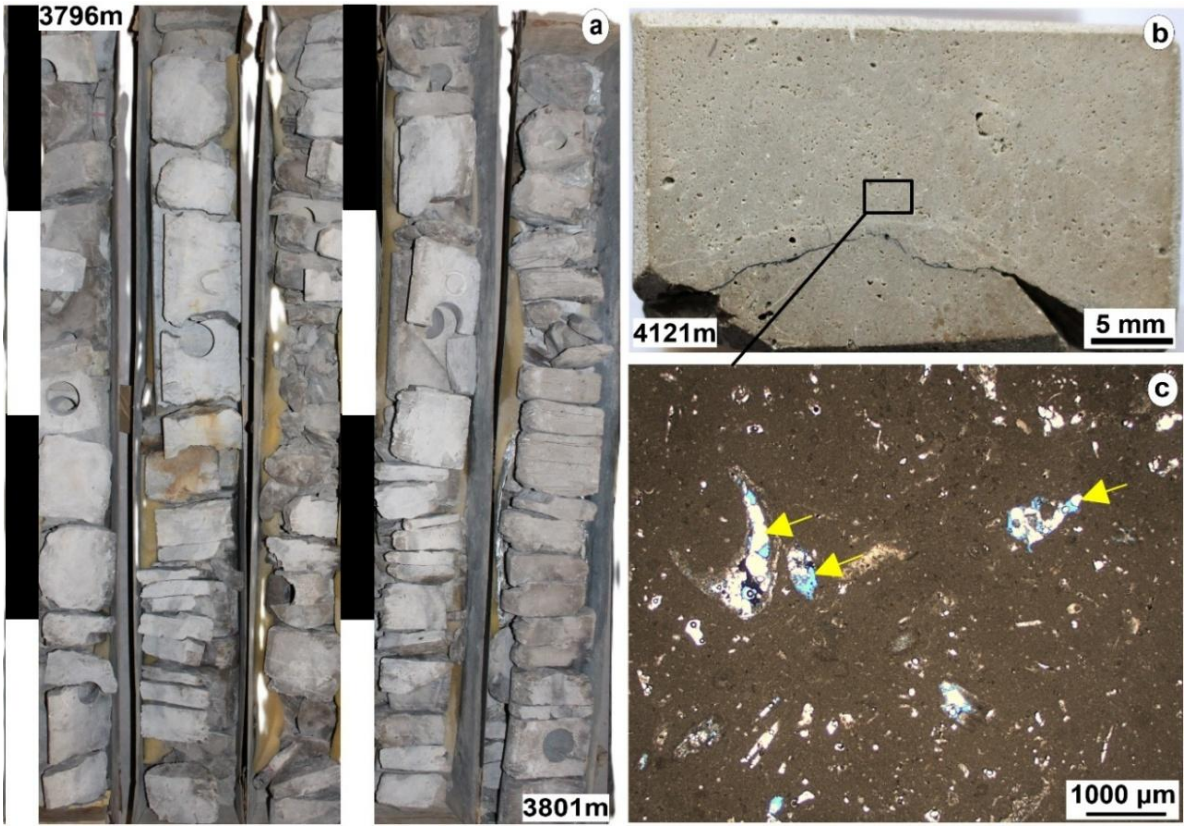

Figure 22. Bioclastic mud- to wackestones microfacies (F-2). ***a*** *and* ***b****) core photos from West Qurna Oilfield. The scale bar in* (***a***) *one meter.* ***c****) showing calcite cement partially filling molds and vuggy pores in Ah'Dimah Oilfield* (*author's own edit*).

Minor quantities of peloids, along with relatively large foraminifera including miliolids as well as echinoderms, are also presented, while smaller foraminifera are absent. Bioturbation is common. The extent of this microfacies is approximately 60 m, constituting 16% of the entire cored intervals. This microfacies is predominantly found in the non-reservoir units of the Yamama Formation and show poor reservoir quality. The porosity varies from 1.7 to 10% with an average of about 6% (Table 4). Predominant porosity types are moldic, intraparticle, and channel pores. The permeability is low, recording an average of about 2mD. Most moldic pores are completely or partially cemented with two cement generation. Fine crystalline cement along the mold's edge followed by blocky calcite cement. It is worth noting that the channels exhibit blocky cement. Blocky cement is a distinctive feature for this microfacies along with stylolites. Volume of shale reaches 20%, with an average of about 13.5%. This facies mostly filled with water, it shows average water saturation of around 55% (Table 4). Dolomite grains are common along the stylolite (see discussion section).

2- Bioclastic cortoidal wacke- to packstones microfacies (F-3)

This facies appeared only in the upper part of the Yamama Formation in Nasiriya Oilfield (Fig. 13), exhibits wacke- to packstone microfacies and comprises 7% of the cored intervals, with a thickness of 27 m (Table 4). It is dominated in the reservoir unit YRA as well as in the non-reservoir unit B1 (Fig. 13). It shows beige to light grey (Fig. 20c, Fig 23a and b) and characterized by cortoids as a result of micritization (Fig. 23c). The cortoids consist of skeletal fragments or algae that are surrounded by micrite envelopes. Some skeletal fragments are completely micritized (Fig. 23c). The grains are dominated by echinoderms, gastropods, benthic foraminifera, and smaller amounts of peloids (≤0.2 mm). The equant calcite cement is common and observed filling interparticle pores (Fig. 23c). The porosity in this microfacies varies from 1-10% with an average of about 4% (Table 4). The volume of shale and water saturation are recorded at 12% and 67%, respectively.

3- Bioclastic dasycladalean wacke- to packstones microfacies (F-4)

This appears in the upper part of the Yamama Formation in all selected wells. It appears in the non-reservoir units B0 and B1 as well as in the poor-to-fair reservoir units YRA and YRB (Fig. 13, 15 and 16). Its thickness is 27.8 m and comprises of about 7.3% of the cored interval (Table

4). This facies has a grey to dark grey color in the core samples (Fig. 20d; Fig. 24 a and b) and dominated by Dasycladaleae algae in mud matrix.

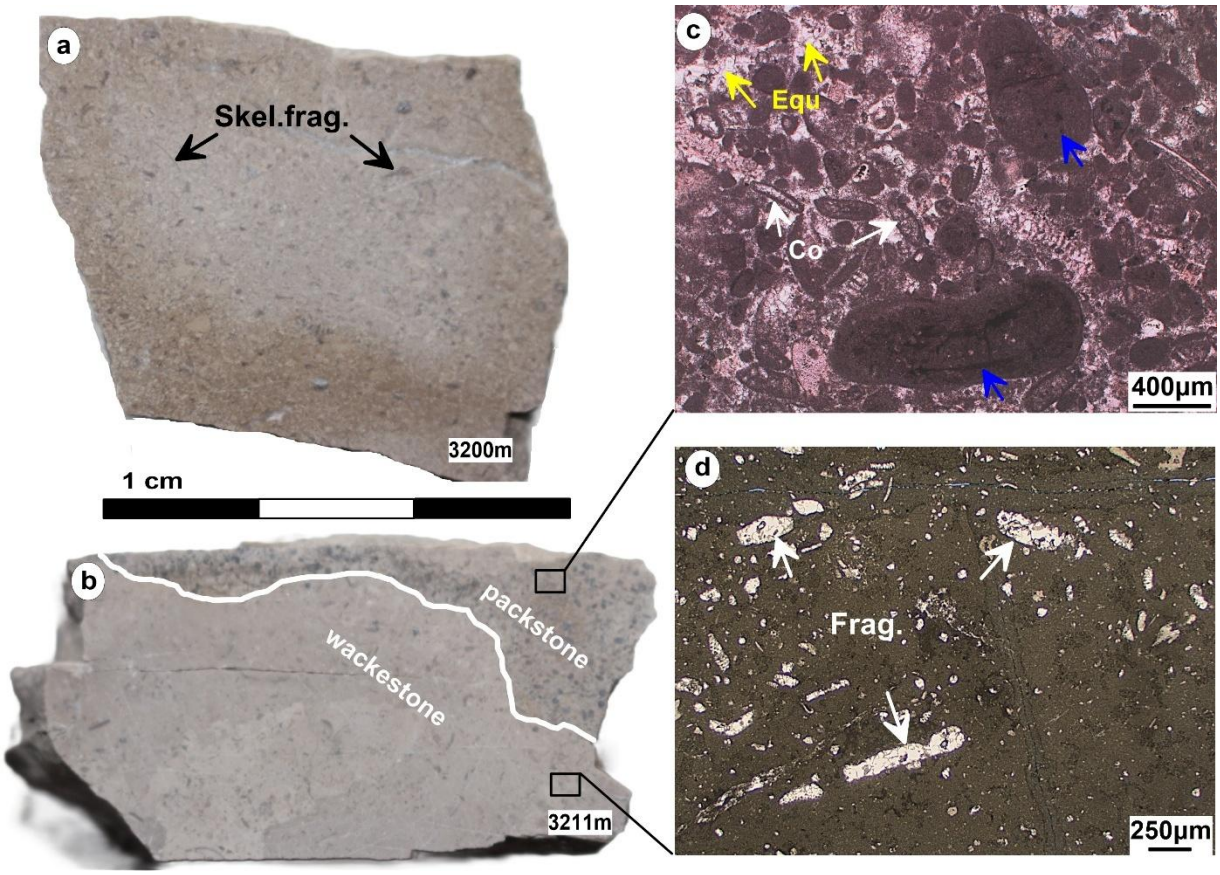

Figure 23. Bioclastic cortoidal wacke- to packstones microfacies (F-3). ***a*** *and* ***b****) slabbed core photos in Nasiriya Oilfield.* ***c*** *and* ***d****) showing the bioclastic cortoids wackestone and packstones, white arrows refer to the cortoids, blue arrows refer to the complete micritized grains, and yellow arrows indicate the equant calcite cement filling interparticle pore space in a packstone texture of this facies* (*author's own edit*).

The presence of Dasycladaleae algae is characteristic in this facies (Fig. 24c-e). Skeletal fragments include benthic foraminifera, Miliolids, *Trocholina*, and shell fragments, bivalves, and echinoderm are common (Fig. 24c). This facies exhibits poor reservoir properties, with average porosity of 5%, shale volume is about 11%, and water saturation of about 45% (Table 4). The equant calcite mainly filled the moldic pores that were formed due to the dissolution of the skeletal grains. The chemical compaction is manifested by the common presence of high-amplitude stylolite.

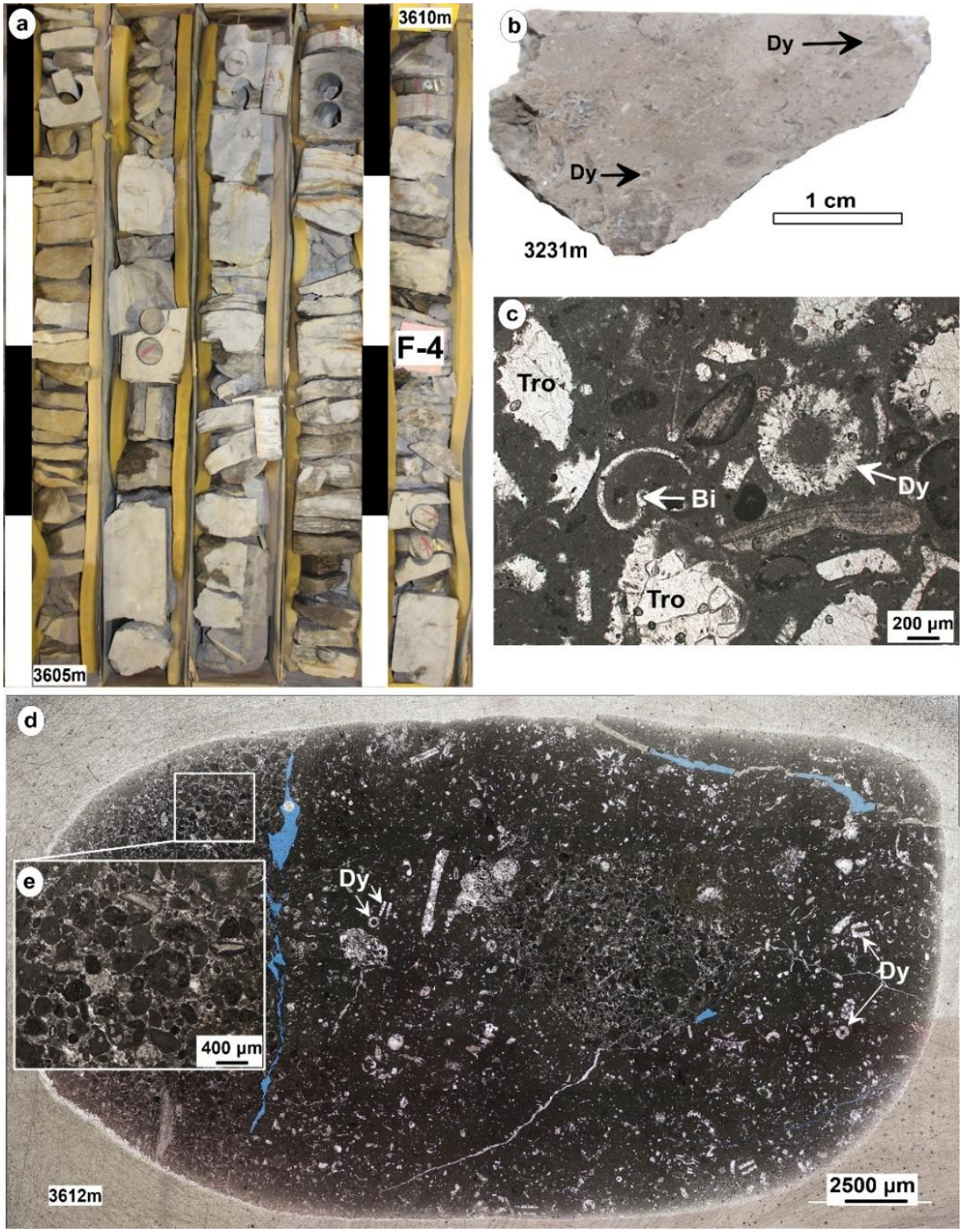

Figure 24. Bioclastic dasycladalean wacke- to packstones microfacies (F-4). ***a*** *and* ***b****) core and slabbed photos from West Qurna and Nasiriya oilfields respectively, the scale bar one meter.* ***c****) dasycladalean algae (Dy), Trocholina foraminifera (Tro), and bivalves (Bi).* ***d****) scanned photo showing the dasyladalean algal wacke- to packstones.* ***e****) zoomed image of the packstone microfacies within the same facies* (*author's own edit*).

Shoal Facies Association (A3)

The shoal facies association is divided into three categories:

- Proximal backshoal
- Shoal
- Distal foreshoal

Two microfacies are recognized within the proximal **backshoal**, these are:

1. Pelletal peloidal pack- to grainstones (F-5)
2. Lithocodium-Bacinella float- to boundstone (F-6)

The **shoal** facies association are characterized by the presence of two different microfacies:

1. Peloidal grainstones (F-7)
2. Ooidal peloidal grain- to rudstones (F-8)

Similarly, two facies are recognized within the distal **foreshoal** microfacies:

1. Reef debris float- to rudstones (F-9)
2. Bioclastic grainstones (F-10)

Backshoal facies

1- Pelletal peloidal pack- to grainstones microfacies (F-5)

This microfacies appears in the lower part of the Yamama Formation in Nasiriya Oilfield only, above F-1. It comprises around 1.7% of the cored intervals with a thickness of 6.5 m (Table 4). It has a light grey to light brown color with dark spots in the slabbed samples (Fig. 20e and Fig. 25a). The black spots are dolomites crystals (Fig. 25a). These dolomites are distinctive for this microfacies at some intervals. This grain-supported limestones facies (packstone to grainstone) are composed mainly of rounded to subrounded, well-sorted, fine-grained (≤0.1 mm) fecal pellets, which are cemented by circumgranular calcite (Fig. 25 c and d). Cortoids, ooids, and intraclasts are less abundant. Some grain aggregates were noticed forming grapstone (Fig. 25d). Skeletal fragments include benthic foraminifera and echinoderm are less common. Interparticle and channel pores are the main pore types. The average porosity is about 11% and reaches up to 16% in some cases (Table 4). Low volume of shale is recorded in this microfacies averaging of about 3%. Syntaxial calcite overgrowth was found around the echinoderms. This microfacies

exhibits extensive dolomitization in the lower part of the formation (Fig. 25b). The compaction is noted within this microfacies (Fig 35c and d).

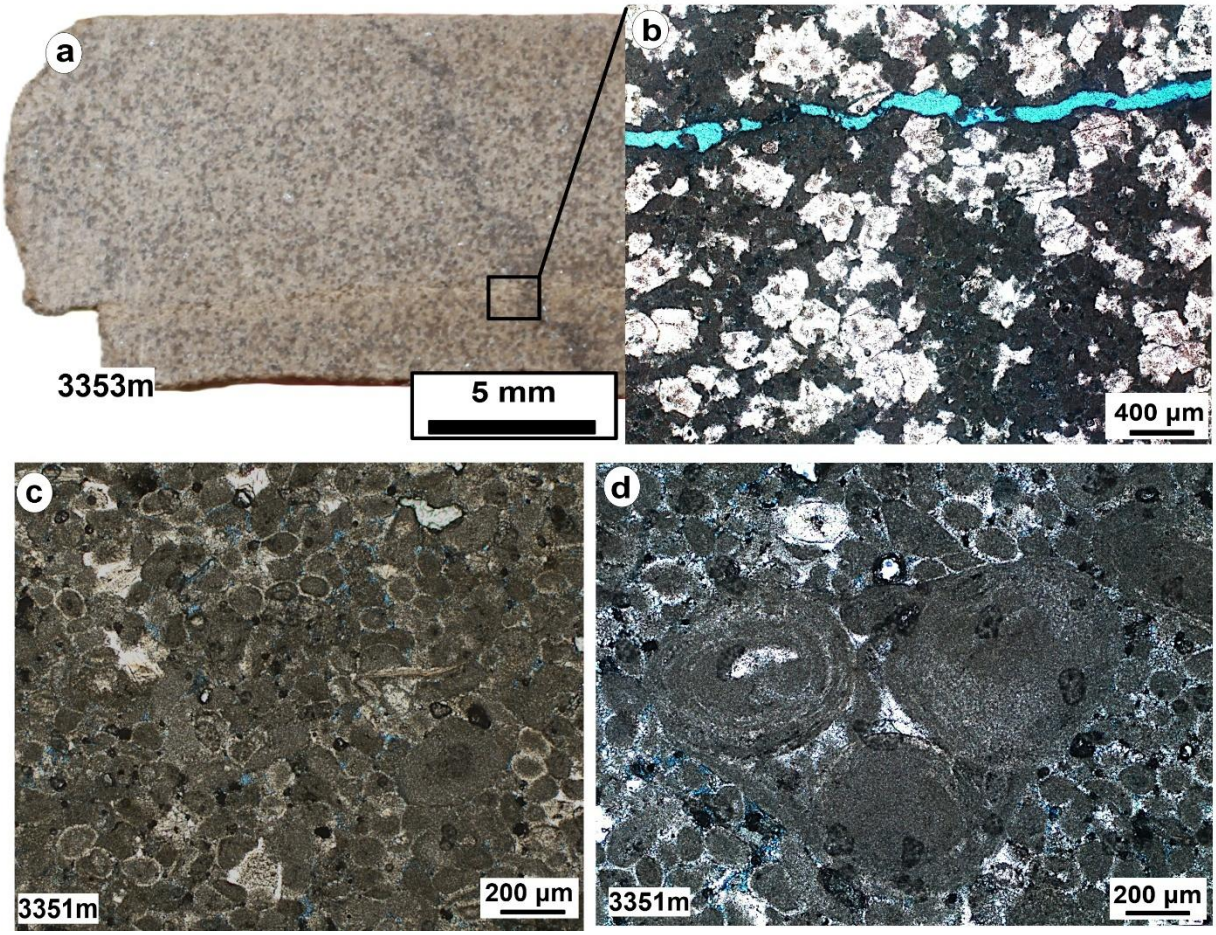

Figure 25. Pelletal peloidal pack- to grainstones microfacies (F-5). ***a****) slabbed core of the dolomitic pelletal pelloidal pack- to grainstones in Nasiriya Oilfield.* ***b****) euhedral-subhedral dolomites and a channel pore.* ***c*** *and* ***d****) pellets and grapestone within the pelletal peloidal pack- to grainstones. Circiumgranular cement around grains is dominated. The grains are generally smaller than 0.1mm and compaction is noted* (*author's own edit*).

2- Lithocodium-Bacinella float- to boundstone microfacies (F-6)

This microfacies found in the upper part of the Yamama Formation in Ah'Dimah and West Qurna oilfield (Fig. 15 and 16), while it is absent in Nasiriya Oilfield. The dominant skeletal grains within this microfacies are the Lithocodium aggregatum- Bacinella irregularis, which is observed floating on a mud matrix (Fig. 26a and b). Additionally, this facies includes common skeletal grains such as large benthic foraminifers, including Miliolids, *Pseudochrysalidina*, and *Pseudocyclammina littus, Cladocoropsis* algae along with shell fragments, echinoderms, and

coral debris (Fig. 26c-g). Peloids and intraclasts are also noted within this microfacies in minor amounts. This microfacies encompassing 12.2% of the overall cored intervals within the Yamama Formation (Table 4).

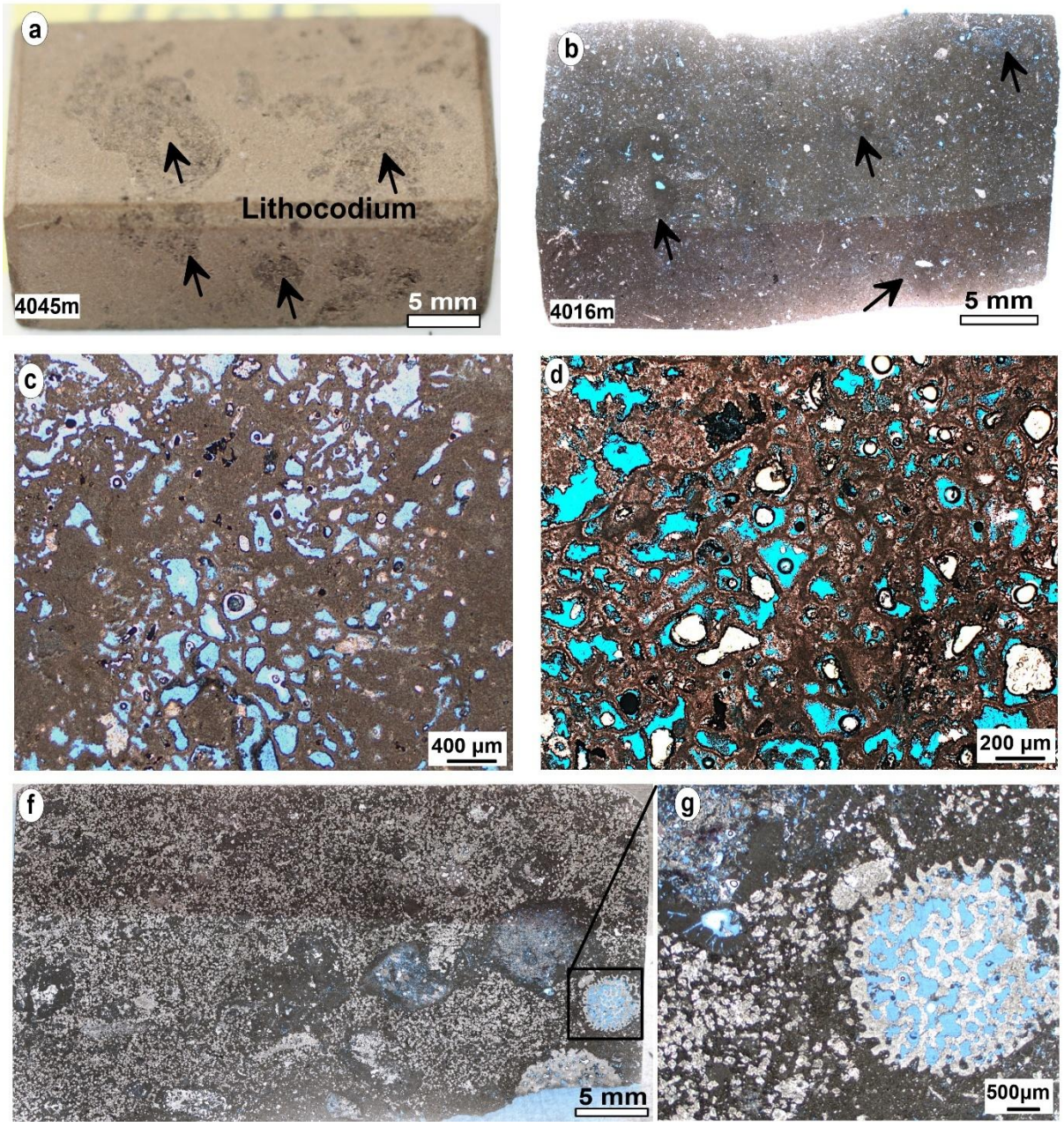

Figure 26. Lithocodium-Bacinella float- to boundstone microfacies (F-6). a) *slabbed core image show Lithocodium-Bacinella from Ah'Dimah Oilfield.* ***b)*** *scanned image showing Lithocodium-Bacinella floating in muddy matrix.* ***c*** *and* ***d)*** *show dominated intraparticle pores with in Lithocodium-Bacinella bodies,* ***f)*** *Pervasive dolomitization.* ***g)*** *dissolution in Cladocoropsis. Note that intraparticle and vuggy porosity are dominant* (*author's own edit*).

It has a considerable thickness of about 46.6 m. It exhibits diagenetic processes involving both euhedral and anhedral dolomite, thereby engendering intercrystalline porosity (Fig. 26f and g). The Lithocodium-Bacinella float- to boundstone is the most extensive facies in Ah'Dimah Oilfield. Remarkably, this facies shows good reservoir quality within the Yamama Formation, where the porosity in varies from 2.5% to 25% with an average of about 15%. Intervals with Lithocodium-Bacinella exhibit higher porosity (15%) values as well as a lower shale volume (9.7%) and water saturation (19.5%), accompanied by varying permeability values (reached 60 mD) when compared to other facies (Fig. 15 and Table 4). Due to considerable dissolution, vuggy and intraparticle pores are noticed, which can be observed within the Lithocodium-Bacinella bodies (Fig. 26c and d). The circumgranular cement and the dissolution are common (Fig. 26d and g). Some intervals show pervasive dolomitization (Fig. 26f and g).

Shoal facies

1- Peloidal grainstones microfacies (F-7)

This microfacies is 67.3 m thick forming 17.7% of the total cored intervals within the Yamama Formation in the studied wells (Table 4). It appears in all selected wells and has a light brown to brown color and massive texture in the core and slabbed samples (Fig. 20g and 27a). It consists of peloids (0.2 to 0.5 mm; poorly sorted, subrounded to rounded) and cortoids (micrite envelops) and smaller amounts of benthic foraminifera, particularly Miliolids, *Pseudochrysalidina*, and *Pseudocyclammina littus*, along with echinoderms and bivalves (Fig. 27b, c and e). Furthermore, Lithocodium-Bacinella fragments are observed in some intervals (Fig 27e). It shows a good reservoir quality and is found exclusively within the reservoir units, YRC in Nasiriya (Fig. 13), YRB in Ah'Dimah (Fig. 15), and YRA in West Qurna (Fig. 16). The average effective porosity is about 12% reaching up to 18%. While volume of shale is 10%, and water saturation is 38% (Table 4). The permeability varies considerably from 2 mD and reaches 51 mD at some intervals. Interparticle porosity is dominant, while intraparticle, vuggy, moldic and channel porosity are less common. Syntaxial calcite overgrowths and circumgranular calcite cements as well as scattered blocky cement are common. The micritization has obvious impact on forming the peloids and cortoids where some grains are partially, and other completely micritized. Pyrite and bitumen are also observed (Fig. 27c).

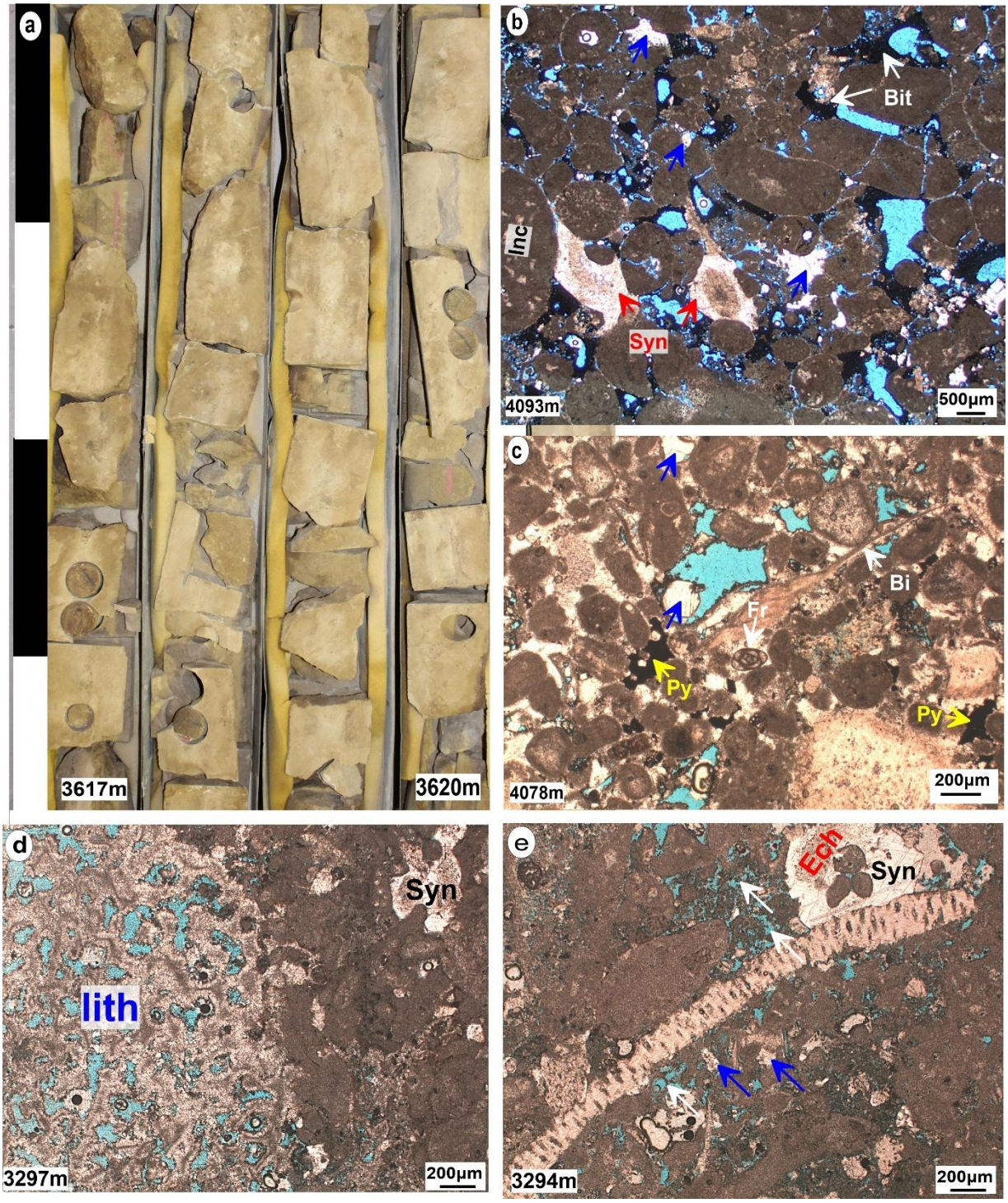

Figure 27. Peloidal grainstones microfacies (F-7). ***a****) core image from West Qurna Oilfield. The scale bar is one meter.* ***c*** *–* ***e****) peloidal grainstones, the interparticle pores, scattered equant calcite (blue arrows) as well as syntaxial overgrowth (Syn) around echinoderms (Ech) are common, Bi = bivalve, Fr = foraminifera, Inc = intraclast.* ***b*** *and* ***c*** *from Ah'Dimah,* ***d*** *and* ***e*** *from Nasiriya Oilfield. The white arrow in* ***e*** *refers to the dissolution of grains. Bit = bitumen, Py = pyrite, lith = Lithocodium (author's own edit).*

2- Ooidal peloidal grain- to rudstones microfacies (F-8)

This appears in the lower part of the formation in the Nasiriya Oilfield, in the reservoir unit YRD1 (Fig. 13), while, based on the available cored intervals, this microfacies is absent in Ah'Dimah and West Qurna oilfields. It is approximately 10 m thick, making up 2.6% of the cored intervals. It is characterized by light brown to brown color and grainstone and in some cases rudstone texture (Fig. 28).

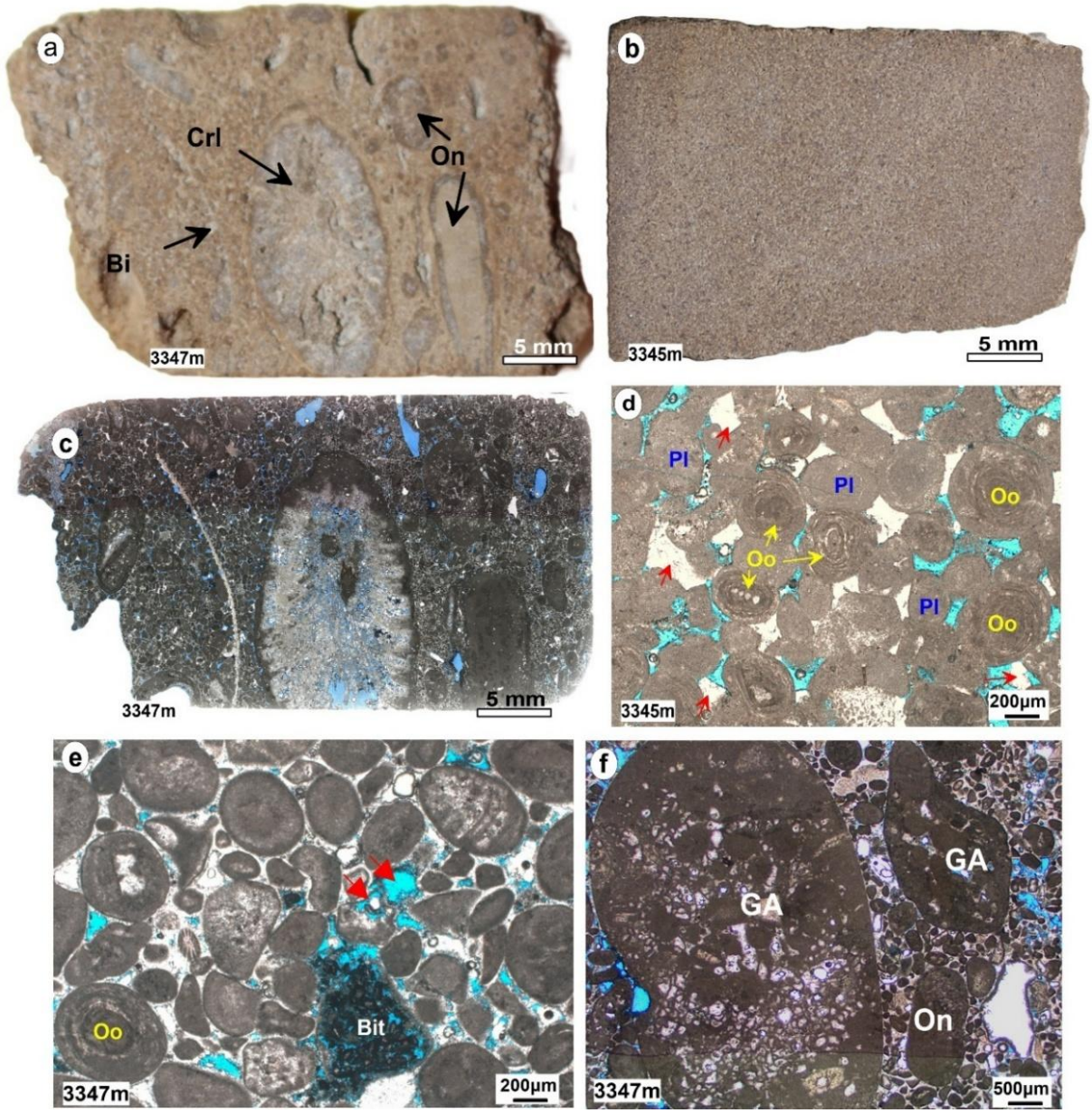

***Figure 28. Ooidal peloidal grain- to rudstones microfacies (F-8)**. **a** and **b**) slabbed core images from Nasiriya Oilfield. **c**) scanned image of the sample (**a**) interparticle and dissolution porosity. **d** and **e**) well preserved ooids, peloids and scattered equant calcite cement (red arrows in **d**),*

the ooids are concentric and composed of cortices around foraminifera and other bioclasts. ***f)*** *grain aggregates composing of Lithocodium-Bacinella fragments and peloids that are cemented and bounded together. Note that interparticle porosity is dominant, dissolution is notable (red arrow in* ***e****), circumgranular cement around grains is common. Crl = coral, Bi = bivalve, On = oncoids, Bit = bitumen, Pl = peloids, Oo = ooids, GA = grain aggregate* (*author's own edit*).

The grains are mainly subrounded peloids (around 2 mm), and rounded ooids (< 2 mm) (Fig. 28d and e). Oncoids (> 2 mm), cortoids, and intraclasts are also observed. The well preserved ooids are characteristic. The ooids are concentric and composed of cortices around foraminiferas, echinoderm, or other skeletal grains. The oncoids are primarily consisting of micritic and sparitic layers around Lithocodium-Bacinella, coral, or shell fragments. The intraclasts are composed of peloids, ooids, and/or Lithocodium-Bacinella fragments that are cemented together by calcite (Fig. 28f). Coral debris, bivalves, and echinoderm fragments are abundant (Fig. 28a and c). This microfacies exhibits high dominantly interparticle porosity (13-22%; average of about 16%), whereas moldic and vuggy porosity are less prevalent. Dissolution affected the grains (Fig. 28e). The circumgranular cement is distinctive, while the scattered calcite equant cement and syntaxial calcite overgrowth are common (Fig. 28d).

Foreshoal facies

1- Reef debris float- to rudstones microfacies (F-9)

This particular microfacies extends over a vertical interval of 37.2 m, representing approximately 9.8% of the entire cored intervals within the Yamama Formation in Ah'Dimah (Fig. 15 and Table 4), while it is absent in Nasiriya and West Qurna oilfields. It shows variety of grains including skeletal and non-skeletal types. The dominant skeletal components include Lithocodium-Bacinella, coral, sponge and cladocoropsis. Large benthic foraminifera (Miliolids, *Pseudochrysalidina, Pseudocyclammina littus, Trocholina sp, Lenticulina sp*.), in addition to shell fragments, bivalves, gastropods, echinoderms, and bryozoa are common (Fig. 29). Notably, bioturbation and the sponge burrows have been observed (Fig. 29a and b). Lithocodium-Bacinella encrusted on coral fragments (Fig. 29c and d). It shows minor amounts of peloids and intraclasts. Pyritization has occurred within the skeletal grains, as well as within the matrix and cement. Circumgranular, blocky and syntaxial cements occluded some pore spaces. Nevertheless, this facies presents a good reservoir quality and is dominantly encountered within the reservoir units of the Yamama Formation (e.g., YRC). The intraparticle and vuggy

porosity are dominant. The porosity varies from 2% to 18% with an average porosity of about 10%. The permeability reaches 62 mD at some intervals.

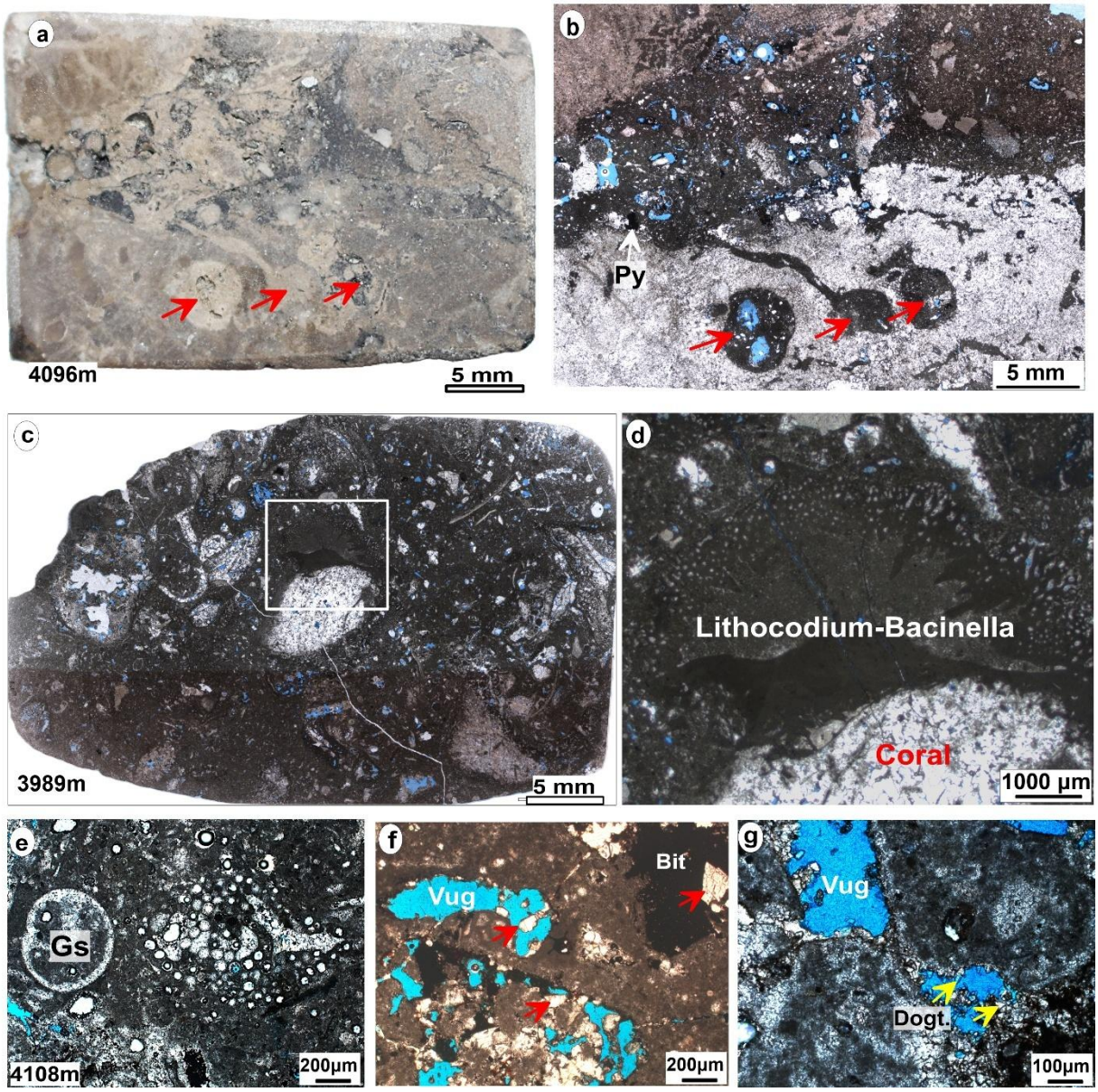

Figure 29. Reef debris float- to rudstones microfacies (F-9). ***a)*** *a slabbed core photo from Ah'Dimah Oilfield, the lower part of the sample is totally calcitized.* ***b)*** *scanned image of sample (**a**) sponge borings, and dissolution (Py =pyrite).* ***c)*** *reef debris float- to rudstones.* ***d)*** *Lithocodium-Bacinella encrusting on coral fragment.* ***e)*** *gastropod (Gs).* ***f*** *and* ***g)*** *Optical petrographic photos showing the vugs (Vug), bitumen (Bit), dogteeth (Dogt.) and calcite cement (red arrows in **f**)* (*author's own edit*).

2- Bioclastic grainstones microfacies (F-10)

This microfacies appears as light brown to brown color (Fig. 30a) in the middle part of the Yamama Formation, within the reservoir unit YRC in Nasiriya Oilfield (Fig. 13). It is 5 m thick, making up 1.5% of the cored intervals (Table 4). The grains (< 0.2 mm) are well sorted and dominated by echinoderms and bivalve fragments while peloids are less frequent. Large, well-preserved benthic foraminifera are rare (Fig. 30d). Partially and completely dissolved grains are observed (Fig. 30d). Organic matters are noted. This facies displays excellent reservoir quality, with dominantly interparticle porosity values ranging from 14-22% with an average of 17% (Table 4). The volume of shale is low (4%), while water saturation is about 39%.

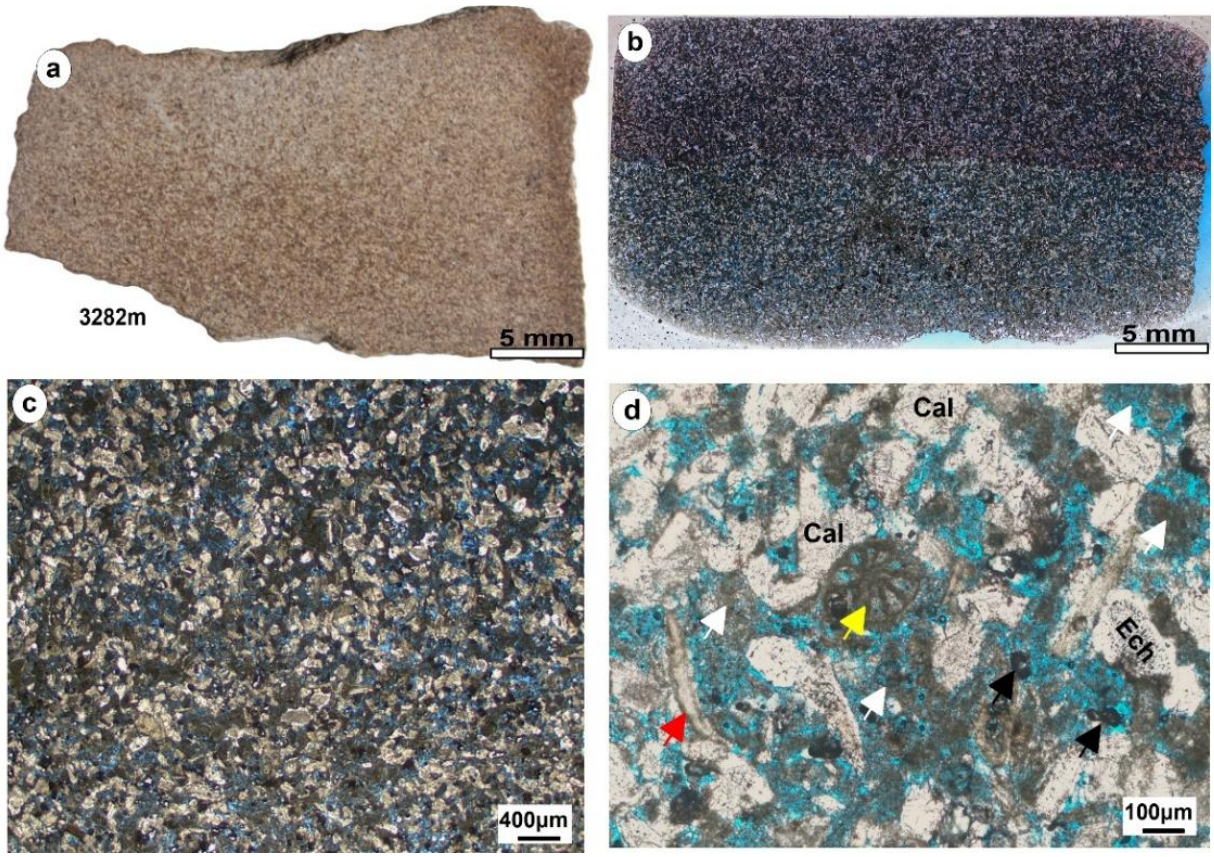

Figure 30. Bioclastic grainstones microfacies (F-10). ***a*** *and* ***b****) core slabbed and scanned photos from Nasiriya Oilfield.* ***c*** *and* ***d****) bioclastic fragments of bivalves (red arrow) and echinoderms (Ech), foraminifera (yellow arrow) and partially and completely dissolved peloids (white arrows), scattered equant calcite cement (Cal), organic matters (black arrows). Note that rare skeletal grains are preserved, dissolved grains and microporosity are common* (*author's own edit*).

Middle-ramp Facies Associations (FA1)

Three distinctive facies are recognized within these facies:

1. Miliolidal pack- to grainstones (F-11)
2. Bioturbated dolomitic wackestones (F-12)
3. Bioclastic foraminiferal wacke- to packstones (F-13)

1- Miliolidal pack- to grainstones microfacies (F-11)

This forms 1.2% (4.7 m) of the entire cored intervals of the Yamama Formation and appears at the upper part of the formation in the reservoir unit YRA and the non-reservoir unit B0 in Ah'Dimah and West Qurna respectively (Fig. 15, Fig. 16 and Table 2). The slabbed samples have grey to dark grey color and show pack- to grainstones (Fig. 20k).

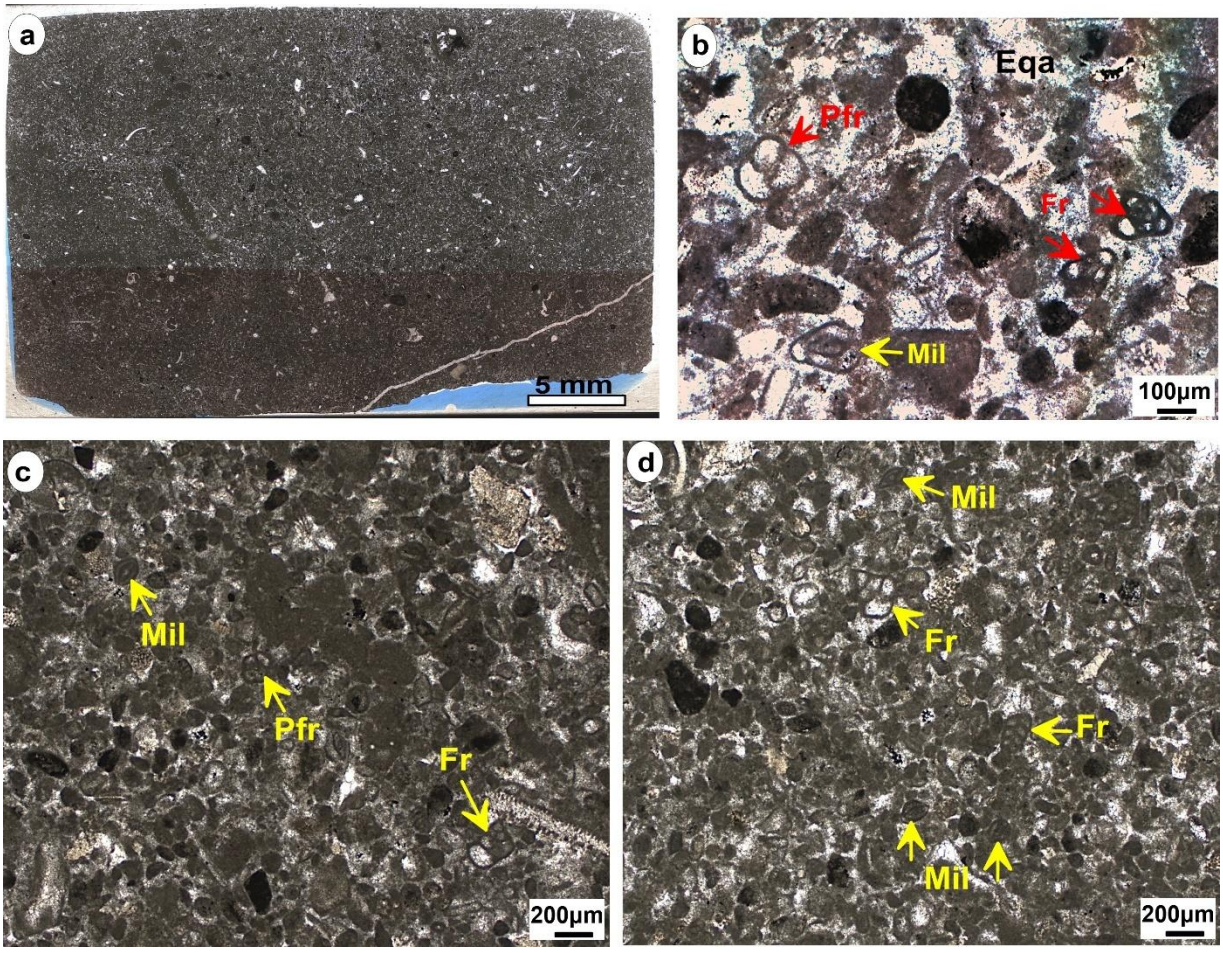

Figure 31. Miliolidal pack- to grainstones microfacies (F-11). a) *A sanned image from Ah'Dimah Oilfield.* ***b-d)*** *small benthic foraminifera (Fr), planktic foraminifera (Pfr), miliolids*

(Mil), and small peloids/pellets (Pl). Note that sparry and equant (Eqa) calcite cements are dominant (author's own edit).

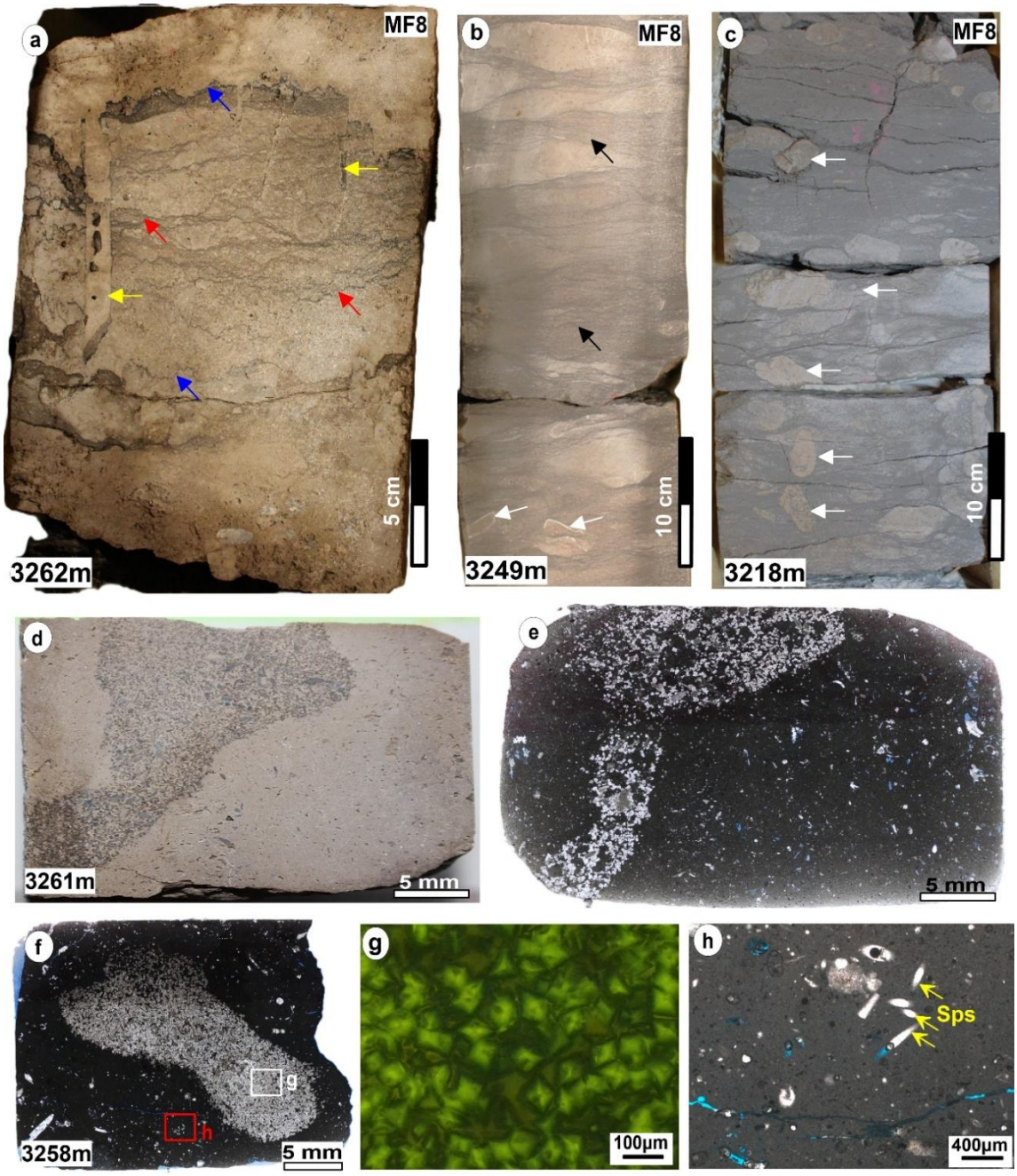

***Figure 32. Bioturbated dolomitic wackestones microfacies (F-12)**. **a-c**) core images, yellow arrows= burrows, blue arrows= stylolites, red arrows= solution seams, black arrows= wavy lamination, white arrows= Thallassinoides? burrows. **d** and **e**) core slabbed and scanned images, dolomites concentrating in a burrow. **f**) dolomitized burrow. **g**) Dolomite rhombs (under fluorescent light) show the presence of fluorescing outer zone (overgrowth) around a non-fluorescing core. **h**) lime mud and sponge spicules (Sps). Samples are from Nasiriya Oilfield* (*author's own edit*).

The main constituents are peloids. The peloids are less than 0.2mm in size and well sorted (Fig. 31b-d). The small miliolid and planktic foraminiferas are common (Fig. 31b-d). It shows similar characters than in F-7. However, for the importance of evaluating the microfacies and their reservoir quality, this facies is distinguished. The main distinctive feature between the F-7 and F-11 is the size of skeletal and non-skeletal grain size. It consists of fine-grained peloids with the abundance of the small size foraminiferas. It exhibits poor reservoir quality compared to F-7. The compaction significantly affected the pore spaces. The porosity varies from 2% to 7.8% with an average of 4%. Notably, it shows a higher volume of shale, reaching an average of about 20% (Table 4).

2- Bioturbated dolomitic wackestones microfacies (F-12)

This microfacies comprises mud-supported, bioturbated limestones, has poor reservoir properties, with 19.5 m thick (5% of the cored intervals) and appears at the middle and upper parts of Yamama Formation within the non-reservoir unit B2 and B1 (Fig. 13, 15 and 16). It has beige to grey color and black to grey color with lighter color spots (Fig. 32a-c). Wavy lamination of clay layers and burrows are noted. Dolomite crystals are concentrated in the burrows (Fig. 32d-g). In other intervals, the dolomite rhombs are scattered within the mud matrix. Bivalves, echinoderms and foraminiferas such as Miliolids and *Pseudochrysalidina littus* and sponge spicules are present in minor amount (Fig. 32h). It shows poor reservoir properties with an average porosity of 5% and high water saturation (57.5%). Moldic and vuggy pores are the main type recognized.

3- Bioclastic foraminiferal wacke- to packstones microfacies (F-13)

This microfacies has bluish grey color (Fig. 33a) and show wacke- to packstone texture. It is comprised of bioclasts fragments, benthic foraminiferas such as Miliolids, *Pseudochrysalidina, Pseudocyclammina littus, Lenticulina sp*, and echinoderms (Fig. 33b-d). It exhibits notable amount of planktic foraminifera as well as sponge spicules, (Fig. 33c and d). It constitutes approximately 6.6% of the total cored intervals, with a vertical extent of 25 m (Table 4). It appears in non-reservoir units (B0 and B2) of Ah'Dimah (Fig. 15), while it is absent in Nasiriya and West Qurna oilfields. This facies exhibits poorer reservoir quality, with low porosity, low permeability, and a higher shale content when compared to other facies (Table 4). The porosity varies from 0.9% to 11% with an average of about 4%. The permeability is low, recording an

average of about 2mD. The limestone is often argillaceous recording shale volume of about 22%. Notably, moldic, vuggy, and channel pores have been entirely occluded by blocky, syntaxial, and drusy cement, resulting in reducing of porosity. This microfacies has undergone dolomitization, stylolitization and pyritization.

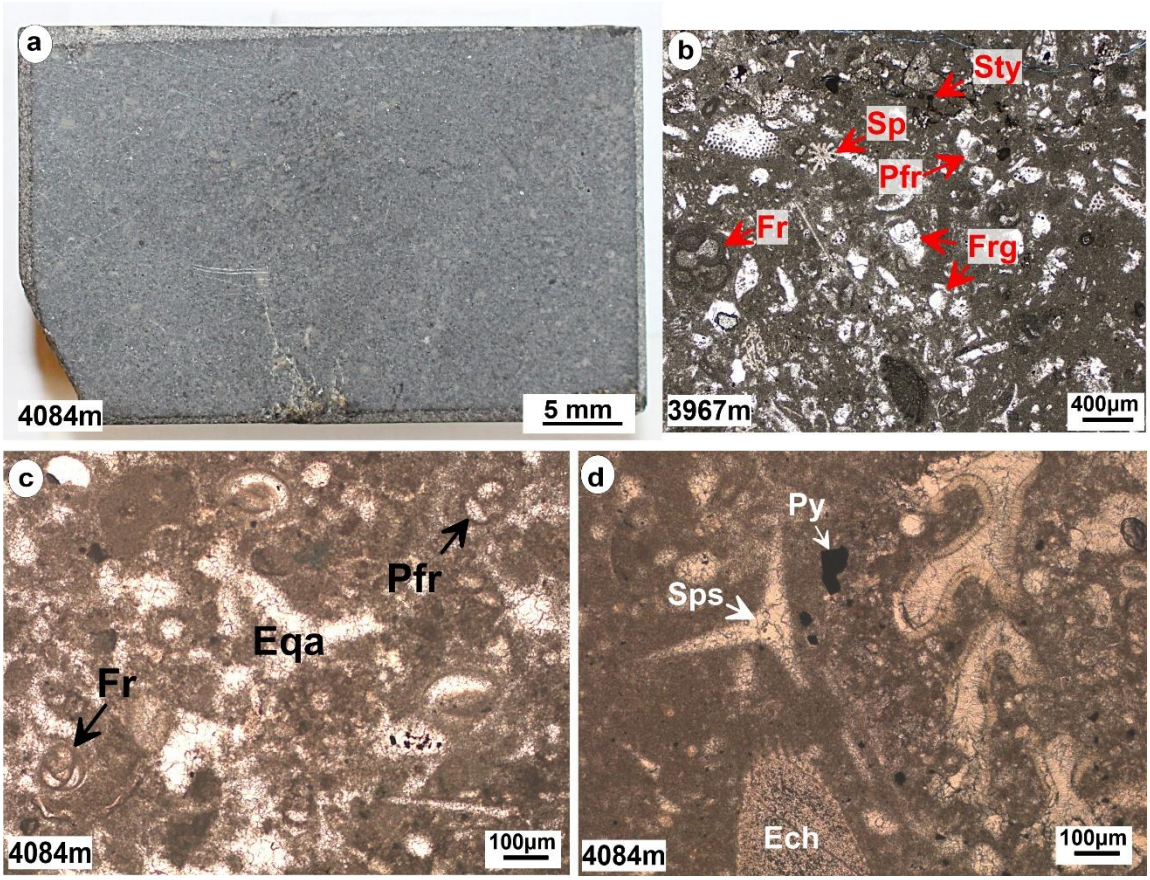

***Figure 33. Bioclastic foraminiferal wacke- to packstones microfacies (F-13)**. **a**) A slabbed image from Ah'Dimah Oilfield. **b-d**) small benthic foraminifers (Fr), planktic foraminifera (Pfr), spine (Sp), bioclasts (Frg), stylolite (Sty), Equant calcite cement (Eqa), oraminifera (Fr), echinoderms (Ech), sponge spicules (Sps), and pyrite (Py) within the bioclastic foraminiferal wacke- to packstones. Sparry and equant calcite cements are common* (*author's own edit*).

Outer-ramp Facies Associations (FA1)

The outer-ramp facies is represented by only one microfacies type:

- Spiculitic skeletal mud- to wackestones microfacies (F-14)

1- Spiculitic skeletal mud- to wackestones microfacies (F-14)

This grey to dark grey mud- to wackestone microfaciesfacies (Fig. 34a and b) is found within the non-reservoir units (B1-B3) in Nasiriya (Fig. 13), Ah'Dimah (Fig. 15), and west Qurna (Fig.

16). It is characterized by argillaceous limestone with a total thickness of 19 m and representing 5% of the cored intervals (Table 4). The grains are represented by sponge spicules small foraminifera, and bioclasts fragments (Fig. 34c-e). Porosity (average 4%) is represented by minor isolated moldic pores, which are mostly filled with blocky calcite cement. Pyrite occurs pseudomorphs after skeletal grains such as the sponge spicules (Fig. 34c) or small foraminifera.

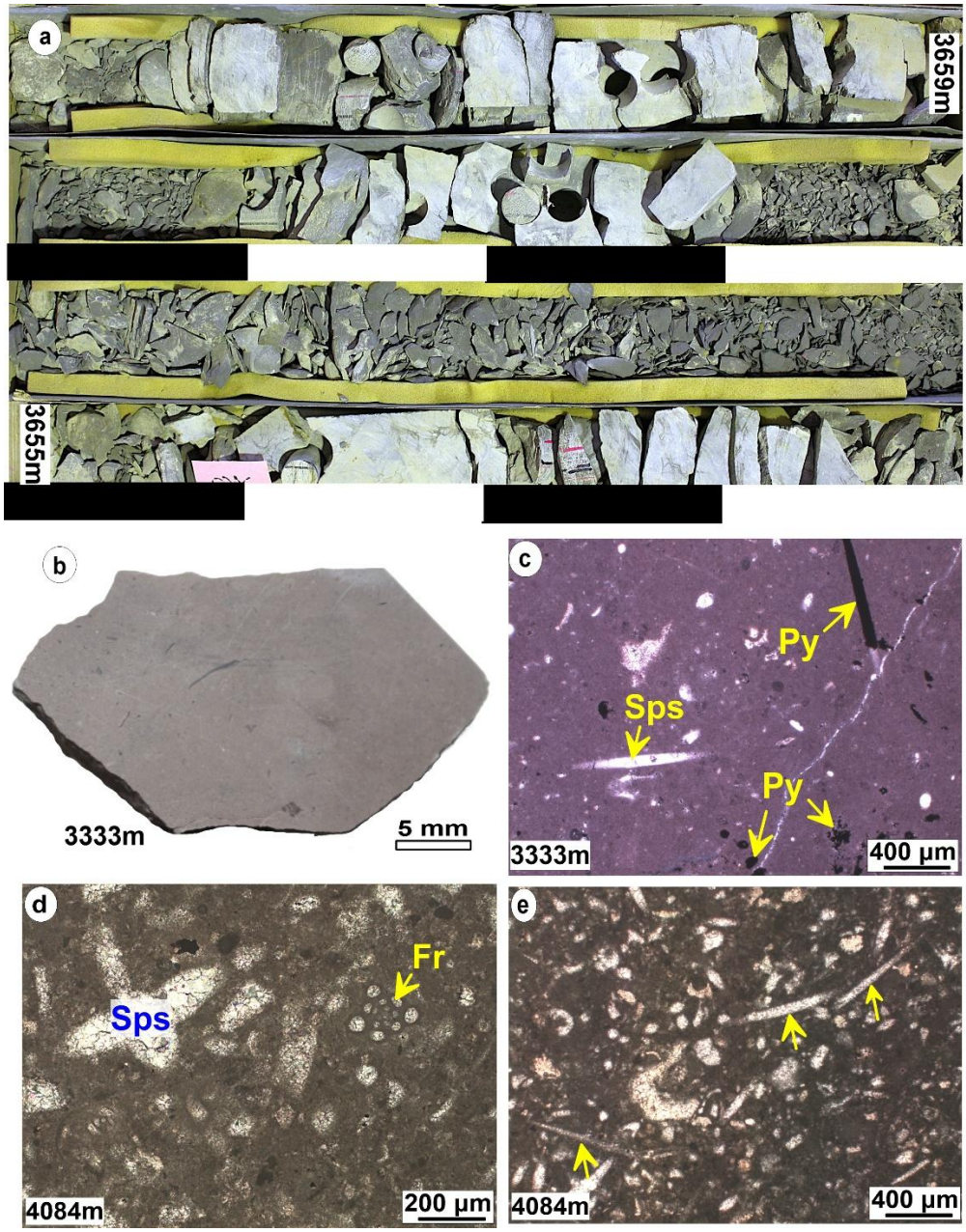

Figure 34. Spiculitic skeletal mud- to wackestones microfacies (F-14). ***a)*** *Core image spiculitic skeletal mud- to wackestones from West Qurna Oilfield.* ***b)*** *slabbed image from Nasiriya Oilfield.* ***c-e)*** *sponge spicules (Sps), small foraminifera (Fr), and pseudomorphs pyrite (Py)* (*author's own edit*).

5. Discussion

5.1 Depositional models of the Yamama Formation

The significant vertical and lateral facies variations are attributed to substantial changes in the depositional conditions across the marine ramp being influenced by interplay between sea-level changes, regional tectonics, and rates of sediment supply (Pitman et al., 2004). The formation and its regional equivalents manifest the depositional evolution of the Arabian carbonate platforms and its intrashelf basins (Fig. 5).

Based on the vertical facies succession, texture, grain types, fauna diversity, and fossil content, the depositional environment of the Yamama Formation is constrained. Changes in the relative sea level during the deposition of the Yamama Formation had a significant impact on the facies distribution across the carbonate ramp. The core observations and facies/microfacies analysis revealed that more than 30% of the facies are grain-supported texture dominated by peloids, ooids, oncoids, cortoids and intraclasts (F-1, F-5, F-7, F-8, F-10, and F-11; Fig. 17d). These grain-supported facies formed barriers and appears as intercalated sheets in the inner ramp, in the shoal and intertidal depositional environments (Fig. 35-37). The Lithocodium-Bacinella facies (F-6 and F-9) form of around 22% of the investigated core intervals. While the mud-supported facies form around 48% (lagoonal, middle and outer ramp facies; F-2 to F-4, F-12 to F-14). No drastic change in sea level is noted during the deposition of Yamama Formation, where the succession remained around the fair-weather wave-base and the storm wave-base (Fig. 35 and 36). The grain-supported limestones show the best reservoir quality with higher porosity and permeability values as well as lower shale volumes and water saturation, whereas the Lithocodium-Bacinella facies exhibit high porosity and relatively lower permeability than the grain-supported facies. While the mud-supported limestones (laggonal, middle and outer ramp) show poor reservoir quality, forming non-reservoir units, separating the reservoir units.

The packstone to grainstone texture and the abundance of non-skeletal grains such as oncoids, peloids, and intraclasts in F-1 (Fig. 21) with the absence of the skeletal grains (e.g., foraminifera and mollusk) suggest a moderate to high energy intertidal environment (Sequero et al. 2020). The irregular and subrounded shapes of these oncoids formed by microbial activities (Pederson et al. 2015; Sequero et al. 2019; Wang et al. 2023). The interparticle porosity provides moderate to good reservoir quality. Local studies carried on the Yamama Formation in south of Iraq including (Van Bellen et al. 1959; Sadooni 1993; Saleh 2014; Chafeet 2016; Idan et al. 2020;

Al-Hassani and Al-Dulaimi 2021; Khazaal and Shakir 2022; Aljibouri et al. 2022; Al-Khafaji et al. 2022; Al-Iessa and Zhang 2023; Alshammary et al. 2024), and regional studies studied the Yamama Formation and its equivalent in Saudi Arabia and Iran including (Jeong et al. 2017; Esrafili-Dizaji et al. 2020; Bahrehvar et al. 2021; Hosseiny and Mohseni 2023; Fallatah et al. 2024; Khalil et al. 2024) have not identified the oncoidal facies within the Yamama Formation. This study confirms the presence of the oncoidal facies within the Yamama Formation, south of Iraq, particularly in Nasiriya Oilfield. The nucleus of oncoids remain unclear, more analytical techniques can be applied to establish the origin and type of the nucleus.

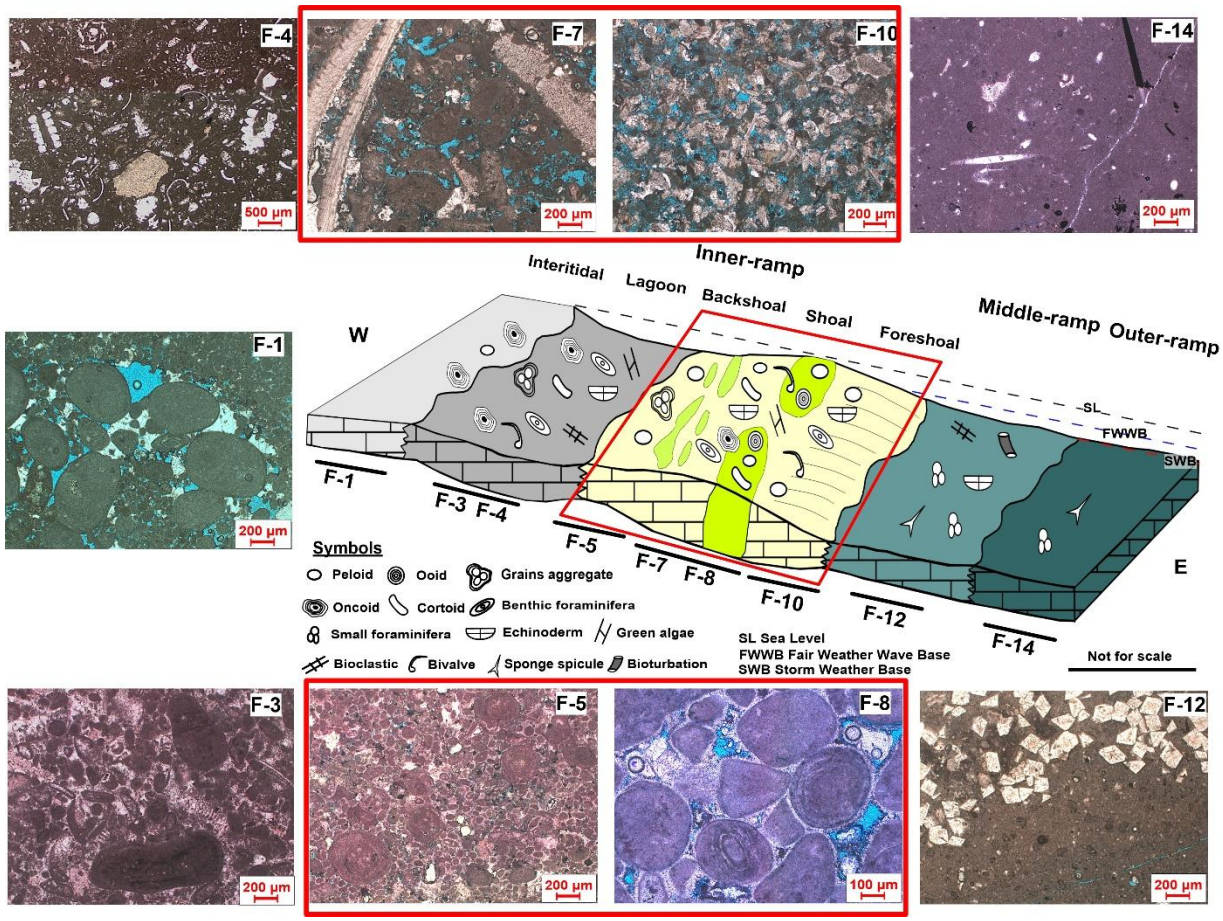

Figure 35. *A conceptual depositional model of the Yamama Formation shows the distribution of facies across intertidal to outer ramp settings in homoclinal shallow-marine carbonate ramp which is distally slightly steepening. The highlighted shoal grain-supported facies represent the best reservoir facies. This model is applicable for Nasiriya Oilfield (author's own edit).*

The presence of abundant micritized skeletal grains in F-2, F-3, and F-4 including foraminifera (Miliolids, *Pseudocyclammina littus, Praechrysalidina infracretacea, Trocholina, Lenticulina sp.*) bivalves, dasycladalean algae, echinoderms, and gastropods, along with the presence of the non-skeletal grains such as peloids and micrite envelopes (Fig. 22-24) suggest that these facies

were deposited in moderate energy with high nutrient level (Nagm et al. 2018; Sabouhi et al. 2022; Deville de Periere et al. 2023).

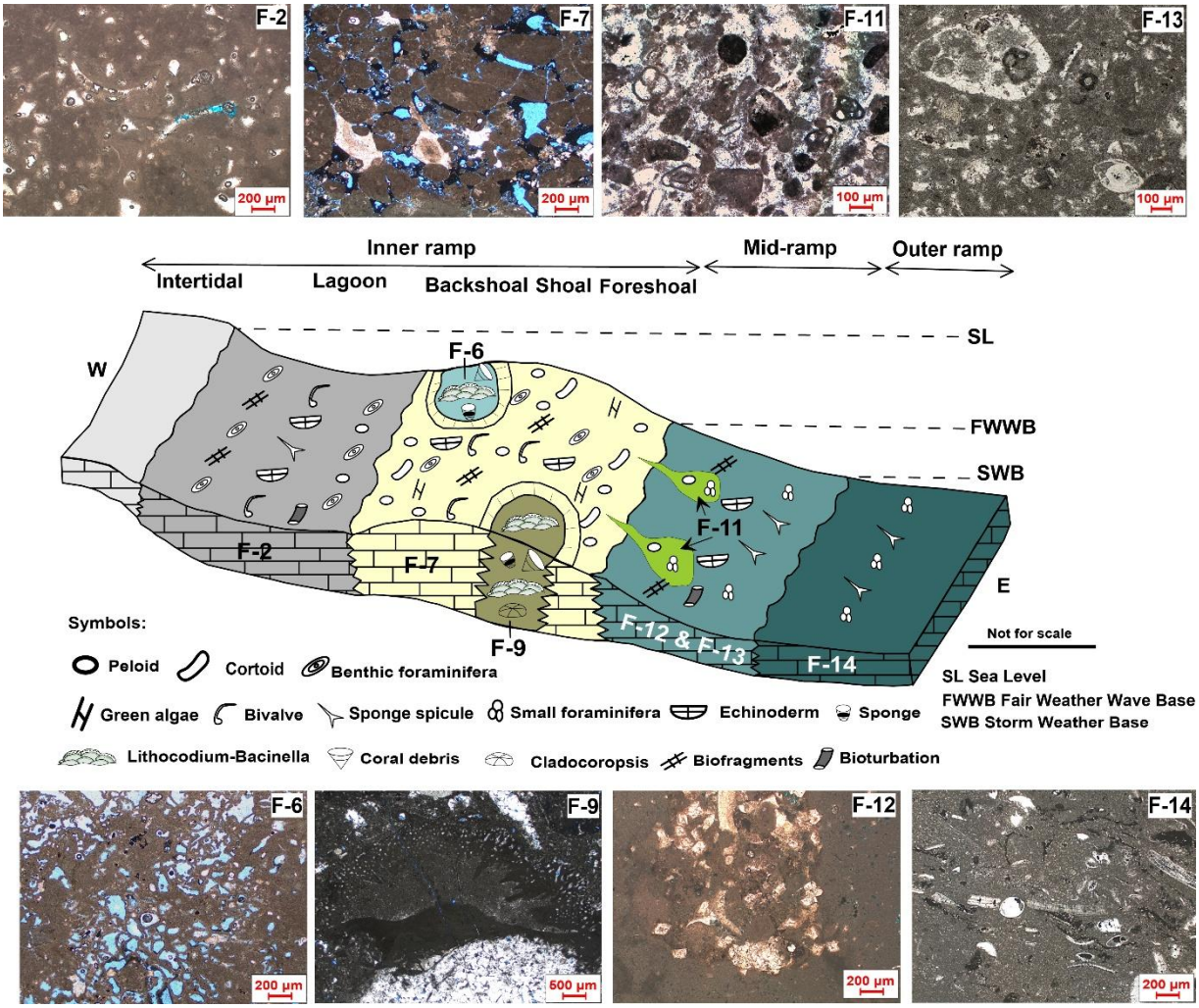

Figure 36. *A conceptual depositional environment model for the Yamama Formation showing distribution of the various facies a slightly steeping homoclinal shallow-marine carbonate ramp. This model is applicable for Ah'Dimah and West Qurna oilfields (author's own edit).*

The pelletal pack- to grainstones and the limited fauna diversity suggest that F-5 (Fig. 35) developed in a restricted moderate energy level, in the backshoal (Fallatah et al. 2024). The distinctive circumgranular cement formed around the non-skeletal grains in marine-phreatic zone (Scholle and Ulmer-Scholle 2003; Flügel 2010; Mohammed et al. 2022b). The grains are small, therefore, the mechanical compaction, caused by the overburden pressure affected this type of microfacies by reducing the porosity (Fig. 25). However, the presence of early circumgranular, scattered equant and syntaxial calcite overgrowths protected the grains from further compaction (Morad et al. 2012).

Within F-6, numerous skeletal and non-skeletal grains were observed interacting with the Lithocodium-Bacinella algae in floatstone texture (Fig. 26). These constituents include peloids, large foraminiferas, algae, echinoderms, and coral debris, cladocoropsis, and the prevalence of circumgranular cement is notable. These collective observations indicate that this facies was deposited in a moderate energy setting and is interpreted to be situated between the lagoon and shoal within the backshoal environment as patches/buildups (Koch et al. 2002).

The grainstones texture including peloids and ooids, and the fauna diversity including the large foraminifera such as Miliolids, *Pseudochrysalidina*, and *Pseudocyclammina littus*, as well as the abundance of echinoderms, bivalves, and coral debris in F-7 and F-8 (Fig. 27 and 28) suggest a shoal environment characterized by high energy depositional conditions (Wilson 1975; Flügel 2010; Valinasab et al. 2023). These facies formed shoal barriers that separate semi-restricted lagoon from the open marine environments.

In contrast, the features observed within F-9 including Lithocodium-Bacinella, sponge, coral, as well as the presence of peloids, large foraminifera, echinoderms and bivalves (Fig. 29) as well as the abundance of circumgranular cement suggest a deposition within a moderate to high energy environment (Longman 1980; Koch et al. 2002; Esrafili-Dizaji et al. 2020). This facies is situated above the fair-weather wave base, within the shoal, subject to daily high and low tides. This facies represent reefs that form reefal patches within the foreshoal area.

The bioclastic grainstones and the abundance of echinoderms and bivalve fragments, and the rarity of foraminifera in F-10 suggest a moderate to high energy environment with normal salinity within the proximal inner-ramp (foreshoal). This facies appeared to be reworked and interpreted to have been deposited in the shoal-slope. This interpretation is supported by angular, well sorted, fine-grained grains (Yousef et al. 2023). The partially and completely dissolved grains including peloids are attributed to episodes of subaerial exposures (Fig. 30).

The small size peloids and foraminiferas and the occurrence of the planktic foraminifera suggest that F-11 (Fig. 31) is likely to have been reworked, transported along the slope and deposited in a lower energy environment compared to F-7 and is presumed to have been deposited within a middle ramp setting. The matrix-supported textures combined with limited fauna diversity and the presence of sponge spicules and planktic foraminifera along with the *Thallassinoides* burrows in F-12 (Fig. 32) suggest low energy middle ramp (Mohammed et al. 2022b). The small

foraminifera, the appearance of the sponge spicules, the absence of non-skeletal grains, in addition to the appearance of the argillaceous limestone in F-13 facies (Fig. 33) all suggest low energy environment (Wilson 1975; Flügel 2010; Valinasab et al. 2023). This facies is interpreted to have been deposited in middle ramp setting below FWWB and above SWB.

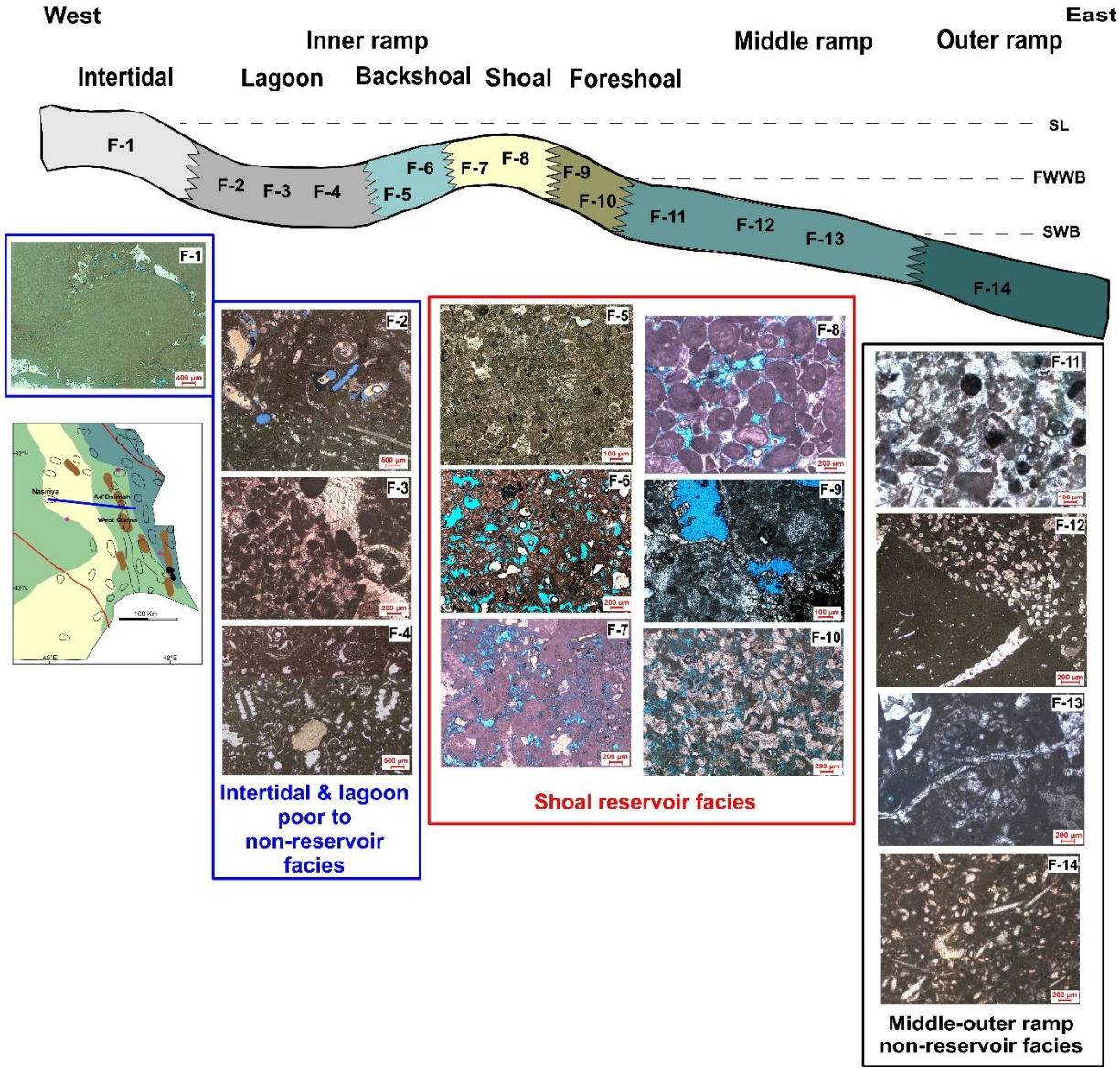

Figure 37. *Facies distribution of the Yamama Formation in the studied area, running from the west (Nasiriya Oilfield) to the east (Ah'Dimah and West Qurna oilfields), illustrating the transition from the inner to the outer ramp. The schematic cross-section depicts facies belts from intertidal, lagoonal, and shoal environments in the inner ramp to deeper-water settings in the middle-outer ramp. The lower panels show photos of the various microfacies, classified into reservoir, non-reservoir, and transitional facies based on their petrographic characteristics. SL = Sea-level, FWWB = Fair-Weather Wave Base, SWB = Storm Wave Base* (*author's own edit*).

The argillaceous limestones and the abundance of sponge spicules and the presence of plankton foraminifers in F-14 (Fig. 34) suggest low energy outer ramp (Esrafili-Dizaji et al. 2020; Fallatah et al. 2024). Dolomitization along bioturbation sites is facilitated by localized increase in carbonate alkalinity and microbial sulfate reduction (Rameil 2008; Morad et al. 2023). Bioturbation can also result in the deterioration of good depositional porosity and permeability through the introduction of the mud matrix (Alsuwaidi et al. 2020).

5.2 Lithocodium-Bacinella facies (F-6 and F-9)

Recognizing the pivotal role of the F-6 and F-9 facies in controlling the reservoir quality of the Yamama Formation within this study, it is important to emphasize the significance of the algal Lithocodium-Bacinella facies. This section will deal with their description, origin, and the geology and sedimentology distribution.

Lithocodium aggregatum, as described by Elliott (Elliott 1956) in 1956, and Bacinella irregularis, identified by Radoičić (Radoičić 1959) in 1959, are mysterious microorganisms known for their encrusting nature. They were once widely distributed across Mesozoic carbonate platforms but have extinct (Rameil et al. 2010). They are frequently encountered within sedimentary rocks dating back to the Middle Jurassic through the Early Cretaceous (174 to 100Ma). They are commonly associated with coral, sponge, and microbial reef frameworks. Additionally, they contribute to the formation of oncoids in lagoonal and shoal environments.

Lithocodium aggregatum is a calcareous alga known for its encrusting growth habit (Fig. 38). It typically forms intricate, branching structures composed of small, rounded or irregularly shaped calcareous segments closely packed together. These segments may resemble small, button-like structures, and the surface of Lithocodium aggregatum often exhibits a granular or textured appearance due to numerous calcified layers. It can be found growing on various substrates, including rocks, shells, coral and other organisms (Elliott 1956; Schmid and Leinfelder 1996; Rameil et al. 2010). Bacinella irregularis, another calcareous organism, is characterized by its fan-shaped or fan-like structures. It comprises fan-shaped plates or blades radiating outward from a central point. These blades can be thin and delicate, featuring a finely textured surface. The fan-shaped structures vary in size, and they often overlap or intertwine, forming intricate patterns (Fig. 38). Like Lithocodium aggregatum, Bacinella irregularis is

commonly associated with other marine organisms, providing valuable insights into ancient marine environments (Radoičić 1959; Schmid and Leinfelder 1996; Rameil et al. 2010).

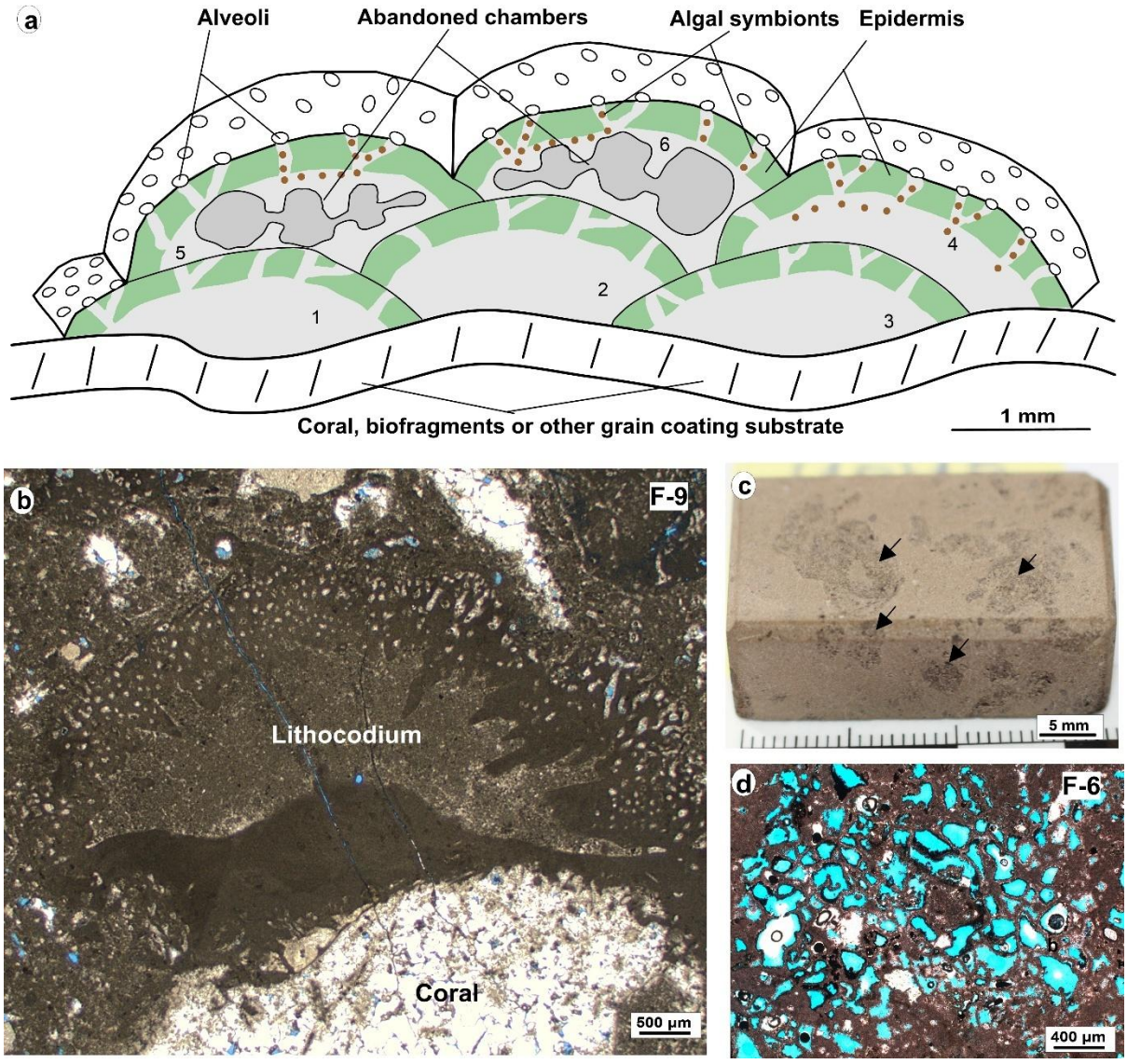

Figure 38. a) *A schematic diagram of the Lithocodium-Bacinella, shows 6 chambers. Modified after Schmid and Leinfelder (1996).* ***b)*** *Lithocodium-Bacinella encrusting a coral (F-9).* ***c)*** *Core slabbed photo showing the Lithocodium-Bacinella floatstones (F-6).* ***d)*** *plan view of the dominated vuggy and intraparticle porosity within F-6 and F-9* (*author's own edit*).

Lithocodium-Bacinella has been identified in various locations worldwide, including, Barremian Hautervian Ratawi Formation in South Iraq (Van Bellen et al. 1959), Hauterivian formations in Southeast France (Conrad and Clavel 2008), Abu Dhabi Onshore Field in the Lekhwair, Kharaib (Jeong et al. 2017), and Lower Shuaiba Formations, Aptian deposits in Oman (Rameil et al. 2010), and Late, Valanginian–Hauterivian in the Fahliyan Formation, eastern

Persian Gulf Basin (Esrafili-Dizaji et al. 2020). Their geographic range further extends from the southern USA and Mexico to NW Africa, the Iberic Plate, and across the Tethyan realm to China (Hüßner 1985; Banner et al. 1990; Lehmann et al. 1999). The Lithocodium-Bacinella were also found in the Lower Aptian of the western Maestrat Basin (Spain) (Schlagintweit et al. 2010). Lithocodium typically thrived in a paleoenvironment characterized by warmth, full marine conditions, ample oxygenation, abundant calcium carbonate, and a mid-shelf sea setting. These conditions point to a shallow, warm environment with normal marine salinity, making it well-suited for the growth of Lithocodium aggregatum (Schmid and Leinfelder 1996).

The reservoir units YRB1, YRB2 and YRC which form as the predominant reservoir units (along with YRB3) within the Yamama Formation in Ah'Dimah Oilfield (Fig. 15), as well as the reservoir unit YRA in West Qurna (Fig. 16) are predominantly composed of Lithocodium-Bacinella facies (F-6 and F-9). In addition to their high intraparticle porosity, the dissolution has played important role in improving the reservoir quality in this facies types of facies. The high porosity of Lithocodium-Bacinella algal facies is a result of their biogenic origin, encrusting growth habit, sediment-trapping capabilities, diagenesis, and their presence in ancient reef and lagoonal environments. These characteristics make them for a significant reservoir rocks and provide valuable insights into past marine ecosystems (James and Choquette 1983; Tucker and Wright 2009). Since Lithocodium-Bacinella grows in lagoonal and reefal environments, the dissolution due to reactions between sediments and marine water is a crucial factor in the formation and modification of porosity. This process can result in the creation of both primary and secondary porosity and contributes to the overall heterogeneity of porosity within these rocks. The early Mg-calcite cement (circumgranular) formed rims inside the pores and likely protected the pores from compaction (Tucker and Wright 2009; Bjorlykke 2010).

The vertical and lateral dimensions of Lithocodium-Bacinella lithosomes exhibit considerable variation, ranging from meter-scale build-ups to massive beds up to 8 m, and as high as 40 m (Alsharhan A. S. 1985; Koch et al. 2002; Rameil et al. 2010). Lithocodium-Bacinella can be characterized by their massive appearance, distinctly differing from adjacent bedded lagoonal facies (Neuweiler and Reitner 1992). In this study F-6 and F-9 formed thickness of 46 m and 37 m in YRB2 and YC, respectively in Ah'Dimah Oilfield. While only F-6 appears in YRA in West Qurna Oilfield. The core of oncoids and grains aggregates is Lithocodium-Bacinella within F-7 and F-8 facies in Nasiriya Oilfield in the reservoir unit YRC (Fig. 27 and Fig. 28).

Evidence from the seismic section shows that there are possible build-ups within the Yamama Formation, where the seismic reflectors are distorted and not continuous in most of the formation's parts (Fig. 7). Similar carbonates build ups were found by Hillgartner et al. (2003) and Valinasab et al. (2023). These build ups are highly likely due to the presence of Lithocodium-Bacinella sediments. Therefore, targeting these build ups, especially, to the northeast part of Ah'Dimah Oilfield is beneficial for developing the Yamama Formation.

5.3 Micropaleontological Content and Its Biostratigraphic Significance

The studied well intervals are located in the Nasiriyah (NS), Ah'Dimah (Da), and West Qurna (WQ) oilfields and represent different types of limestone (including argillaceous, dolomitic, and bioturbated dolomitic limestones), all belonging to a single lithostratigraphic unit, the Yamama Formation. The microfossils have been determined by Dr. Daria Ivanova (Bulgarian Academy of Science, Sofia, Bulgaria).

Regarding the distribution of foraminifera in the studied wells, the lowest abundance was observed in Nasiriyah, with an average of about 15 foraminiferal specimens per thin section. A significantly higher quantity was found in samples from well West Qurna, with an average of about 30 specimens, and in some thin sections (at depth 3657 and 3640 m), over 50 specimens were recorded. The highest abundance was observed in well Ah'Dimah, with an average of about 40 specimens per thin section; in samples at 3999.50, 3967.50, and 3964 m, more than 70 were recorded, while sample 3984 m contained over 150 foraminiferal specimens.

The thin sections of the Yamama Formation contain diverse benthic foraminiferal communities, agglutinated foraminifera being predominant. Although most of the identified species have a wide stratigraphic range, the assemblages they form are reliable indicators of the age of the Yamama Formation. The foraminiferal assemblage consists of *Paravalvulina arabica* (Henson), *Patellovalvulina patruliusi* Neagu, *Bramkampella arabica* Redmond, *Pseudocyclammina lituus* (Yokoyama), *Mayncina bulgarica* Laug, Peybernès & Rey, *Freixialina planispiralis* Ramalho, *Melathrokerion valserinensis* Broennimann and Conrad, *Charentia cuvillieri* Neumann, *Nautiloculina bronnimanni* Arnaud-Vanneau & Peybernès, *Montsalevia salevensis* (Charollais, Brönnimann & Zaninetti), *Haplophragmoides joukowskyi* (Charollais, Brönnimann & Zaninetti), *Protopeneroplis ultragranulata* (Gorbatchik), *Vercorsella camposaurii* (Sartoni & Crescenti), *Coscinophragma cribrosum* (Reuss), *Siphovalvulina variabilis* Septfontaine,

Redmondoides lugeoni (Septfontaine), *Scythiolina/Histerolina* div. sp., and representatives of the genus *Coscinoconus*, among others (Fig. 39-41).

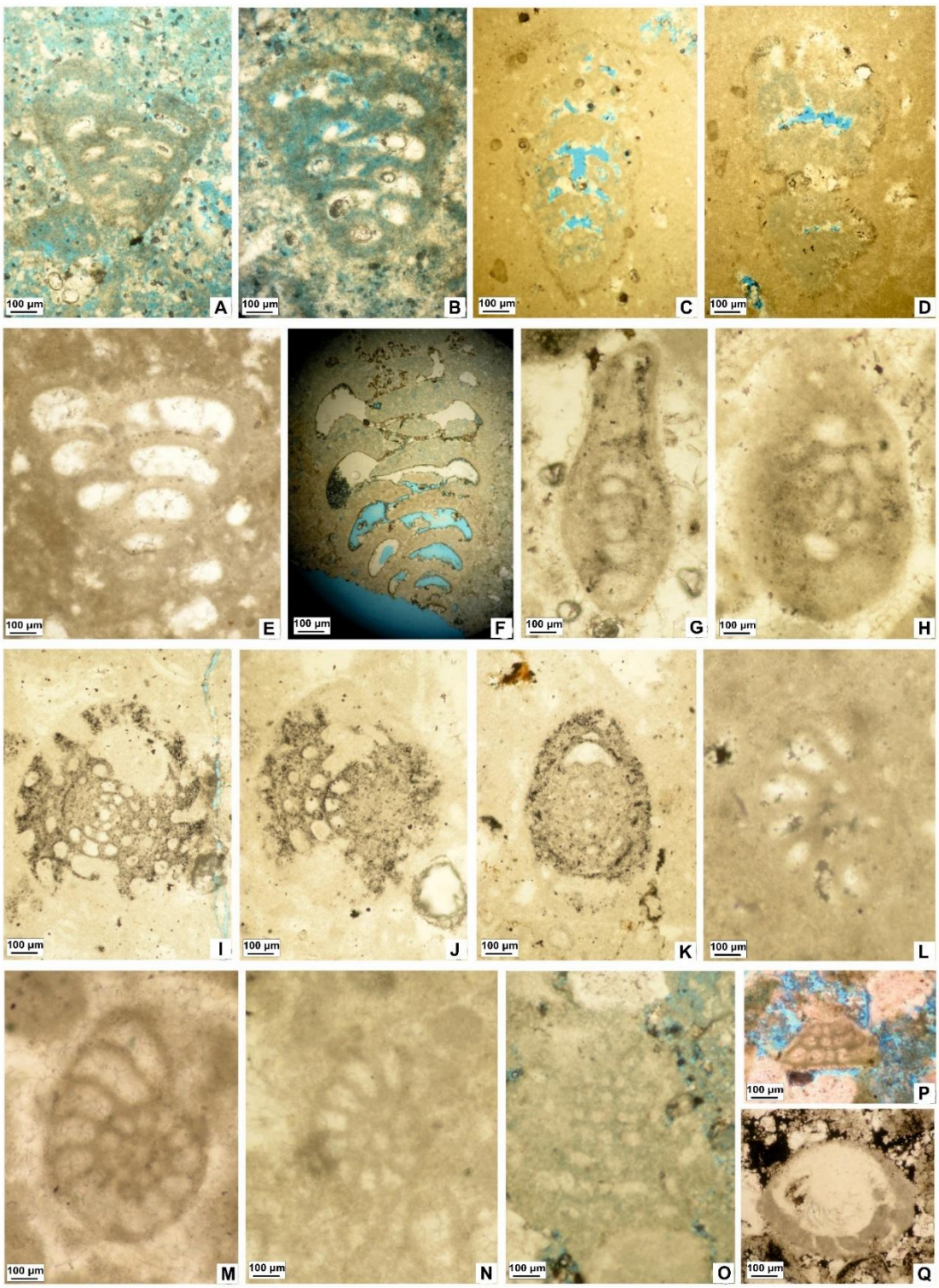

Figure 39. Plate 1:

A, B. *Paravalvulina arabica (Henson);* ***A.*** *Well WQ, sample 3622 m;* ***B.*** *Well WQ, sample 3623 m*
C, D. *Bramkampella arabica Redmond; Well Da, sample 4120 m*
E. *Patellovalvulina patruliusi Neagu; Well NS, sample 3179 m*
F. *Praechrysalidina infracretacea Luperto Sinni; Well Da, sample 4068 m*
G, H. *Charentia cuvillieri Neumann; Well Da, sample 4078 m*
I-K. *Nautiloculina bronnimanni Arnaud-Vanneau & Peybernès; Well Da, sample 3967 m*
L. *Freixialina planispiralis Ramalho; Well NS, sample 3333 m*
M, N. *Mayncina bulgarica Laug, Peybernès & Rey;* ***M.*** *Well Da, sample 3984 m;* ***N.*** *Well NS, sample 3210 m*
O, P. *Montsalevia salevensis (Charollais, Brönnimann & Zaninetti);* ***O***. *Well Da, sample 4047 m;* ***P***. *Well NS, sample 3282 m*
Q. *Protopeneroplis ultragranulata (Gorbatchik); Well Da, sample 3981 m. (author's own edit).*

While some species in this assemblage have wide stratigraphic ranges, many exhibit restricted stratigraphic distributions, limited to the Berriasian–lower Valanginian (or, at most, the upper Tithonian–Valanginian). In the uppermost part of the studied Yamama Formation, there is a notable decline in the abundance of benthic foraminifera probably due to deepening of the sea level. However, several species with calcareous tests appear, including *Meandrospira favrei* (Charollais, Brönnimann & Zaninetti), *Rumanolina turriculata* (Dieni & Massari), *Istriloculina eliptica* (Iovcheva), *Istriloculina emiliae* Neagu, and *Ichnusella infragranulata* (Noth).

5.3.1 Stratigraphic Range of the Identified Microfossils

Paravalvulina arabica (Henson) (Fig. 39A and B) is an important marker species in the Valanginian Yamama and Zakum formations across several locations on the Arabian Plate, including Saudi Arabia, Qatar, the United Arab Emirates, Kuwait, Bahrain, and Iraq (Granier 2008; Hosseini et al. 2016)

Patellovalvulina patruliusi Neagu (Fig. 39E) was first described by Neagu (1975) from the earliest Cretaceous deposits of the Perșani Mountains, Romania. It was later reported from various Lower Cretaceous sediments by Bucur (1988), (Bernaus et al. 2002) and (Neagu and Cirnaru 2004). The known stratigraphic range of the species extends from the Berriasian to the Bedoulian (lower Aptian).

Bramkampella arabica (Fig. 39C and D) was first described from deposits attributed to the basal Cretaceous (Berriasian) by Redmond (1964). The species was later identified in limestones ranging from the Kimmeridgian to the lower Valanginian (Bucur and Săsăran 2005; Pleş et al. 2015; Mircescu et al. 2019; Bucur and Lazăr 2023).

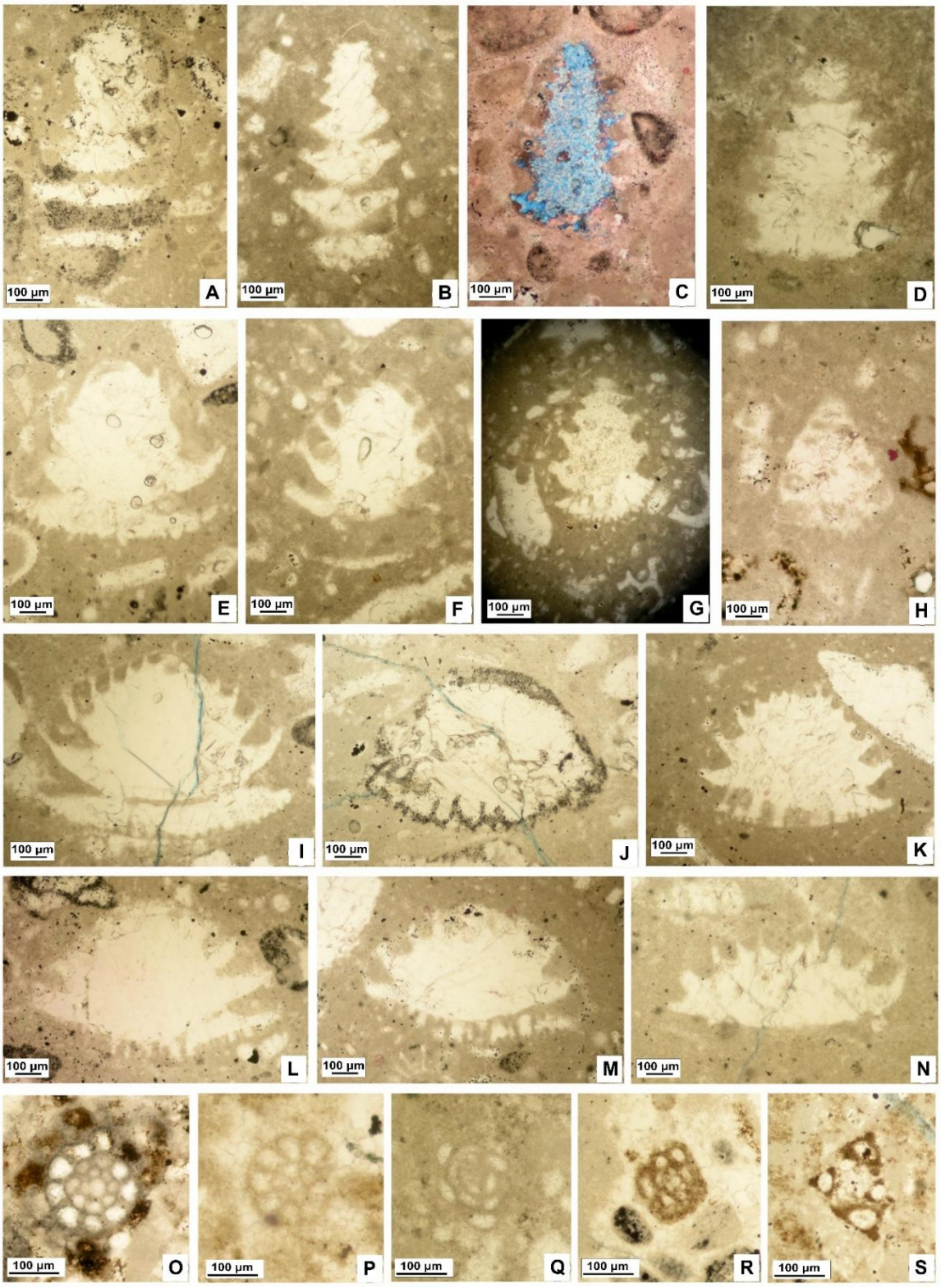

Figure 40. Plate 2:
A-N*. Representatives of the genus Coscinoconus: Well Da, samples 4093 m, 3988 m; Well WQ, samples 3657 m, 3640 m, 3617 m.*

O, P. *Haplophragmoides joukowskyi (Charollais, Brönnimann & Zaninetti);* ***O****. Well Da, sample 3999 m;* ***P****. Well WQ, sample 3611 m*
Q, R. *Meandrospira favrei (Charollais, Brönnimann & Zaninetti);* ***Q****. Well Da, sample 4082 m;* ***R.*** *Well WQ, sample 3612 m*
S. *Moesiloculina danubiana (Neagu); Well WQ, sample 3611.5 m. (author's own edit).*

Montsalevia salevensis (Charollais, Brönnimann and Zaninetti) (Fig. 39O and P) is a well-known species ranging from the upper Berriasian to the Hauterivian (Charollais et al. 1965; Darsac 1983; Zaninetti et al. 1987; Bucur 1988; Ivanova et al. 2015; Mircescu et al. 2019).

Haplophragmoides joukowskyi (Charollais, Brönnimann & Zaninetti) (Fig. 40O and P), was first reported from Valanginian – lower Hauterivian deposits by (Charollais et al. 1965). However, it is more commonly found in the Berriasian–lower Valanginian interval (Darsac, 1983; Ivanova et al., 2015; Mircescu et al., 2019).

Mayncina bulgarica Laug, Peybernes & Rey (Fig. 39M and N) was first described from Lower Aptian deposits in Bulgaria. The species has subsequently been reported from various sediments ranging from the Upper Berriasian to the Aptian.

Freixialina planispiralis Ramalho (Fig. 39L) was first described by (Ramalho 1969) in Portugal from the Upper Jurassic. Later on it was reported from the Kimmeridgian to Barremian (Ivanova and Kolodziej 2010; Ivanova et al. 2015).

Meandrospira favrei (Charollais, Brönnimann & Zaninetti) (Fig. 40) was originally described by Charollais et al. (1965) from upper Valanginian to upper Hauterivian deposits in Haute-Savoie, France. The species has also been identified in Valanginian strata (Bucur et al. 1995; Pop and Bucur 2001), as well as in upper Valanginian to lower Hauterivian deposits (Bucur 1988; Altiner 1991; Ivanova 2000; Ivanova and Kołodziej 2010). Its known stratigraphic range extends from the Valanginian to the lower Aptian.

Representatives of the genus *Coscinoconus* (e.g., *Coscinoconus alpinus* Leupold, *C. elongatus* Leupold, *C. cherchiae* (Charollais, Brönnimann & Zaninetti), *C. campanellus* (Charollais, Brönnimann & Zaninetti), *C. delphinensis* (Charollais, Brönnimann & Zaninetti), and *C. chouberti* (Hottinger)) (Fig. 40) are characteristic of the middle Berriasian to lower Valanginian interval (Mancinelli and Coccia 1999; Ivanova 2000; Mircescu et al. 2019).

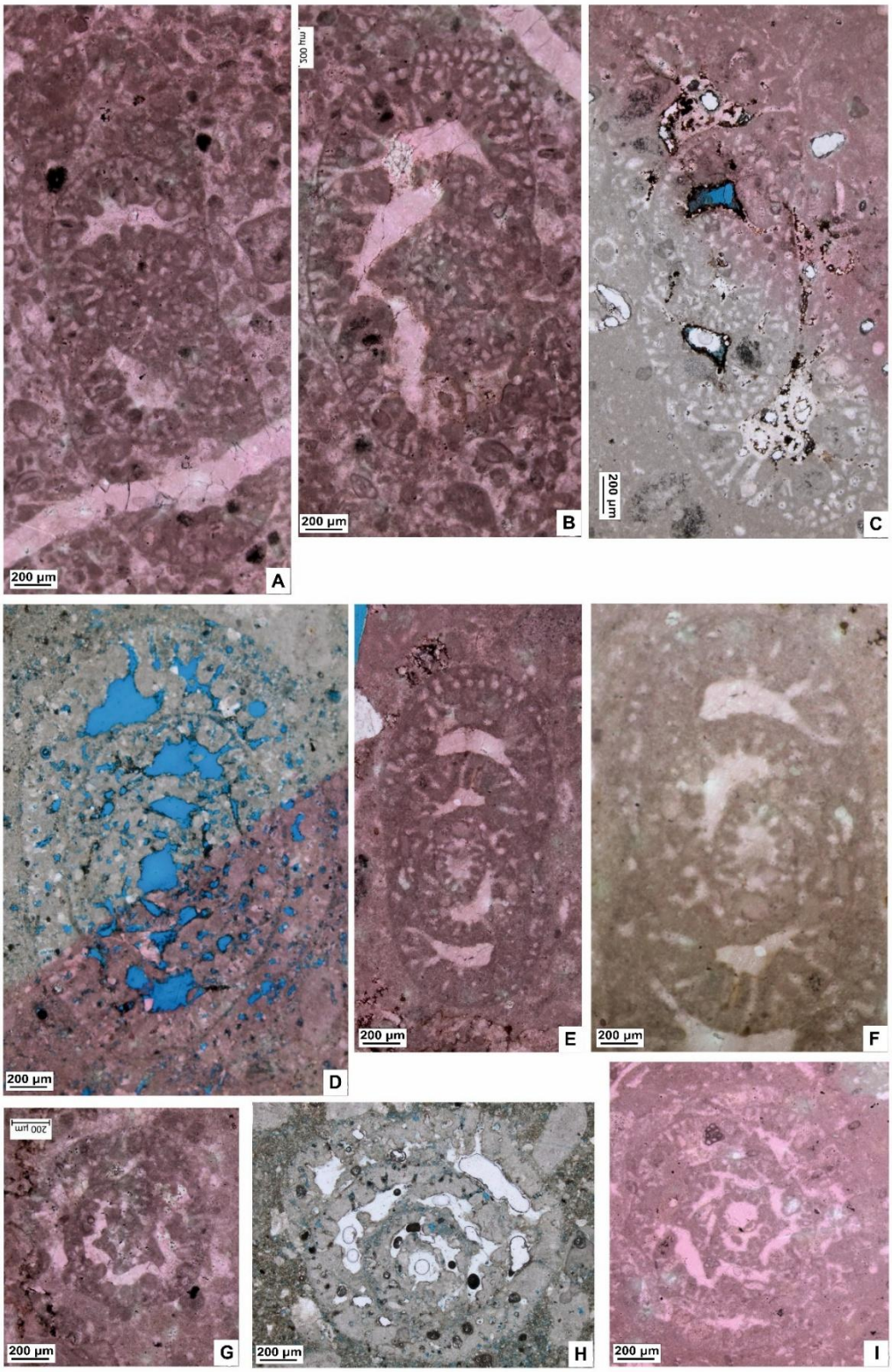

Figure 41. Plate 3:
A-C, E, F. *Pseudocyclammina lituus (Yokoyama);* ***A, B.*** *Well Da, sample 3984 m;* ***C.*** *Well Da, sample 3988 m;* ***E, F****. Well Da, sample 4061 m*
D. *Paracyclammina sp.; Well Da, sample 4014 m*

G-I. *Pseudocyclammina sphaeroidalis Hottinger;* ***G, I****. Well Da, sample 4061 m;* ***H****. Well WQ, sample 3617 m. (author's own edit).*

Pseudocyclammina lituus (Yokoyama) was originally described by Yokoyama (1890) from Lower Kimmeridgian strata under the name *Cyclammina lituus*. This widespread taxon was later reported by various authors from different regions within an interval extending from the Oxfordian(?) to the Lower Hauterivian. More recently, Bucur et al. (2020) refined its stratigraphic range to the Kimmeridgian–Lower Valanginian.

The entire assemblage of benthic foraminifera observed in the studied thin sections from three wells in south of Iraq (Nasiriyah, Ah'Dimah, and West Qurna) indicates a Berriasian to earliest Valanginian age (Darsac 1983; Salvini-Bonnard et al. 1984; Arnaud-Vanneau and Boisseau 1988; Altiner 1991; Chiocchini et al. 1994; Bucur et al. 1995, 2020; Ivanova 2000; Granier and Bucur 2011; Schlagintweit and Enos 2013; Ivanova et al. 2015; Hosseini et al. 2016; Mircescu et al. 2019) (Fig. 42).

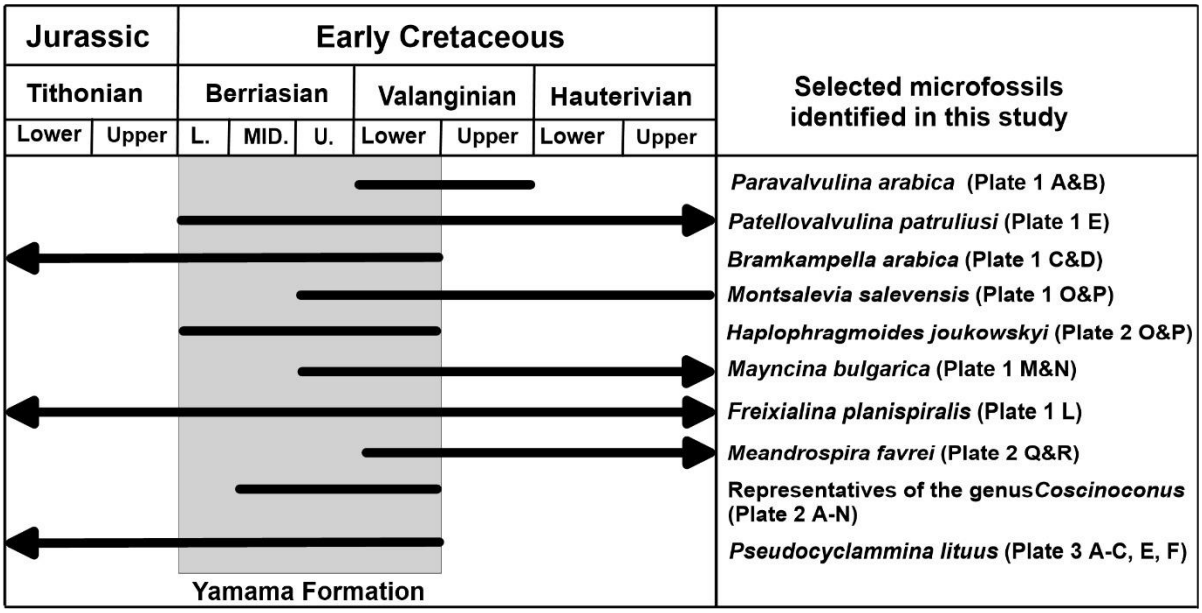

Figure 42. *Stratigraphic range of the Yamama Formation based on some selected foraminiferal species identified in this study (author's own edit).*

5.4 Diagenetic Alterations and Impact on Reservoir Properties

The reservoir quality and heterogeneity of the Yamama Formation are intricately influenced by a variety of diagenetic alterations (Fig. 43-45). These alterations have taken place under various conditions ranging from near seafloor to deep burial, i.e. eogenesis and mesogenesis, respectively (Choquette and Pray 1970). Most of the diagenetic alterations have caused

deterioration and improvement of depositional porosity and permeability. A comprehensive understanding of these processes is essential for accurately evaluating and predicting the capacity of the formation to store and transmit hydrocarbons. These include micritization, dissolution, cementations, dolomitization, as well as physical and chemical compaction.

Mechanical compaction of grain-supported Yamama limestones exerted by the load of the overburden sediments has caused reduction of pore spaces through re-arrangement of the grains and pseudoplastic deformation of the peloids between the more rigid skeletal fragments (Fig. 43a and b; Fig. 45i). The degree of compaction and consequent reduction in size of interparticle and intraparticle pores within the Lithocodium-Bacinella is lower in the grain-supported limestones that are cemented by circumgranular calcite and/or scattered interparticle equant calcite and syntaxial calcite overgrowths around echinoderm fragments.

Dissolution significantly contributed to the formation of vugs, moldic pores, channels, and enhanced the intraparticle porosity. Both fabric-selective and non-fabric-selective dissolution played pivotal roles in developing the porosity. The grain-supported facies (F-7, F-8, and F-10) exhibit notable dissolution (Fig. 43c and h; Fig. 45e, h, j, and k). The Lithocodium-Bacinella F-6 and F-9 facies showed abundance of intraparticle and vuggy porosity (Fig. 43c, Fig. 45e, f, and j) contributing to forming good reservoir units (see Lithocodium-Bacinella facies F-6 and F-9 section). These dissolution can reflect episodes of subaerial exposures within the Yamama Formation (Tucker and Wright 2009; Moore and Wade 2013). This is evident from the difference in the effective porosity (PHIE) and sonic porosity (PHIS) values (Table 4). The higher PHIE values than PHIS values arises because sonic measurements mainly capture primary porosity, as sonic waves typically travel through connected pores, while density-neutron measurements account for total porosity, including both primary and secondary porosity (Asquith et al. 2004). The difference between PHIE and PHIS porosities exceeds 5% in some of the shoal facies due to the dissolution that generated secondary porosity.

Micritization of the grains by microbial boring results in the formation of abundant microporosity and commonly cause the alteration of unimodal macroporous grainstones to bimodal macro and micropore dominated (Morad et al. 2019). Furthermore, the micritization has an influence on the texture transformation from wackestones to packstones (e.g., F-3 and F-4 facies), where these facies they different texture (Fig. 23 and 24).

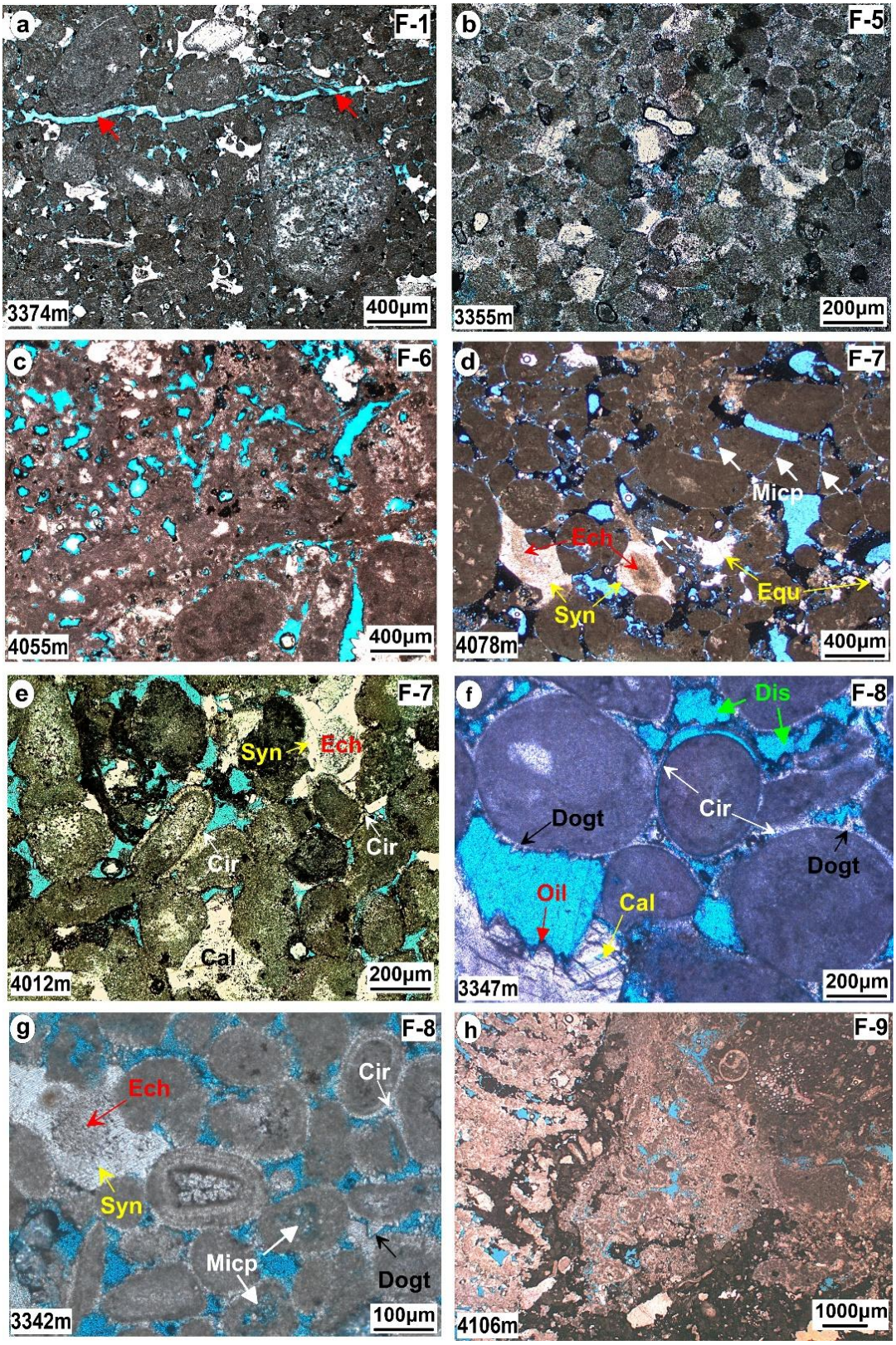

Figure 43. *Diagenetic features in the reservoir facies of the Yamama Formation.* ***a****) channel (red arrows) and limited interparticle pores in the poorly sorted oncoidal peloidal grainstones*

in Nasiriya Oilfield. ***b****) Abundance of circumgranular cement around the fine-grained pellets in Nasiriya Oilfield.* ***c*** *and* ***h****) Dissolution forming vyggy and intraparticle pores in the F-6 and F-9 (Ah'Dimah).* ***d*** *–* ***g****) Circumgranular cement (Cir) forming rims around peloids and ooids, scattered syntaxial overgrowth (Syn) around echinoderms (Ech), equant calcite cements (Cal), dissolution of grains (Dis), dogteeth cement (Dogt), Micro-porosity inside peloids (Micp).* ***d*** *and* ***e*** *from Ah'Dimah,* ***f*** *and* ***g*** *from Nasiriya Oilfield (author's own edit).*

The circumgranular calcite cement, which is common in the grain-supported shoal limestones, F-5 to F-9 (Fig. 43b, e, f, and g) was presumably originally high-Mg-calcite cement (Cao et al. 2024). This cement together with the scattered equant and syntaxial calcite overgrowth protected the grain-supported limestones deposited in the shoal facies from further compaction during burial (Morad et al. 2012, 2019). The high porosity (≤22%) was preserved despite the deep burial depth of the formation (>4000m). The lower porosity in similar circumgranular calcite cemented limestones (e.g., F-5) is attributed to their fine grains size rich in ductile pellets (Fig. 43b), which undergo porosity loss due to compaction more than in the coarse-grained sediments. Some grain-supported limestones (e.g., F-11) have experienced massive equant calcite cement, which resulted in significant reduction in the interparticle porosity prior to compaction (Fig. 44e).

Limited amounts of scattered syntaxial overgrowth and equant calcite cement in F-7 and F-8 (Fig. 43d-g, Fig. 45h) helped in protecting the porosity in the main reservoir units due to preservation of interparticle pores (Morad et al. 2012). It is recommended that further exploration and development focus on areas where grain-supported limestone facies are prevalent, given their superior reservoir quality. Enhanced reservoir characterization using well logs and seismic data could help delineate high-potential zones. Furthermore, targeting nearby fields with similar grain-supported limestone facies could present promising opportunities, contributing to overall economic potential.

Backscattered electron imaging (BSE) and energy dispersive spectroscopy (EDS) analysis revealed the presence of scattered patches of booklet-like kaolin crystals in the lagoonal facies (F-2 to F-4) of the Yamama Formation (Fig. 46a and b). The formation of diagenetic kaolin in limestones has been attributed to the flow of aggressive, basinal brines enriched in organic acids capable of dissolving and mobilizing Al^{3+} (Paganoni et al. 2016). These authors have suggested that the flow of such brines takes place along stylolites during lateral compression of the basin.

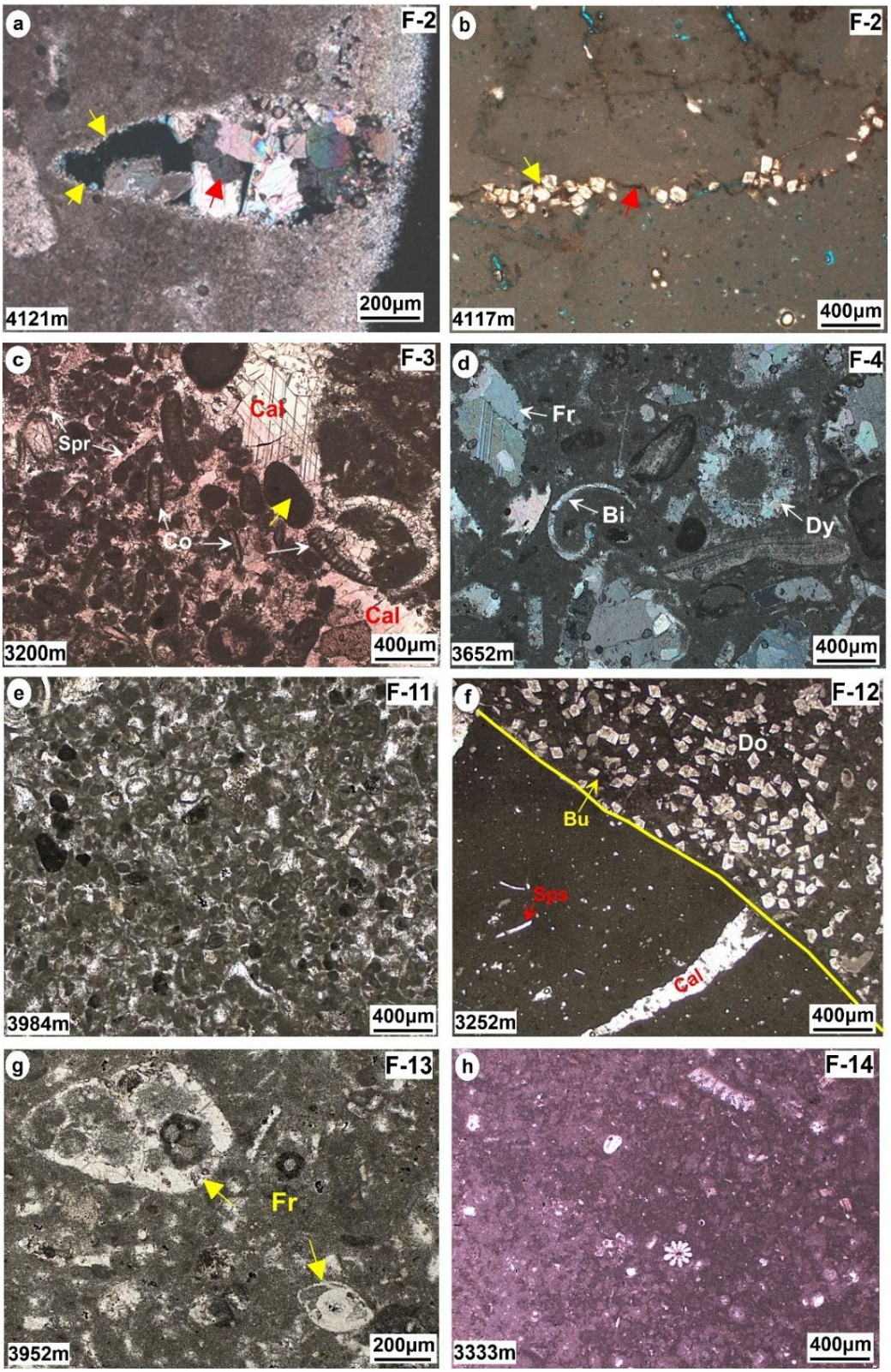

Figure 44. *Diagenetic features in the non-reservoir microfacies in the Yamama Formation.* ***a****) Partially cemented moldic pore with two cement generations (XPL), fine crystalline cement (yellow arrows) along the mold's edge followed by blocky calcite cement (red arrows) in*

Ah'Dimah. ***b****) Dolomite rhombs (yellow arrow) along stylolite (red arrow) in Ah'Dimah.* ***c****) Extensive calcite blocky and spar cement filled interparticle pores in packstone texture in Nasiriya.* ***d****) Dissolution of aragonite grains followed by calcite cementation, XPL (West Qurna), Bi= bivalve, Dy= Dasycladalean algae, Fr= foraminifera.* ***e****) Equant, spar cement, and compaction in the fine-grains of the F-11(Ah'Dimah).* ***f****) Dolomites concentrating within a burrow (Nasiriya).* ***g*** *and* ***h****) Foraminiferal wackestone (F-13), from Nasiriya.* ***h****) lime mud in (F-14), from Ah'Dimah (author's own edit).*

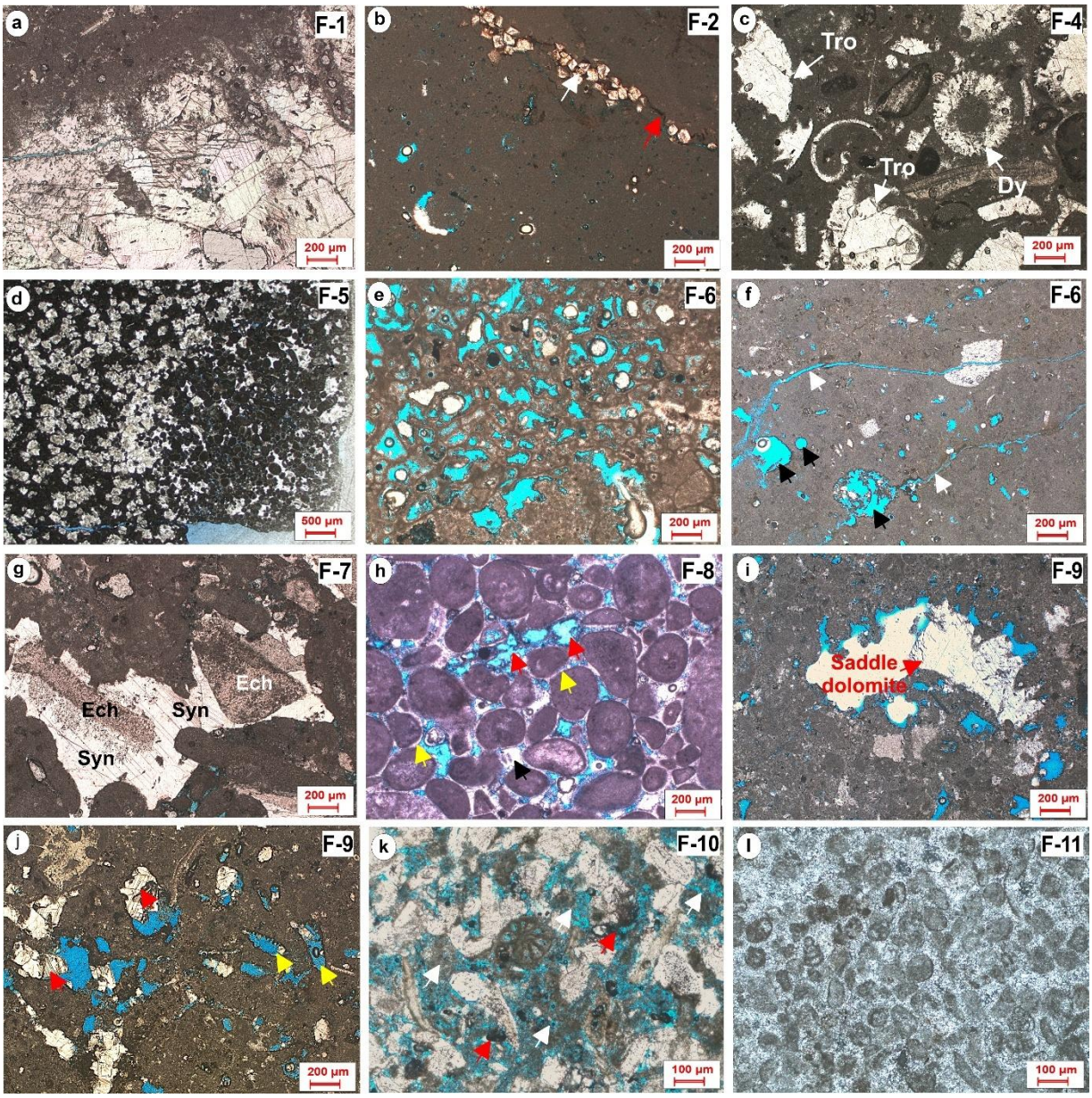

Figure 45. *Various diagenetic features recognized in the Yamama Formation. (****a****) pore space filled by large blocky calcite. (****b****) dolomite rhombs (white arrow) along stylolite (red arrow) in bioclastic mud- to wackestones (****c****) equant calcite and sparry calcite have replaced low-Mg calcite and aragonite of Trocholina (Tro) and dasyclads (Dy), respectively in lagoonal facies, (****d****) dolomitization in grain-supported pelettal limestones, (****e****) intraparticle and vuggy pores in Lithocodium-Bacinella facies, (****f****) molds (black arrows) and channels pores (white arrows) in*

*Lithocodium-Bacinella facies, (**g**) syntaxial calcite overgrowth (Syn), filling pore spaces around echinoderms (Ech) saddle dolomite partially filling a moldic pore, (**h**) circumgranular cement around grains (yellow arrows), scattered equant calcite (black arrows), and completely dissolved grains (red arrows) in grain-supported, interparticle dominated limestones, (**i**) saddle dolomite partially filling pore space, (**j**) molds (yellow arrows) and equant calcite partially filling vugs (red arrows) in Lithocodium-Bacinella facies, (**k**) dissolved grains (white arrows), and residues organic matter (red arrows) in grain-supported limestones, (**l**) grain-supported facies with extensive sparry calcite cement (author's own edit).*

Two such tectonic events have occurred in the basin, including the obduction of ophiolites in later Cretaceous-early Tertiary and the Zagros Orogeny caused by the collision of the Arabian and Eurasian plates in Oligocene (Agard et al. 2011). The flow of such basinal brines is further evidenced by the presence of discrete euhedral, thermochemical pyrite (TSR) and saddle dolomite in the vicinity of stylolite (Fig. 45b, i and Fig. 46d). Where the occurrence of the saddle dolomites is attributed to the flow of hydrothermal fluids (Mansurbeg et al. 2024). Dolomite rhombs found along the stylolites (Fig. 44b) indicate that precipitation occurred from magnesium-rich fluids during the basin's lateral compression, which was likely caused by the obduction of the Oman Ophiolites in the Late Cretaceous period (Paganoni et al. 2016). The pervasive euhedral to subhedral dolomite rhombs in the backshoal pelletal grainstones and Lithocodium-Bacinella facies (F-5 and F-6; Fig. 25; Fig. 26 and Fig. 45d) indicates early dolomitization, likely during shallow burial or even at/near the sediment–water interface. The preservation of grain outlines (e.g., peloids and pellets) suggests that dolomitization occurred prior to significant compaction and cementation, consistent with eogenesis.

Framboidal pyrite aggregates are characterized by their distinctive raspberry-like morphology composed of tightly packed microcrystals (Fig. 46c). This is attributed to microbial sulfate reduction (BSR) during early anoxic eogenesis, within organic-rich microenvironments in pore spaces during shallow burial or even syn-depositional (Cavalazzi et al. 2014; Morad et al. 2019). In contrast, the euhedral to subhedral crystal forms, associated with dolomitic limestones and in the vicinity of stylolites (Fig. 46d) indicating later-stage (mesogenetic) diagenetic growth is presumably related to the derivation of H_2S from thermochemical sulfate reduction (TSR) through the interaction of gypsum/anhydrite with hydrocarbons upon burial of the formation to depths at which temperatures exceeding 130 °C (Worden et al. 1995; Worden and Carrigan 2005). The spatial and textural evolution of pyrite thus reflects a diagenetic transition from early microbial to later thermochemical processes under reduced porewater flow regimes.

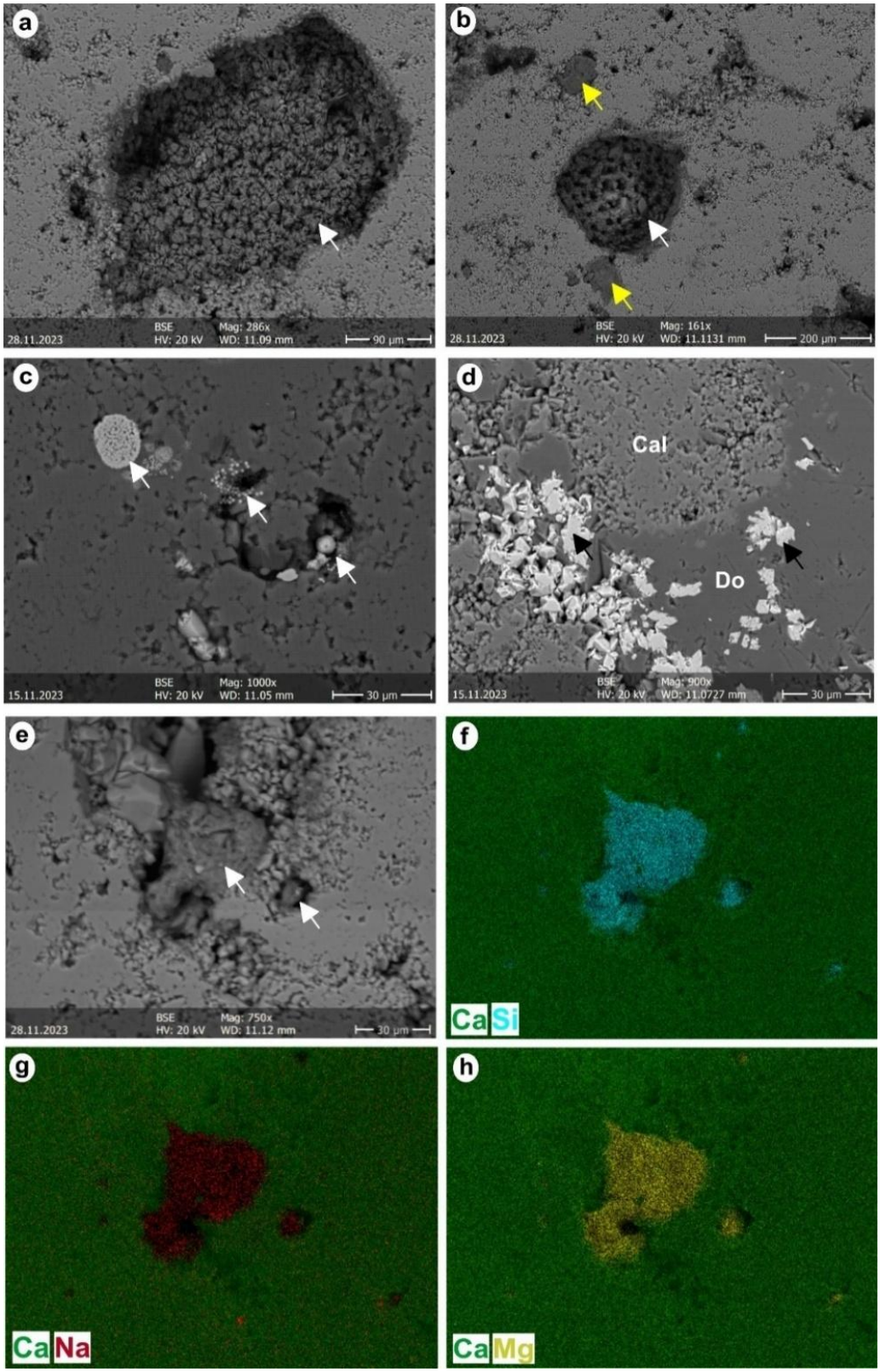

Figure 46. *Backscattered electron (BSE) images and Energy Dispersive Spectroscopy (EDS) maps shows pore-filling clay minerals and pyrite in the Yamama Formation. (**a**, **b**) Pore-filling kaolinite (white arrows) and saponite (yellow arrows) in the lagoonal facies. (**c**) Framboidal*

*pyrite (white arrows). (**d**) Euhedral pyrite crystals (black arrows) replace dolomite. (**e**) Pore-filling saponite (white arrows). (**f–h**) EDS elemental maps: (**f**) Calcite-silicon Ca–Si, (**g**) Calcite-sodium Ca–Na, and (**h**) Calcite-magnesium Ca–Mg in Na-rich saponite (author's own edit).*

The pore fillings saponite within the lagoonal facies (F-2 to F-4) of the Yamama Formation is interpreted as authigenic pore filling mineral (Na-saponite) (Fig. 46b, e-h). The high Mg, Si, and Na content, with low Al, is consistent with a trioctahedral smectite, typical of saponite formed in early diagenetic conditions in restricted, Mg-rich carbonate settings. This is likely the result of early diagenetic reaction of alkaline carbonate with Mg-rich porewaters, under restricted, evaporative marine conditions (Bristow et al. 2009).

5.5 Stable Isotopic Composition and Fluid Inclusion Microthermometry

Stable carbon and oxygen isotope analyses of blocky calcite cement ($\delta^{18}O_{VPDB}$ = -6.79‰ to -3.69‰; $\delta^{13}C_{VPDB}$ = +2.1‰ to +2.4‰) and dolomite ($\delta^{18}O_{VPDB}$ = -4.2‰ to -3.9‰; $\delta^{13}C_{VPDB}$ = +0.53‰ to +1.56‰) as well as bulk limestones of grain and mud-supported limestones ($\delta^{18}O_{VPDB}$ = -6.43‰ to -3.35‰; $\delta^{13}C_{VPDB}$ = +0.41‰ to +1.74‰) with various depositional textures (Fig. 47) provide important clues to the geochemical conditions. The dolomite samples, which occur along bioturbations sites, and the blocky calcite crystals were obtained by micro-drill. The $\delta^{13}C_{VPDB}$ values of these different carbonate types fall within the range inferred for Lower Cretaceous seawater (0 to +3‰: according to Moldovanyi and Lohmann (1984)) suggesting that dissolved carbon is derived from marine porewaters and dissolution of the grains. Regarding the bulk samples (mud- and grain-supported), the isotopic values also reflect the marine mud matrix and grains components in the matrix-supported and grain-supported limestones, respectively.

Nevertheless, the highest $\delta^{13}C_{VPDB}$ values recorded in the dolomite samples may suggest partial derivation of dissolved carbon from microbial methanogenesis (Irwin et al. 1977). The $\delta^{18}O_{VPDB}$ values obtained are lower than those calculated for calcite precipitated at 20-30°C ($\delta^{18}O_{VPDB}$ = -3‰ to -2‰) in isotopic equilibrium with Lower Cretaceous seawater ($\delta^{18}O_{VSMOW}$ = -1‰) using the oxygen isotopes fractionation equation of Kim and O'Neil (1997). Enrichment of marine diagenetic carbonates with ^{16}O is attributed to carbonate precipitation at elevated temperatures during burial diagenesis. The low $\delta^{18}O_{VPDB}$ values of the bulk samples is attributed to the presence of significant amounts of calcite cement which is dominated by micro-overgrowths

around micrite mud in the matrix-supported limestones (Alsuwaidi et al. 2021), and to the circumgranular, the scattered syntaxial and equant calcite cements of the grain-supported limestones. The overall lower $\delta^{18}O_{VPDB}$ values of the grain-supported limestones is attributed to greater amounts of intergranular calcite cement compared to the matrix supported limestones (Fig. 47). This interpretation is supported by the lowest $\delta^{18}O_{VPDB}$ values are measured in the calcite cement.

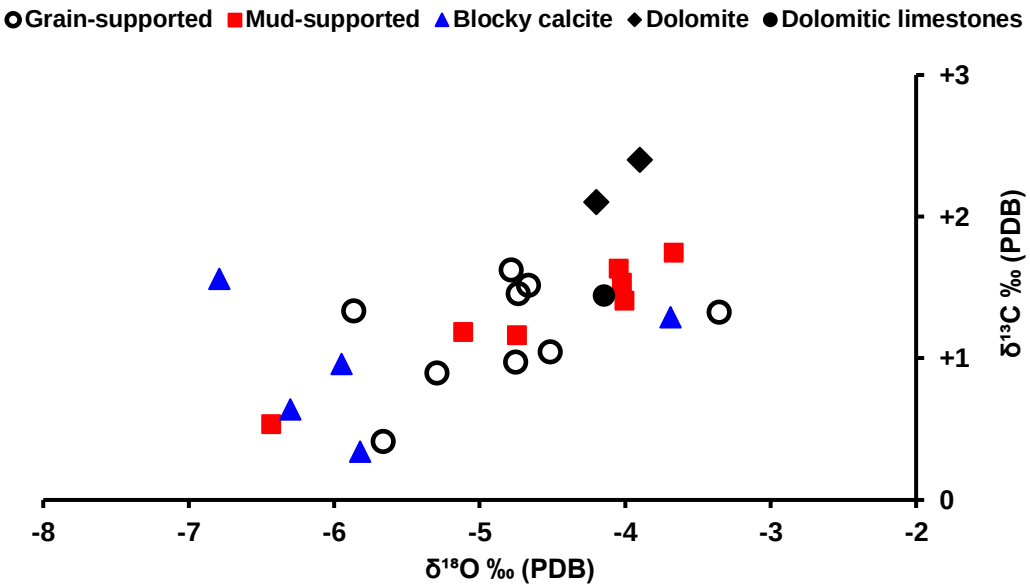

Figure 47. *Cross plot of $\delta^{13}C$ and $\delta^{18}O$ isotope values for various components from the Yamama Formation, illustrating isotopic variations among different carbonate facies and components (author's own edit).*

Fluid inclusion microthermometry of calcite cement is crucial for reconstructing the temperature and composition of paleo-fluids, providing insights into diagenetic conditions and fluid flow history in sedimentary basins. Fluid inclusion petrography in calcite cement helps identify inclusion types, origins, and entrapment sequences, offering vital context for interpreting fluid evolution and diagenetic processes. Petrographic examinations revealed the presence of aqueous two phase (liquid and vapor). Primary fluid inclusions were identified by their presence in alternating inclusion-rich and inclusion-poor zones, and the preferential orientation or shape of such inclusions in the direction of crystal growth. Secondary fluid inclusions were mostly found as trails cutting across the calcite crystals. Homogenization temperatures (minimum fluid entrapment temperatures; T_h) and final ice melting temperatures (Tmice) were measured. The latter, which reflects fluid salinity (wt% NaCl eq.; Bodnar 1993; Goldstein and Reynolds 1994),

is the temperature at which the last ice crystal melts in an aqueous fluid inclusion. Synthetic pure water and CO_2 inclusions were used to calibrate the stage thermocouple.

Microthermometric analyses, which were performed on the primary fluid inclusion in the calcite cements, revealed that the T_h range from 80°C to 145°C. These values are consistent with estimated maximum burial temperatures (~116°C at 3200 m depth, assuming a 30°C/km geothermal gradient). This elevated Th, that exceeds the maximum burial temperature of the formation, suggests that the brine originated from deeper, higher-temperature formations. Evidence of thermochemical sulfate reduction (TSR) and saddle dolomite further indicates that these brines are likely sourced from the evaporitic Gotnia Formation. The eutectic temperatures vary between -12°C and -10°C and the final ice melting temperature of -7°C to -6°C. Using the empirical formula of Bodnar (1993), these values indicate NaCl–KCl-H_2O dominated brines with total salinity of about 10 wt.% NaCl equivalent. Using the most common $\delta^{18}O_{VPDB}$ values of calcite cement (around -6.8‰ to -5.8‰; Fig. 47) and the T_h range from 80°C to 145°C, the $\delta^{18}O_{VSMOW}$ values of the brines +4‰ to +8‰ according to the oxygen fractionation equation of Kim and O'Neil (1997). These positive oxygen isotopic values are typical for basinal brines (e.g., Egeberg and Aagaard 1989). The presence of calcite cement in the vicinity of stylolites support the burial diagenetic origin and the chemical compaction of the limestones acted as source of the required dissolved mass. Moreover, stylolites have likely acted as conduits for flow of basinal brines (Paganoni et al. 2016; Morad et al. 2018b).

5.6 Reservoir-quality evolution of the limestones

The porosity and permeability of limestones are controlled by a complex interplay between depositional texture and diagenetic factors (Morad et al. 2018a). Depositional texture, encompassing grain size and sorting, exerts profound control on primary porosity and, most importantly, permeability. There are several types of pores and pore sizes (micro, meso and macropores) the distribution of which is strongly linked to the depositional texture of the limestones and the diagenetic alterations. Macro and meso porosity in the grain-supported limestones of the Yamama Formation is dominantly primary/depositional interparticle and intraparticle pores, and less frequent moldic and vuggy pores (Fig. 43-45). The primary intraparticle pores occur within Lithocodium-Bacinella algal facies arises from their biogenic nature (Mohammed and Velledits 2024a). Microporosity in the grainstones occurs within the

peloids, which include micritized grains, peloids and fecal pellets which shows frequent sparry calcite cements filling interparticle pores.

The grain-supported Yamama limestones are dominated by macropores, which thus account for the higher initial permeability than matrix-supported limestones (Fig. 43; Fig. 44e, f, h-k). However, the wide ranges of porosity and permeability suggest modifications by a variety diagenetic process, such as cementation, micritization, compaction, dissolution, and dolomitization. Closer packing of the grains and pseudoplastic deformation of the ductile peloids by mechanical compaction has caused most of the porosity and permeability reduction (Fig. 43a and b; Fig. 44e; Fig.45l). These limestones experienced limited improvement to reservoir quality by diagenetic processes, including dolomitization and dissolution of the grains.

The core-plug porosity and permeability measurements of the formation reveal up to 25-27% porosity, and the permeability ranges from 1 to 1000 mD (Fig. 17). The wide ranges of permeability for each porosity value in the grain-supported limestones reflect the amounts of mud matrix (e.g., in packstones) and of moldic and intraparticle pores that are poorly connected to the overall pore system (e.g., in the Lithocodium-Bacinella bodies). Micritization of the grains resulted in the formation of abundant intragranular micropores. This process converted the macropore dominated grain-supported limestones to bimodal macro- and micropore dominated limestones (cf. Morad et al., 2018). Moreover, these limestones will be characterized by high total porosity and variable permeability values (Fig. 17).

Limestones with the lowest most porosity and permeability include the wackestones and mudstones as well as grain-supported limestones which are extensively cemented by calcite (Fig. 44c and e) or suffered extensive mechanical compaction (e.g., F-5; Fig. 43a and b; Fig. 45l) owing to their peloidal composition (small peloids and pellets) combined with the lack of scattered fabric-supporting cements, such as circumgranular and scattered equant calcite cements.

5.7 Porosity Evolution and Paragenetic Sequence in the Yamama Formation

A paragenetic sequence and a conceptual model have been constrained to illustrate the spatial and temporal diagenetic evolution and porosity development of the Yamama Formation carbonates (Fig. 48 and 49). These models are based on integrated petrographic observations,

fluid inclusion microthermometry, and stable isotope geochemistry, allowing for a robust reconstruction of burial-related diagenetic processes across a carbonate ramp system.

Grain-supported facies (e.g., oncoidal grainstones, peloidal and ooidal facies, and Lithocodium-Bacinella facies) deposited in the intertidal and shoal facies formed the reservoir units in the Yamama formation. These contain abundant primary interparticle and intraparticle pores. These facies undergo early cementation by circumgranular (arounds grains), scattered equant and syntaxial calcite overgrowths, which led to partial occlusion of primary porosity during eogenesis. The observed dissolution of unstable grains (aragonitic) during episodes of subaerial exposure, increased porosity by creating secondary porosity. In mesogenesis, precipitation of the scattered equant calcite and saddle dolomite further help protecting porosity from the compaction. Therefore, preserved good porosity in the reservoir units.

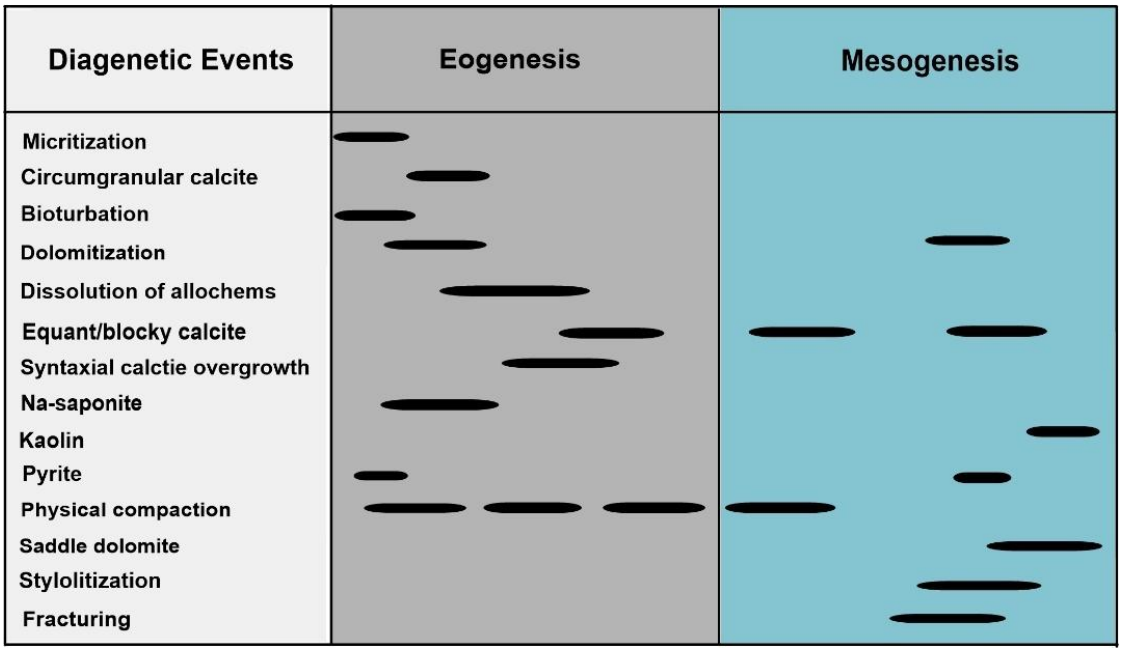

Figure 48. *A paragenetic sequence of the main diagenetic features in the Yamama Formation Adapted from Mohammed and Velledits (2024b).*

Mud-supported facies (e.g., lagoonal wackestones and outer ramp mudstones) exhibit initially low primary porosity dominated by intraparticle and micropores in the mud matrix. Early diagenesis is characterized by micritization, bioturbation, and formation of authigenic minerals (e.g., kaolinite and Na-saponite), especially in restricted lagoonal environments. The eogenesis bioturbation and micritization helped in texture transformation from wackestones to packstones (e.g., F-4; Fig. 24). Dissolution of grains during eogenesis was followed by the precipitation of

equant calcite cement and pore-filling authigenic minerals. While interparticle microporosity within mud was reduced by mechanical compaction and occluded by calcite micro-overgrowths (Fig. 49). During mesogenesis, the development of stylolites acted as a source of calcium carbonate, further contributing to the formation of blocky calcite cement. These stylolites filled bitumen and dissoluble materials and later acted as barrier for the vertical fluid flow in the non-reservoir units, therefore, separated the reservoir units.

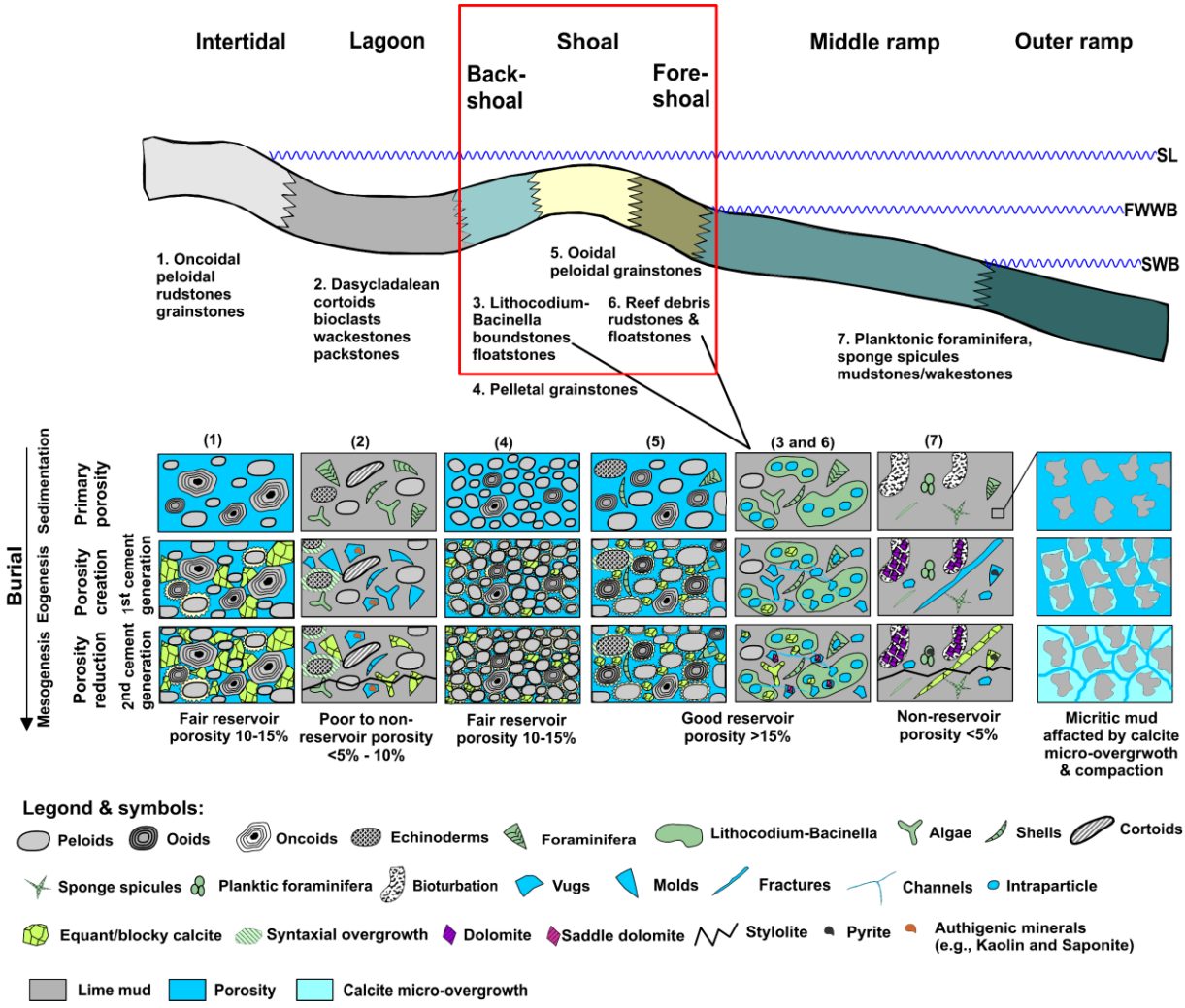

Figure 49. *Conceptual model shows porosity and diagenetic processes evolution across the Yamama carbonate ramp during burial. The three panels on the right illustrate the progressive compaction and cementation of lime mud with depth, representing the diagenetic evolution of lime mud in mud-supported facies (lagoonal, middle and outer ramp). The shoal ooidal, peloidal facies, Lithocodium-Bacinella float- to boundstones, and the reef debris facies represent good reservoir facies, while mud-supported middle and outer-ramp facies are non-reservoir facies. The mud-supported lagoonal facies form poor to non-reservoir facies. The intertidal oncoidal and the backshoal pelletal grainstones facies form fair reservoir facies (author's own edit).*

These models reveal a complex interplay between depositional texture, mineral stability, and burial diagenesis in controlling reservoir quality. Grain-supported facies tend to retain better porosity if early dissolution was effective before deep cementation, while mud-supported facies generally suffer pervasive occlusion due to compaction and cement precipitation. These findings highlight the importance of facies-controlled diagenetic pathways in the heterogeneity of the Yamama Formation reservoir.

5.8 Facies distribution

Distinct facies types control the hydrocarbon storage potential in each reservoir and non-reservoir units in the Yamama Formation. The porosity results obtained from well logs show a clear matching with the porosity in thin sections. The non-reservoir units (B0-B3) are characterized by low porosity values (generally <5%) and higher volume of shale and high-water saturation. These units are predominantly composed of mud-supported facies, including the lagoonal facies (F-2, F-3, F-4), the middle-ramp facies (F-11, F-12, F-13), the outer-ramp facies (F-14). Consequently, these facies formed barriers that separate the reservoir units causing compartmentalization within the formation. The reservoir units (YRA-YRD) are characterized by the grain-supported facies and the Lithocodium-Bacinella facies (F-1, F-5 to F-10). These facies are defined by the abundance of the interparticle, interparticle and vuggy porosity (Table 3).

The reservoir unit YRA shows poor to fair reservoir properties in Nasiriya (Fig. 13) and Ah'Dimah (Fig. 15) oilfields (Table 3). This unit is dominated by the lagoonal F-3 and F-4 facies in Nasiriya, turning into F-7, F-9 and F-11 in Ah'Dimah. The F-7 and F-9 show good reservoir properties in most cases. Although F-11 exhibits a grain-supported texture, it has poor reservoir quality and is classified as a non-reservoir facies. This is due to the predominance of fine grains (including peloids, pellets, and foraminifera), which are more susceptible to compaction than the larger grains found in other facies, and to subsequent pervasive cementation. Therefore, deteriorated the reservoir quality of the YRA in Nasiriya and Ah'Dimah oilfields. In contrast, the YRA is good reservoir unit that is dominated by F-6 and F-7 in West Qurna. The reservoir unit YRB fair, good, and poor reservoir characters in Nasiriya, Ah'Dimah, and west Qurna respectively. The YRB is dominated by the F-4 in Nasiriya, turning into F-6, F-7 and F-9 in Ah'Dimah, and defined by the presence of EF-2 in West Qurna Oilfield.

In contrast, the reservoir unit YRC demonstrates high porosity values in Nasiriya and Ah'Dimah oilfields, reaching up to 22% in some intervals, due to the presence of grain-supported limestone (F-7, F-10) in Nasiriya, turning into the reefal facies (F-9) in Ah'Dimah Oilfield. However, this unit shows the presence of the F-2 in West Qurna, therefore, deteriorated the reservoir quality. The domination of the F-8 in the reservoir unit YRD1 in Nasiriya Oilfield caused the good reservoir properties in this unit. YRD1 exhibits high porosity and low water saturation and forms a good reservoir unit. While YRD2, which is dominated by the intertidal oncoidal limestones, shows high-moderate porosity but is water-bearing. The fluids density differences have likely resulted in water saturating the lower part of the formation (YRD1), due to its position below the hydrocarbon-bearing zones. This highlights how fluid density, gravitational forces, and facies distribution collectively influence fluid segregation, shaping the heterogeneity and reservoir potential within the Yamama Formation.

5.9 Sequence stratigraphy of the Yamama Formation

The Yamama Formation is heterogeneous and divided into four reservoir units, from top to bottom as Yamama Reservoir A (YRA), Yamama Reservoir B (YRB), Yamama Reservoir C (YRC), and Yamama Reservoir D (YRD). The YRD was subdivided into YRD1 (hydrocarbon bearing) and YRD2 (water bearing). These reservoir units are separated by four non-reservoir intervals, as Barrier 0 (B0), Barrier 1 (B1), Barrier 2 (B2), and Barrier 3 (B3), which act as seals or flow barriers within the formation. The formation exhibits considerable variability in reservoir quality, both between different fields and within the same field, presenting a significant challenge for distinguishing the reservoir from non-reservoir units. Another debated issue is the determination of its lower and upper boundaries with the underlying Sulaiy and overlying Ratawi formations, as these three formations are part of a regressive 2nd-order, first cycle of the megasequence AP8 (Sharland et al., 2004).

Sequence stratigraphy offers a critical tool to decipher the distribution of the reservoir and non-reservoir units within the formation across different fields. The depositional sequence framework of the Yamama Formation is poorly constrained in Iraq. The AP8 megasequence, as described by Sharland et al. (2004) is bounded by the Late Tithonian unconformity (149 Ma) at the base and the Middle Turonian unconformity (marked by ophiolite obduction, 92 Ma), at the top (Fig. 2). This sequence comprises six second order cycles. The lower cycle (Late Tithonian-Middle Valanginian) includes the Sulaiy, Yamama, and Ratawi formations in southern Iraq, the

Makhul and Zangura formations in central Iraq, and Garagu, Sarmord, Karimia, and Chia Gara formations in northern Iraq (subsurface), Garagu, Sarmord, Balambo, and Chia Gara (outcrops), with the Rayda and Salil formations in Oman, Makhul and Minagish in Kuwait, and the Sulaiy and Habshan formations in Qatar and the UAE (Fig. 7; Aziz and El-Sattar, 1997; Nagm et al., 2018; Mohammed and Velledits, 2024a). This cycle comprises four MFSs, including J110, K30, K20, and K10 (Sharland et al. 2004; Haq and Al-Qahtani 2005). The combination of sequence stratigraphy, facies analysis, and regional correlation provides a powerful framework for: (i) understanding the facies distribution of the Yamama Formation, and (ii) allowing more accurate reservoir characterization, stratigraphic modeling, and hydrocarbon exploration throughout the Arabian Plate.

The Yamama formation is divided into three 3rd order sequences (Li et al. 2024), where the Sulaiy-Yamama boundary considered the Jurassic-Cretaceous contact. However, Sharland et al. (2004) considered the upper part of the Sulaiy Formation as belonging to the Lower Cretaceous, marked by the Middle Tithonian unconformity separating the AP7 and AP8 megasequences (Fig. 2 and 3). Whereas the formation has been divided into three cycle represented by three (Jameel and Al-Zaidy 2022) and four (Al Mafraji and Al-Zaidy, 2019) highstand system tracts (HST) with no transgressive system tracts, while Idan et al. (2020) described it as consisting of a seaward stepping (progradation) and landward stepping (retrogradation) separated by a sequence boundary. The Garagu Formation (equivalent to the Yamama Formation in northern Iraq) subdivided into multiple HST: two in Jambur, three in Khabbaz, and four in Qara Chauq (Mahdi and Al-Zaidy 2024). These studies have not considered the relative and global sea-level changes. Sadooni (1993) delineated three reservoir units within the formation, separated by impermeable units based on depositional facies, without incorporating sequence stratigraphy or stacking patterns of each the depositional sequences. The Habshan Formation in eastern Abu Dhabi has been subdivided into three sequences (Aziz and El-Sattar, 1997). Sequences 1 and 3 comprising transgressive systems tract (TST) and HST, while sequence 2 linked to a lowstand system tract. The Yamama Formation consists of three depositional cycles bounded by MFS in Saudi Arabia (Nagm et al., 2018). The latter authors further noted that the upper boundary of the Yamama Formation with the Buwaib Formation (equivalent to the Ratawi Formation in southern Iraq) is delineated by a sequence boundary, and that the Yamama-Sulaiy contact represents the Berriasian–Valanginian boundary.

In this study, critical features such as the Yamama Formation tops and bottoms, sequence boundaries (SBs), maximum flooding surfaces (MFSs), and reservoir units have been identified using an integrated and comprehensive approach including borehole well reports, well logs, core samples, petrography, regional correlations, and previously published studies for the Yamama Formation in Iraq and Middle East. This approach provided a better understanding of reservoir distribution in relation to sequence stratigraphy. Sequence stratigraphy of the Yamama Formation was built based on the approach of Catuneanu (2022).

The Yamama Formation was deposited within a shallow-water carbonate ramp system during a 2nd transgressive cycle, in association with the underlying Sulaiy and the overlying Ratawi formations (Sharland et al. 2004). This stratigraphic setting rises challenges in confidently identifying sequence boundaries (SBs) and maximum flooding surfaces (MFSs), due to the transitional nature of facies and the lack of clear stratigraphic breaks. Furthermore, in southern Iraq (the studied area), the Yamama Formation is deeply buried (>4000m), making continuous coring operations technically difficult and economically unfeasible across the entire interval. The SBs and MFSs are identified based on facies change correlated with petrophysical data (well logs). The MFSs were recognized based on facies change from mud-supported limestones with low skeletal components and/or those with planktonic foraminifera and sponge spicules reflecting facies deposited in deeper water settings (middle and outer ramp) into the shallower facies represented by more grain-supported limestones with abundance of skeletal and non-skeletal grains.

Sequence boundaries within the Yamama Formation were defined based on vertical facies transitions. The change from high-energy, grain-supported or reefal limestones into overlying low-energy, mud-supported limestones. These abrupt changes in depositional energy are interpreted to reflect a rise in relative sea level. Although direct evidence of subaerial exposure (e.g., karstification or paleosols) is not clearly observed within the formation, indirect indicators are present. Notably, observable dissolution and syntaxial calcite overgrowths occur in the upper highstand systems tracts, within grain-supported facies. The dissolution affected both skeletal and non-skeletal grains and may be linked to episodes of subaerial exposure. Consequently, the sequence boundaries are interpreted as correlative sequence boundaries (Type 2), representing subtle or poorly preserved subaerial exposure surfaces (Wagoner et al. 1988; Read 1995).

The sequence stratigraphy of the Yamama Formation is defined by four depositional sequences (DS-1 to DS-4) that are characterized by coarsening-upward cycles (Fig. 50 and 51). Transitional contacts between the Yamama Formation and the underlying Sulaiy and the overlying Ratawi formations represented by MFSs. However, these MFSs belong to the Ratawi and Sulaiy rather than to the Yamama Formation.

The depositional environment models presented for the Yamama Formation illustrate the spatial and temporal facies distribution across a carbonate ramp system during relative sea-level change (Fig. 52). These models correspond to the TST and HST of four successive depositional sequences (DS-1 to DS-4), reflecting dynamic shifts in depositional settings. Facies types range from restricted lagoonal wackestones in the inner ramp to high-energy shoal grainstones and spiculitic wackestones in the outer ramp. Notably, the formation emphasizes the lateral migration of facies belts in response to fluctuating sea levels, which played a critical role in the evolution and distribution of reservoir-prone units. The ooidal and peloidal grainstones, Lithocodium–Bacinella boundstones, and reefal build-ups are key facies contributing to enhanced reservoir quality. The facies retrograded landward (west- southwest), during sea level rise (transgression system tract TST) forward Nasiriya oilfield. While they prograded basinward (north- northeast) forward Ah'Dimah and West Qurna oilfields during sea level fall (highstand system tract HST).

5.9.1 Depositional sequence 1 (DS-1)

Transgressive system tract (TST1) (Sulaiy Formation)

The TST1, which represents the upper most Sulaiy Formation, is composed of mud-supported limestones and exhibits abundance of organic matters/bitumen and pyritization (Fig. 18).

Highstand systems tract (HST1)

The HST1 corresponds to the reservoir unit Yamama Reservoir D (YRD) (Fig. 50; Fig. 51 and Table 3), which is located at the base of the Yamama Formation and above the Sulaiy Formation. The boundary between the Sulaiy and Yamama formations is not well-defined due to gradual facies change and lack in continuous core interval data. In the Nasiriya area (Fig. 51), the top of the Sulaiy Formation is characterized by fine-grained and marly limestones, transitioning into argillaceous and marly limestones, to the east, in the Ah'Dimah (Fig. 50). In Ah'Dimah, the boundary between the non-reservoir unit B4 (the very base of the Yamama Formation) and the

overlying water-bearing unit YRD2 likely marks the contact between the Sulaiy and Yamama formations. This depositional sequence is identified by abrupt decrease in gamma-ray values and a corresponding relative increase in sonic log readings.

The HST1 represented by the intertidal oncoidal-peloidal grainstones/rudstones, the backshoal pelletal grainstones, and the ooidal-peloidal grainstones dominated facies. These facies are developed in the Nasiriya Oilfield (e.g., F-1, F-5, and F-8; Fig. 51). The thickness of this system tract varies across the regions between 43 m in Nasiriya, 80 m in Ah'Dimah, and 20 m in West Qurna (Table 3). The sequence is dominated by the porous electrofacies, the EF-3 and EF-4 in Nasiriya and Ah'Dimah, and the EF-5 in West Qurna. The lower part (YRD2) of this cycle consists of water-bearing units, while the upper part (YRD1) is reservoir unit in the Nasiriya and Ah'Dimah oilfields. Notably, and based on the data availability, the water-bearing zone (YRD2) within this cycle is absent in the studied well of West Qurna (Fig. 50 and Table 3). The late HST1 is dominated by good interparticle porosity accounting for the reservoir unit YRD1 in the studied area. Dissolution observed in the skeletal and non-skeletal grains (e.g., peloids).

5.9.2 Depositional sequence 2 (DS-2)

The DS-2 is interpreted as TST2 separated by the HST by MFS1. The sequence boundary (SB1) between DS-1 and DS-2 is defined by a shift from the ooidal-peloidal shoal grainstones in the upper most HST1 to the outer-ramp spiculitic mud- to wackestones of lower most TST2 in the DS-2. The SB1 is defined by abrupt increase in gamma-ray values, decrease in sonic logs, and the occurrence of the dense and marly limestones electrofacies overlying the porous limestones.

Transgressive system tract 2 (TST2)

The TST2 corresponds to the non-reservoir unit B3 (Table 3). The TST2 is characterized by the argillaceous limestone lithofacies and defined by the marly limestone (EF-1) and the dense limestones (EF-2) electrofacies (Fig. 50). The thickness ranges from 20 m, 15 m, and 30 m in Nasiriya, Ah'Dimah and West Qurna oilfields, respectively. This system tract is dominated by the outer-ramp spiculitic mud- to wackestones (F-14) in the Nasiriya oilfield, turning into the lagoonal bioclastic mud- to wakcestones (F-2) in the Ah'Dimah and West Qurna, reflecting lateral facies changes within the TST2 across the ramp from west to east. The TST2 encounters the appearance of the *Bramkampella arabica* and *Freixialina planispiralis* (Fig. 51).

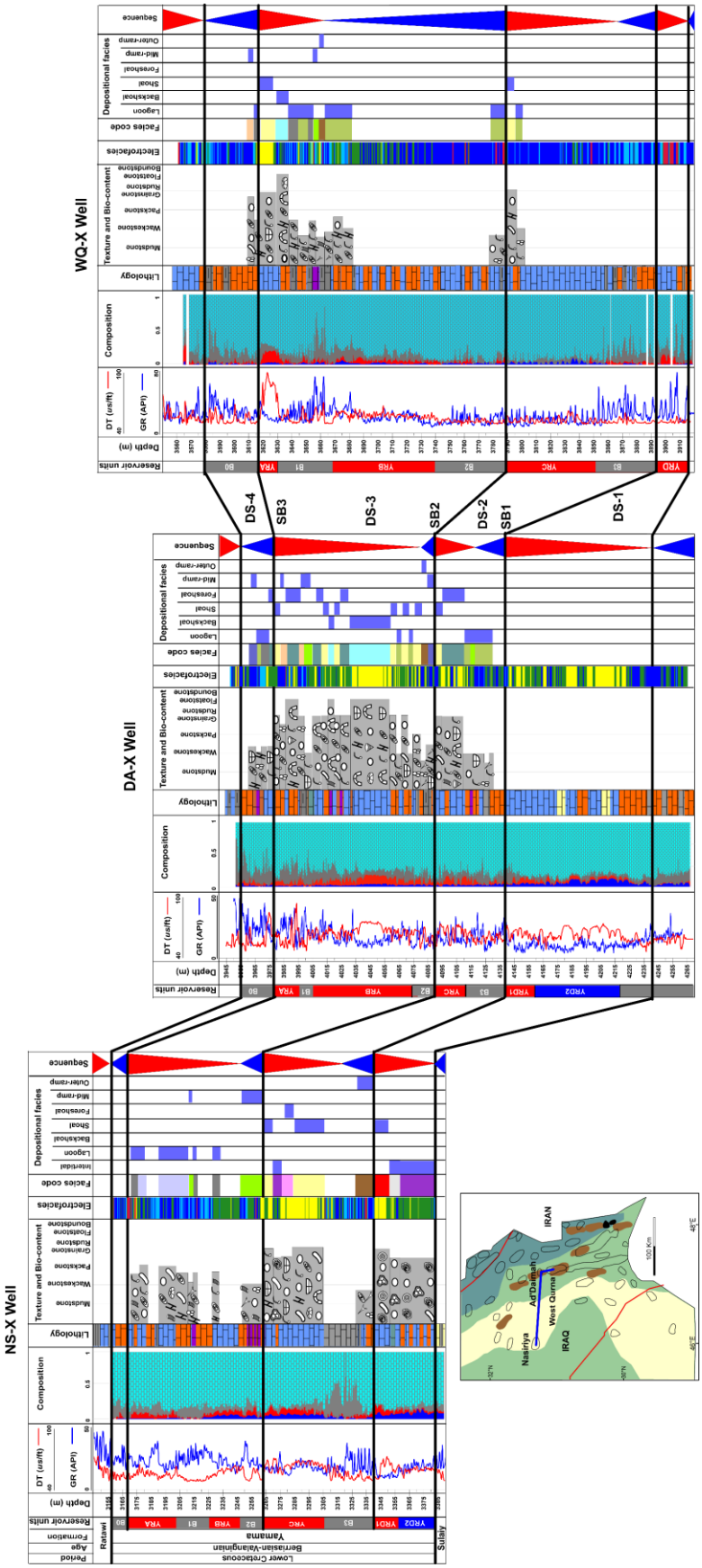
WQ-X Well
DA-X Well
NS-X Well
DS-4
SB3
DS-3
SB2
DS-2
SB1
DS-1
Sequence
Depositional facies
Outer-ramp
Mid-ramp
Foreshoal
Shoal
Backshoal
Lagoon
Facies code
ElectroFacies
Texture and Bio-content
Mudstone
Wackestone
Packstone
Grainstone
Rudstone
Floatstone
Boundstone
Lithology
Composition
DT (us/ft)
GR (API)
Depth (m)
Reservoir units
Lower Cretaceous
Berriasian-Valanginian
Yamama
Ratawi
Sulaiy
IRAN
IRAQ
Nasiriya
Ad Diwaniyah
West Qurna
100 Km

Figure 50. *Sequence stratigraphy correlation of the Yamama Formation in south of Iraq running between Nasiriya (NS-X), Ah'Dimah (DA-X), and West Qurna (WQ-X) oilfields, showing four depositional sequences (DS-1–DS-4), sequence boundaries (SB1–SB3), and lateral and vertical facies changes. The integration of lithology, petrography, electrofacies, and petrophysical well logs data emphasizes lateral heterogeneity, reservoir distribution, and system tracts (author's own edit).*

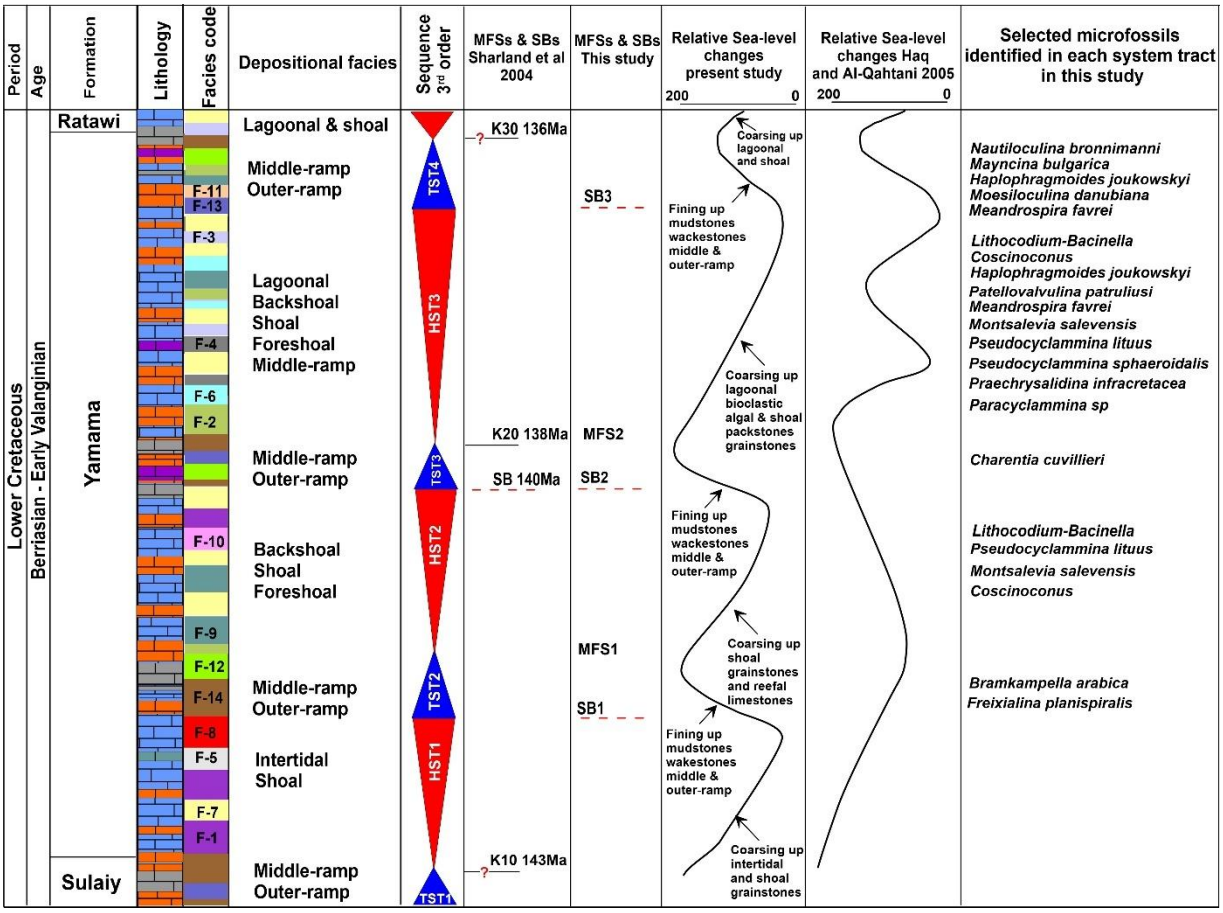

Figure 51. *Synthetic sedimentological/graphic log of the Lower Cretaceous Yamama Formation showing lithology, microfacies, depositional environments, and the distribution of foraminifers in each system tract. Color-coded facies are used to interpret third-order depositional sequences and relative sea-level changes. MFSs (K10, K20, K30) and sequence boundaries (SBs) are correlated with Sharland et al. (2004) and compared with the regional sea-level curve of Haq and Al-Qahtani (2005), highlighting transgressive–regressive trends and reservoir-related facies transitions. Refer to Figure 14 for legend (author's own edit).*

Maximum flooding surface 1 (MFS1)

The MFS1 of the DS-2 is characterized by the presence of the outer-ramp spiculitic mud- to wackestones (F-14) in Nasiriya Oilfield, and the middle-ramp bioturbated dolomitic mud- to wackestones (F-12) in Ah'Dimah Oilfield. This defined by the higher gamma-ray readings, and the occurrence of the marly limestones (EF-1) in studied area.

Highstand system tract 2 (HST2)

The HST2 corresponds to the reservoir unit YRC with thickness of 50 m, 35 m, and 75 m in Nasiriya, Ah'Dimah and West Qurna, respectively (Fig. 50 and Table 3). A gradual change in facies is observed within the HST2 from the intertidal and shoal grain-supported limestones. These include the intertidal (F-1), the shoal (F-7), and foreshoal (F-10) in the Nasiriya, transitioning into the reefal (F-9) and the shoal (F-7) in the Ah'Dimah Oilfield (Fig. 50). These grainstones are dominated by good interparticle and dissolution of skeletal and non-skeletal grains, in addition to the presence of syntaxial calcite overgrowth (typical for the F-7, F-10, and F-9; Fig. 43 and 45) that are characterized by the EF-3 in the Nasiriya and Ah'Dimah. The HST2 turns into dense limestones (EF-2) in West Qurna Oilfield and reducing the reservoir quality in the field. Several foraminifers occur within the HST2, including *Montsalevia salevensis, Pseudocyclammina lituus,* and Representatives of the genus *Coscinoconus.*

5.9.3 Depositional sequence 3 (DS-3)

The DS-3 is represented by TST3, MFS2, and HST3 (Fig. 50). The sequence boundary SB-2 between DS-2 and DS-3 is defined by abrupt facies change from the shoal peloidal grainstones (F-7) of the uppermost HST2 to the mud-supported middle-ramp bioturbated dolomitic limestones (F-12), and foraminiferal wackestones (F-13) in the Nasiriya and Ah'Dimah oilfields into the lagoonal bioclastic mud- to wackestones (F-2) in the West Qurna Oilfield (Fig. 50). This depositional sequence is marked by the appearance of the Lithocodium-Bacinella along with the *Dasycladales, Salpingoporella,* and *Pseudocyclammina lituus.*

Transgressive system tract 3 (TST3)

The TST3 has a thickness of around 6 m, 10 m, and 120 m in the Nasiriya, Ah'Dimah, and West Qurna oilfields, respectively (Fig. 50). In Nasiriya and Ah'Dimah, this systems tract corresponds to the non-reservoir unit B2, while in West Qurna, it corresponds to the non-reservoir unit B2 and the reservoir unit YRB, and lower part of the non-reservoir unit B1. Notably, the YRB in West Qurna shows poor to fair reservoir properties. The TST3 is dominated by the middle-ramp facies (F-12) in Nasiriya, the middle-ramp facies (F-13) and the outer-ramp facies (F-14) in Ah'Dimah, and by the lagoonal (F-2) in West Qurna Oilfield. The TST3 is characterized by the dolomitic and argillaceous limestones in Nasiriya, the marly and argillaceous limestones in Ah'Dimah and West Qurna. The dense limestones (EF-2) and the

presence of the marly limestones (EF-1) electrofacies are characteristic for this system tract. Thin streaks of the vuggy limestones (EF-5) occurred in the lower part of the TST3 in West Qurna. The *Charentia cuvillieri* foraminifera encounters in this system tract.

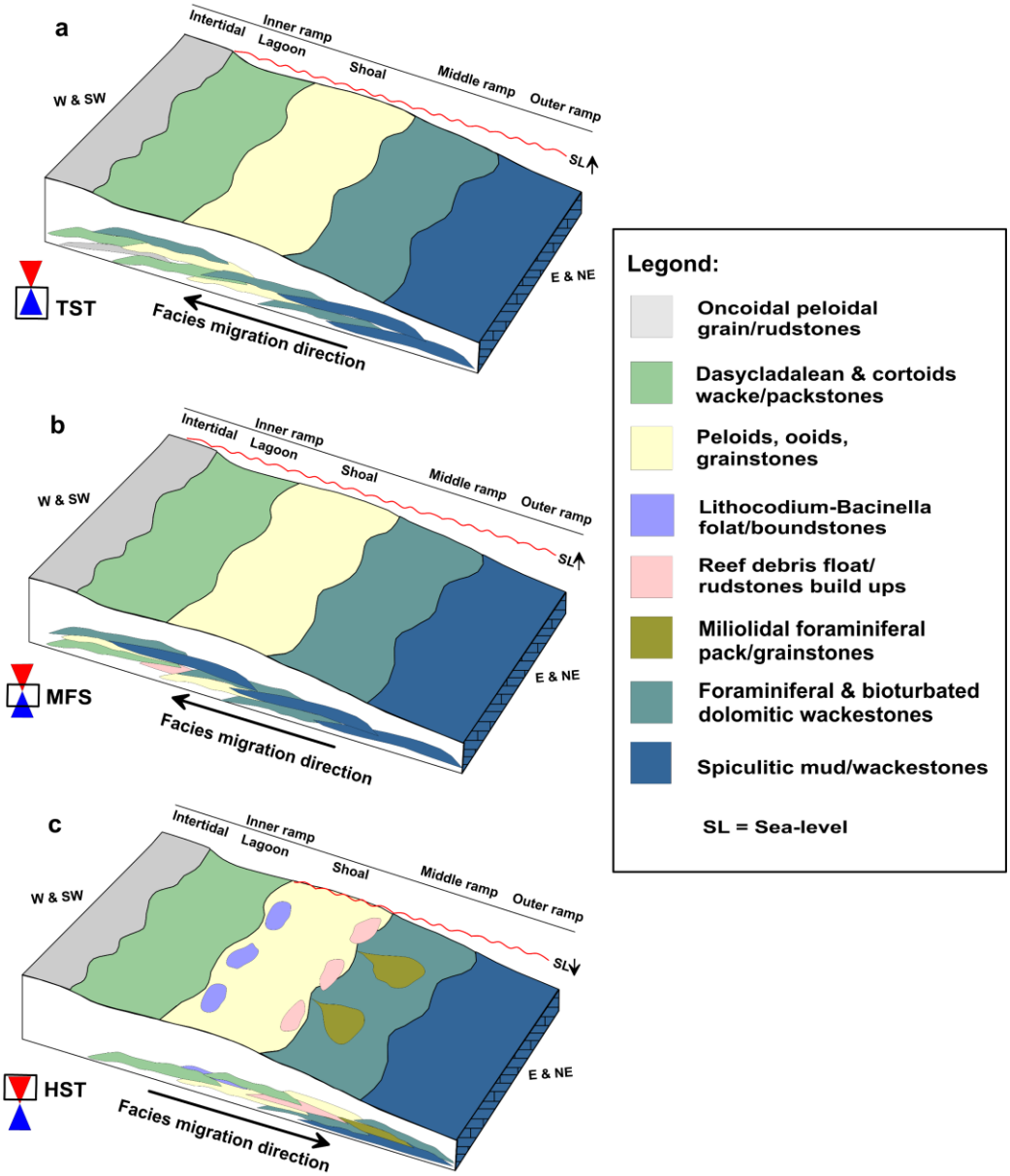

Figure 52. *Schematic depositional environment models showing the spatial facies distribution across the Yamama carbonate ramp during relative sea-level change. The depositional facies range from intertidal, restricted lagoonal wackestones to high-energy shoal grainstones and outer-ramp mudstones. The models illustrate: (**a**) during the transgressive systems tract (TST), facies retrograde landward and the ramp is dominated by mud-supported middle- to outer-ramp deposits; (**b**) at the maximum flooding surface (MFS), facies retrograde to their maximum landward position and the ramp is dominated by outer-ramp facies; and (**c**) during the highstand systems tract (HST), facies prograde basinward and the ramp is dominated by grain-supported shoal and Lithocodium–Bacinella reefal facies (author's own edit).*

The TST3 is dominated by the middle-ramp facies (F-12) in Nasiriya, the middle-ramp facies (F-13) and the outer-ramp facies (F-14) in Ah'Dimah, and by the lagoonal (F-2) in West Qurna Oilfield. The TST3 is characterized by the dolomitic and argillaceous limestones in Nasiriya, the marly and argillaceous limestones in Ah'Dimah and West Qurna. The dense limestones (EF-2) and the presence of the marly limestones (EF-1) electrofacies are characteristic for this system tract. Thin streaks of the vuggy limestones (EF-5) occurred in the lower part of the TST3 in West Qurna. The *Charentia cuvillieri* foraminifera encounters in this system tract.

Maximum flooding surface 2 (MFS2)

MFS2 of the DS-3 is defined based on the high gamma-ray readings, the presence of marly and argillaceous limestones of the middle ramp bioturbated dolomitic limestones in Nasiriya Oilfield (west and northwest) that graded into the outer ramp spiculitic mudstones in Ah'Dimah and West Qurna oilfields (east and southeast) (Fig. 50).

Highstand system tract 3 (HST3)

The HST3 ranges in thickness from 80 m in Nasiriya, to 100 m in Ah'Dimah, and 45 m in West Qurna Oilfield. The YRB represents the lower part of the HST3, while the upper part of the HST3, corresponds to the non-reservoir unit B1 and the reservoir unit YRA in Nasiriya and Ah'Dimah (Fig. 51). In West Qurna, the lower part of the HST3 corresponds to the non-reservoir unit B1 and upper part represents the reservoir unit YRA. The HST3 is characterized by limestones that interbedded with the argillaceous limestones and dominated by the lagoonal (F-3) and (F-4) facies in Nasiriya. The early HST3 in Ah'Dimah (corresponds to YRB) is characterized by the shoal peloidal grainstones (F-7), and the backshoal Lithocodium-Bacinella float/boundstones (F-6) (Fig. 50). The late HST3 in Ah'Dimah is defined by the occurrence of the foreshoal reefal facies (F-9) that interbedded with the shoal facies (F-7). The middle part of the YRB is dominated by the Lithocodium-Bacinella and defined by the domination of the porous limestones (EF-4), forming a good reservoir unit. The HST3 in West Qurna is dominated by the shoal peloidal grainstones (F-7) and the backshoal Lithocodium-Bacinella float- to boundstones (F-6), forming a good reservoir unit (YRA) that is characterized by porous limestones (EF-4). The occurrence of the middle ramp bioturbated dolomitic wackestones (F-12), and the Miliolidal packstones (F-11) encounter the non-reservoir unit B1 in Nasiriya and Ah'Dimah. The middle ramp mliolidal grainstones (F-11) probably formed due to reworking of

shoal sediments due to the lack in accommodation space during the upper most of the HST3. Several foraminifers occur within the HST3, such as *Patellovalvulina patrulius, Haplophragmoides joukowskyi, Montsalevia salevensis,* and *Meandrospira favrei, Pseudocyclammina lituus, Praechrysalidina infracretacea* Luperto Sinni and Representatives of the genus *Coscinoconus.*

5.9.4 Depositional sequence 4 (DS-4)

This depositional sequence is represented by transgressive system tract (TST4) of the upper most Yamama Formation.

Transgressive system tract 4 (TST4)

The thickness of TST4 varies from 15 m, 20 m, and 35 m in the Nasiriya, Ah'Dimah, and West Qurna, respectively, reflecting an increase in its thickness from the west to the east. This corresponds to the B0 (the uppermost of the Yamama) in the entire area (Table 3). The sequence boundary SB3 is manifested by change from the porous limestones (EF-4) of the uppermost HST3 to the marly and dense limestones (EF-1 and EF-2), and from the shoal peloidal grainstones (F-7) to the middle ramp miliolidal packstones (F-11) and bioclastic wackestones (F-13). The TST4 is characterized by increase in gamma ray log, marly and dense limestones (EF-1 and EF-2), lagoonal and middle ramp facies (F-2, F-3, F-11 and F-13). The lowermost part of the underlying Ratawi shows changing in lithology from the marly and dense limestones and a higher gamma ray readings of the TST4 in the uppermost Yamama into the peloidal grainstones of the lowermost Ratawi marked as the MFS that separates the two formations. Several foraminifers occur within the TST4 including *Haplophragmoides joukowskyi* and *Meandrospira favrei*, *Nautiloculina bronnimanni*, *Mayncina bulgarica*, and *Moesiloculina danubiana* (Fig. 51). According to Sadooni (1993), the upper part of Yamama is considered as reservoir units across south of Iraq based on SP and sonic well logs. In contrast, this study revealed that the upper part of the formation has a poor reservoir quality, with dense, marly and argillaceous limestones that characterized by low porosity values and a high shale content across the area, therefore, considered as non-reservoir and a seal layer of the formation in this study.

Highstand system tract (HST4) (Ratawi Formation)

The HST4, which represents the lower most Ratawi Formation, is composed of grain-supported peloidal and oncoidal limestones that are sparry calcite cemented (Fig. 19).

6. Concluding Remarks

The main conclusions derived from this study on the sedimentology, depositional sequences and diagenesis of the Lower Cretaceous Yamama Formation, which is an important carbonate reservoir in southern Iraq and across the Arabian Gulf, include:

- The formation is heterogeneous and comprises pure limestones, argillaceous, marly, dolomitic limestones, and bioturbated dolomitic limestones, divided into reservoir and non-reservoir units and composed of fourteen distinct depositional facies/microfacies (F-1 to F-14) that vary with depth in the different localities within the reservoir and non-reservoir units. These were deposited in intertidal to outer ramp settings in west-east homoclinal shallow-marine carbonate ramp, which is distally slightly steepening.
- The Yamama carbonate ramp influenced by tectonic events including; (i) the opening of the Neo-Tethys Ocean that created accommodation space during the early Cretaceous, (ii) by the Oman ophiolite obduction during middle-late Cretaceous, (iii) and the Zagros orogeny during Miocene.
- The Yamama Formation yields diverse benthic foraminiferal assemblages, including *Paravalvulina arabica*, *Patellovalvulina patruliusi*, *Bramkampella arabica*, *Montsalevia salevensis*, *Haplophragmoides joukowskyi*, *Mayncina bulgarica*, *Freixialina planispiralis*, *Meandrospira favrei*, species of genus *Coscinoconus, Praechrysalidina infracretacea*, and *Pseudocyclammina lituus* confirming and representing its age to Berriasian–early Valanginian.
- The shoal grain-supported and reefal facies including the ooidal and peloidal grainstones, the backshoal Lithocodium-Bacinella floatstones and foreshoal reefal debris rudstones represent excellent reservoir facies.
- The Lithocodium-Bacinella float/boundstones and reefal debris rudstones facies formed build-ups within the shoal area, and of significant interest for the development of the Yamama Formation. Special attention should be directed towards areas northeast of the Ah'Dimah Oilfield for further exploration and development efforts.
- Hydrocarbon migrations are related to two phases of tectonic activity, including: (i) the Late Cretaceous ophiolite obduction during which hydrocarbon was derived from Jurassic source rocks, and (ii) the Zagros orogeny in the Miocene during which hydrocarbon was

derived from Upper Jurassic and Lower Cretaceous source rocks. The upper of the formation is charactrized by dense marly limestones that act as an effective seal, whereas, regionally, mudstones of the deep-water facies of the Chia Gara, Lower Sarmord, and Sulaiy formations prevented lateral hydrocarbon migration.

- Two types of traps are proposed, including: (i) structural traps, such as anticlines and fault closures, and (ii) stratigraphic traps created by lateral facies changes and the build-ups of the Lithocodium facies. The denser, mud-supported facies combine with the local faulting formed the seal for these rocks.

- The lateral and vertical reservoir heterogeneity is attributed to shift in depositional facies, and to various diagenetic alterations. The early circumgranular cement as well as small amounts of scattered syntaxial calcite overgrowths and equant calcite cement reduced the compaction of the grain-supported and reefal limestones and preserved good primary/depositional porosity and permeability. The dissolution of grains and the formation of moldic and vuggy pores in the Yamama limestones locally enhanced porosity, likely due to episodes of subaerial exposure. Conversely, fine pellets/peloids (>50 μm) experienced greater porosity loss than coarser grains as a result of compaction.

- Micritization of the grains resulted in the formation of abundant intragranular micropores in the grain-supported limestones. This process converted the macropore dominated grain-supported limestones to bimodal macro- and microporous limestones with high content of high water saturation even subsequent to oil emplacement. Moreover, these limestones will be characterized by high total porosity and commonly low permeability.

- The occurrence of pore-filling kaolin and Na-rich saponite in the mud-supported facies of the Yamama Formation further reduced porosity through mineral precipitation during early to burial diagenesis. Kaolin formed during mesogenesis from alumina-bearing acidic brines migrating along stylolites, during tectonic compression. While saponite developed earlier from micrite–brine reactions under restricted, evaporative conditions. Framboidal and euhedral pyrite indicate a diagenetic shift from microbial to thermochemical sulfate reduction, both contributing to porosity loss through pore-filling and dolomite replacement.

- Fluid-inclusions microthermometry in the blocky calcite filling moldic/vuggy pores revealed that precipitation took place at temperatures ranging from 85-140°C from brines composed of NaCl-KCl-H_2O with total salinity of 10 wt.% NaCl eq and $\delta^{18}O_{VSMOW}$ of +4‰

to +8‰. Precipitation at elevated temperatures corroborates the negative $\delta^{18}O_{VPDB}$ (mostly -6.9‰ to -5.6‰). The carbon isotopic signatures and presence of this calcite cement in the vicinity of stylolites suggest that dissolved carbon was derived from the pressure dissolution of host limestones. The low $\delta^{18}O$ values of the mud-supported and grain-supported limestones reflect the abundance of calcite cement, including micro-overgrowths in mud-supported limestones, and to the circumgranular and the scattered equant cements in grain-supported limestones confirmed by the lowest $\delta^{18}O$ values measured in the blocky cement itself.

- Restriction of dolomitization to bioturbation sites, which was due to local increase in carbonate alkalinity of the pore waters by oxidation of organic matter, had local impact on improvement of reservoir properties by the formation of intercrystalline pores. Moreover, these pores were reduced in size due to the development of dolomite overgrowths around the rhombs. while the backshoal dolomitic pelletal limestones most likely formed through early diagenetic evaporative reflux under restricted, high-Mg conditions.
- The depositional sequence of the Yamama Formation comprises four cycles bounded by three Type 2 sequence boundaries, which represent episodes subaerial exposure surfaces. The lower and upper contact with the undelaying Sulaiy and the overlaying Ratawi formations are represented by maximum flooding surfaces.
- The reservoir and non-reservoir units of the formation coincide with the depositional sequences in Nasiriya and Ah'Dimah oilfields (but not always in West Qurna Oilfield). The grain-supported, reservoir facies deposited during regressive cycles, whereas the mud-supported, non-reservoir facies deposited during transgressive cycles.

7. Applicability of the results

The integration of facies/microfacies, electrofacies, and petrophysical data provides a refined framework for distinguishing between reservoir and non-reservoir units in the carbonate reservoirs. This offers a practical guide for reservoir zonation, well targeting, and enhances the predictability of fluid distribution and improves hydrocarbon recovery strategies.

The recognition of grain-supported shoal and Lithocodium–Bacinella reefal facies (F-6 to F-10) as excellent reservoir facies emphasizes the importance of targeting these lithologies in exploration and development. Their distribution along a homoclinal carbonate ramp controlled by regional sea-level fluctuations suggests predictable trends that can be mapped regionally. Areas with Lithocodium–Bacinella buildups and reefal debris rudstones are of interest in exploration plans due to their high reservoir potential.

The study highlights the dual role of diagenetic processes in both preserving and destroying reservoir quality. Early cementation helped maintain primary porosity, whereas later cementation and authigenic mineral precipitation reduced pore space in mud-supported facies. Understanding these diagenetic pathways allows operators to better predict heterogeneity and reservoir quality across different facies in a carbonate ramp.

The stable isotope and fluid inclusion data reveal the influence of basinal brines, stylolites, and tectonic compression on fluid flow and cementation. These highlight the roles of regional tectonic activities (e.g., Oman ophiolite obduction and Zagros orogeny) in modifying reservoir quality through fluid migration. This is applicable to broader Middle East carbonate systems where similar tectono-diagenetic processes occurred.

The establishment of a depositional sequence model linked to reservoir and non-reservoir intervals provides a predictive tool for correlating facies architecture across fields. Grain-supported reservoir facies are commonly associated with regressive systems tracts, while transgressive cycles are dominated by mud-supported non-reservoir facies. This can be applied in other oilfields within the area to anticipate reservoir distribution and continuity.

The study demonstrates how an integrated sedimentological, petrographic, geochemical, and stratigraphic approach can reveal the complexity and heterogeneity of Lower Cretaceous reservoirs. The findings are relevant to carbonate ramp systems in other parts along the Tethyan Ocean, offering analogs for exploration and production in comparable settings.

8. Recommendations

- The lower part of the Yamama Formation can be cored to investigate the presence of ooidal and oncoidal limestones within the formation in the Ah'Dimah, West Qurna or any adjacent oilfields, as these facies are known to exist in the lower part of the Yamama Formation in Nasiriya Oilfield. In the case that such facies are found, and considering that no study has yet proposed a type section for the Yamama Formation, the Yamama Formation in the Ah'Dimah Oilfield could serve as the type section. Otherwise, two type sections are proposed here, one in Nasiriya and one in Ah'Dimah.
- The Lithocodium–Bacinella float-boundstone and reefal rudstone facies, which form reefal patches and build-ups within the shoal, dominated in YRB2 and YRC in Ah'Dimah. Targeting these patches in the northeast part of the field appears promising for field development when guided by seismic data. It is also recommended that further exploration and development focus on areas where grain-supported limestone facies are prevalent, given their superior reservoir quality. Enhanced reservoir characterization using well logs and seismic data could help delineate high-potential zones. Moreover, targeting nearby fields with similar grain-supported limestone facies could present additional promising opportunities, thereby contributing to the overall economic potential.
- Dividing the formation into hydraulic flow units and reservoir rock types based on porosity-permeability measurements is a valuable method. Although this approach was not utilized in the present study, it is recommended for future research to enhance our understanding of the formation's reservoir characteristics. However, more porosity-permeability laboratory measurements are needed.
- The modal analyses have not yet been undertaken to quantify the effects of the various diagenetic processes on reservoir quality. Diagenetic alterations such as physical compaction which has had the most substantial impact on reservoir quality, are difficult to quantify.
- Advanced geological modeling, 3D seismic imaging, and well logs integration will improve reservoir characterization and enhance exploration efficiency. The integration of sequence stratigraphy with biostratigraphic analysis will further refine our understanding of the reservoir characteristics and distribution.

9. References

Abd OK, Abd N (2024) Seismic Sequence Stratigraphic Model and Hydrocarbon Potential of Yamama Formation in Al-Fao Area, Southeastern Iraq. The Iraqi Geological Journal 56–69. https://doi.org/10.46717/igj.57.1A.6ms-2024-1-17

Abeed Q, Alkhafaji A, Littke R (2011) Source Rock Potential of the Upper Jurassic – Lower Cretaceous Succession in the Southern Mesopotamian Basin, Southern Iraq. Journal of Petroleum Geology 34:117–134. https://doi.org/10.1111/j.1747-5457.2011.00497.x

Abeed Q, Leythaeuser D, Littke R (2012) Geochemistry, origin and correlation of crude oils in Lower Cretaceous sedimentary sequences of the southern Mesopotamian Basin, southern Iraq. Organic Geochemistry 46:113–126. https://doi.org/10.1016/j.orggeochem.2012.02.007

Abeed Q, Littke R, Strozyk F, Uffmann AK (2013) The Upper Jurassic–Cretaceous petroleum system of southern Iraq: A 3-D basin modelling study. GeoArabia 18:179–200. https://doi.org/10.2113/geoarabia1801179

Agard P, Omrani J, Jolivet L, et al (2011) Zagros orogeny: a subduction-dominated process. Geological Magazine 148:692–725. https://doi.org/10.1017/S001675681100046X

Ahmad W (2016) Sulfur in Petroleum: Petroleum Desulfurization Techniques. In: Applying Nanotechnology to the Desulfurization Process in Petroleum Engineering. IGI Global Scientific Publishing, pp 1–52

Ahmed A, Al-Hameedy R (2023) Sedimentological Study of the Chia Gara Formation Successions in Selected Outcrop Sections of Northern Iraq,. Iraqi National Journal of Earth Science 23:1.0-18.0. https://doi.org/10.33899/earth.2022.134929.1020

Al Mafraji TGZ, Al-Zaidy AAH (2019) Microfacies Architecture and Stratigraphic Development of the Yamama Formation, Southern Iraq. Iraqi J Sci 60:1115–1128. https://doi.org/10.24996/ijs.2019.60.5.20

Al Naqib KMA (1967) Geology of the Arabian Peninsula; southwestern Iraq. United States Geological Survey. https://doi.org/10.3133/pp560G

Al-Ameri T, Al-Ibrahim R (2015) Crude oil analysis of the Yamama Formation in the Subbah, Tuba and Luhais oil fields, Southern Iraq. Iraqi Journal of Science 56:1425–1437

Alavi M (2004) Regional stratigraphy of the Zagros fold-thrust belt of Iran and its proforeland evolution. American Journal of Science 304:1–20. https://doi.org/10.2475/ajs.304.1.1

Al-Habba YQ, Abdullah M (1989) A geochemical study of hydrocarbon source rocks in Northern Iraq. Oil and Arab Cooperation Journal 15:11–15

Al-Hassani M, Al-Dulaimi S (2021) Biostratigraphy of Yamama Formation in Faihaa Oil Field, Southern Iraq. Iraqi J Sci 62:1570–1586. https://doi.org/10.24996/ijs.2021.62.5.20

Al-Helal A, Al-Refaia Y, Al-Kandari A, Abdullah M (2023) Subsurface Stratigraphy of Kuwait. In: Abd el-aal A el-aziz K, Al-Awadhi JM, Al-Dousari A (eds) The Geology of Kuwait. Springer International Publishing, Cham, pp 27–50

Al-Iessa IA, Zhang WZ (2023) Facies evaluation and sedimentary environments of the Yamama Formation in the Ratawi oil field, South Iraq. Sci Rep 13:5305. https://doi.org/10.1038/s41598-023-32342-9

Aljibouri RD, Al-Hakeem NSA, Nasser ME (2022) 3D geological modeling for Yamama reservoir in Al-Nasiriyah oil field Southern Iraq. International journal of health sciences 6:8949–8962. https://doi.org/10.53730/ijhs.v6nS6.12376

Al-Khafaji AJ, Al-Najm FM, Al-Refaia RAK, et al (2022) Source rock evaluation and petroleum generation of the Lower Cretaceous Yamama Formation: Its ability to contribute to generating and expelling petroleum to cretaceous reservoirs of the Mesopotamian Basin, Iraq. J Pet Sci Eng 217:110919. https://doi.org/10.1016/j.petrol.2022.110919

Almalichy A, Aljawad MS, Turzo Z, Al-Yaseri A (2024) A study of the optimum injection rate of carbonic acid during matrix acidizing of carbonate reservoirs: Implications for reducing CO2 emissions. Heliyon 10:e39955. https://doi.org/10.1016/j.heliyon.2024.e39955

Almalichy A, Aljawad MS, Turzo Z, Al-Yaseri A (2025) A novel approach to assess acid diversion efficiency in horizontal wells. Sci Rep 15:1080. https://doi.org/10.1038/s41598-024-84671-y

Alobaidy AR, Al-Banna AS (2021) Density - Velocity Relationship and Prediction of Lithology Variation Using Physical Analysis in Kf-4 Well of The Kifl Oil Field, Yamama Formation, South of Iraq. Iraqi Journal of Science 3601–3611. https://doi.org/10.24996/ijs.2021.62.10.18

Alshammary ZS, Al-Khafaji AJ, Al-Najm FM (2024) Characterization of the Yamama Reservoir in the Abu-Amood Oil Field, Nasiriya, Southern Iraq. The Iraqi Geological Journal 14–28. https://doi.org/10.46717/igj.57.1C.2ms-2024-3-14

Alsharhan A. S. (1985) Depositional Environment, Reservoir Units Evolution, and Hydrocarbon Habitat of Shuaiba Formation, Lower Cretaceous, Abu Dhabi, United Arab Emirates. AAPG Bulletin 69:. https://doi.org/10.1306/AD462B19-16F7-11D7-8645000102C1865D

Alsuwaidi M, Mohamed AAI, Mansurbeg H, et al (2021) Depositional and diagenetic controls on reservoir quality of microporous basinal lime mudstones (Aptian), United Arab Emirates. Sedimentary Geology 420:105925. https://doi.org/10.1016/j.sedgeo.2021.105925

Alsuwaidi M, Morad S, Mansurbeg H, Sulieman H (2020) Packstones and floatstones: Ambiguous textures and origins in need of critical appraisal. Marine and Petroleum Geology 118:104425. https://doi.org/10.1016/j.marpetgeo.2020.104425

Altiner D (1991) Microfossil biostratigraphy (mainly foraminifers) of the Jurassic-Lower Cretaceous carbonate successions in north-western Anatolia (Turkey). Geologica Romana 27:167–213

Archie GE (1942) The Electrical Resistivity Log as an Aid in Determining Some Reservoir Characteristics. Transactions of the AIME 146:54–62. https://doi.org/10.2118/942054-G

Arnaud-Vanneau A, Boisseau T (1988) Le genre Trocholina Paalzow 1922 et ses principales espèces au Crétacé. Revue de paléobiologie 353–377

Asquith GB, Krygowski D, Gibson CR (2004) Basic well log analysis. AAPG Tulsa

Aziz SK, El-Sattar MMA (1997) Sequence Stratigraphic Modeling of the Lower Thamama Group, East Onshore Abu Dhabi, United Arab Emirates. GeoArabia 2:179–202. https://doi.org/10.2113/geoarabia0202179

Bahrehvar M, Mehrabi H, Akbarzadeh S, Rahimpour-Bonab H (2021) Depositional and diagenetic controls on reservoir quality of the uppermost Jurassic–Lower Cretaceous sequences in the Persian Gulf; a focus on J–K boundary. J Pet Sci Eng 201:108512. https://doi.org/10.1016/j.petrol.2021.108512

Banner FT, Finch EM, Simmons MD (1990) On Lithocodium Elliott (Calcareous algae); its paleobiological and stratigraphical significance. J Micropalaeontol 9:21–35. https://doi.org/10.1144/jm.9.1.21

Bernaus JM, Arnaud-Vanneau A, Caus E (2002) Stratigraphic distribution of Valanginian–Early Aptian shallow-water benthic foraminifera and algae, and depositional sequences of a carbonate platform in a tectonically-controlled basin: the Organyà Basin, Pyrenees, Spain. Cretaceous Research 23:25–36. https://doi.org/10.1006/cres.2001.0300

Berner RA (1984) Sedimentary pyrite formation: An update. Geochimica et Cosmochimica Acta 48:605–615. https://doi.org/10.1016/0016-7037(84)90089-9

Bice KL, Huber BT, Norris RD (2003) Extreme polar warmth during the Cretaceous greenhouse? Paradox of the late Turonian δ^{18} O record at Deep Sea Drilling Project Site 511. Paleoceanography 18:2002PA000848. https://doi.org/10.1029/2002PA000848

Bjorlykke K (2010) Petroleum Geoscience: From Sedimentary Environments To Rock Physics. Springer Science & Business Media

Bodnar RJ (1993) Revised equation and table for determining the freezing point depression of H2O-Nacl solutions. Geochimica et Cosmochimica Acta 57:683–684. https://doi.org/10.1016/0016-7037(93)90378-A

Bristow TF, Kennedy MJ, Derkowski A, et al (2009) Mineralogical constraints on the paleoenvironments of the Ediacaran Doushantuo Formation. Proceedings of the National Academy of Sciences 106:13190–13195. https://doi.org/10.1073/pnas.0901080106

Bucur II (1988) Les foraminifères du Crétacé inférieur (Berriasien–Hauterivien) de la zone de Resita-Moldova Noua (Carpathes Méridionales, Roumanie). Remarques biostratigraphiques. Revue de Paléobiologie volume Spécial 2:379–389

Bucur II, Conrad MA, Radoicic R (1995) Foraminifers and calcareous algae from Valanginian limestones in the Jerma River Canyon, Eastern Serbia. Muséum d'histoire naturelle

Bucur II, Lazăr I (2023) UPPER JURASSIC TO LOWERMOST CRETACEOUS MICROFOSSILS FROM THE HĂGHIMAŞ MOUNTAINS (EASTERN CARPATHIANS, ROMANIA). Acta Palaeontologica Romaniae 19:

Bucur II, Săsăran E (2005) Micropaleontological assemblages from the Upper Jurassic-Lower Cretaceous deposits of Trascău Mountains and their biostratigraphic significance. Acta Palaeontologica Romaniae 5:27–38

Bucur II, Sudar M, Schlagintweit F, et al (2020) Lowermost Cretaceous limestones from the Kučaj zone (Carpatho–Balkanides, Eastern Serbia): new data on their age assignment. Cretaceous Research 116:104575. https://doi.org/10.1016/j.cretres.2020.104575

Burchette TP (2012) Carbonate rocks and petroleum reservoirs: a geological perspective from the industry. Geological Society, London, Special Publications 370:17–37. https://doi.org/10.1144/SP370.14

Cao T, Alsuwaidi M, Antler G, et al (2024) Depositional control on composition, texture and diagenesis of modern carbonate sediments: A comparative study of tidal channels and marshes, Abu Dhabi, United Arab Emirates. Sedimentary Geology 472:106744. https://doi.org/10.1016/j.sedgeo.2024.106744

Catuneanu O (2022) Principles of Sequence Stratigraphy. Newnes

Cavalazzi B, Agangi A, Barbieri R, et al (2014) The formation of low-temperature sedimentary pyrite and its relationship with biologically-induced processes. Geol Ore Deposits 56:395–408. https://doi.org/10.1134/S107570151405002X

Chafeet HA (2016) Yamama reservoir characterization in the West Qurna oil field, Southern Iraq. Iraqi J Sci 57:938–947

Charollais J-J, Brönnimann P, Zaninetti L (1965) Troisieme note sur les foraminifères du Crétacé inférieur de la région genevoise. Remarques stratigraphiques et description de Pseudotextulariella salevensis, n. sp.; Haplophragmoides joukowskyi, n. sp.; Citaella? favrei, n. sp. Archives des Sciences 19:23. https://doi.org/10.5169/seals-739322

Chiocchini M, Farinacci A, Mancinelli A, et al (1994) Biostratigrafia a foraminiferi, dasicladali e calpionelle delle successioni carbonatiche mesozoiche dell'Appennino centrale (Italia). Studi Geologici Camerti Special Volume "Biostratigrafia dell'Italia centrale":9–128

Choquette PW, Pray LC (1970) Geologic Nomenclature and Classification of Porosity in Sedimentary Carbonates1. AAPG Bulletin 54:207–250. https://doi.org/10.1306/5D25C98B-16C1-11D7-8645000102C1865D

Conrad MA, Clavel B (2008) A Lithocodium and Bacinella signature of a late Hauterivian, local microbial event: the Urgonian limestone in south-east France. Geol Cro 61:239–250

Crain ER (1986) Log analysis handbook

Darsac C (1983) La plate-forme berriaso-valanginienne du Jura méridional aux massifs subalpins (Ain, Savoie)

Datta K, Ghosh D, Al-Nasheet A, et al (2013) Depositional and Diagenetic Controls on Carbonate Reservoir Distribution - A Study in Minagish Formation, Burgan Field, Kuwait. European Association of Geoscientists & Engineers, p cp

Davis JC (2018) Electrofacies in Reservoir Characterization. In: Daya Sagar BS, Cheng Q, Agterberg F (eds) Handbook of Mathematical Geosciences: Fifty Years of IAMG. Springer International Publishing, Cham, pp 211–223

Deville de Periere M, Brenac P, Hilali I, et al (2023) Paleoenvironments and stratigraphy of the Valanginian–Hauterivian carbonates of the Arabian Platform: Implications for the recognition of the Weissert Event on the Southern Tethys. Cretaceous Research 148:105541. https://doi.org/10.1016/j.cretres.2023.105541

Droste HJ (2013) Upper Jurassic to Lower Cretaceous stratigraphic model for the eastern Arabian Plate. GeoArabia 18:197–202. https://doi.org/10.2113/geoarabia1802197

Dunham RJ (1962) Classification of carbonate rocks according to depositional textures. In: Classification of Carbonate Rocks. AAPG Mem.1

Egeberg PK, Aagaard P (1989) Origin and evolution of formation waters from oil fields on the Norwegian shelf. Applied Geochemistry 4:131–142. https://doi.org/10.1016/0883-2927(89)90044-9

Elliott GF (1956) Further records of fossil calcareous algae from the Middle East. Micropaleontology 2:327–334

Embry AF, Klovan JE (1971) A Late Devonian Reef Tract on Northeastern Banks Island, N.W.T. Bulletin of Canadian Petroleum Geology 19:730–781

Esrafili-Dizaji B, Hajikazemi E, Dalvand M, et al (2020) Diagenesis and reservoir characteristics of the Lithocodium–Bacinella facies in a Lower Cretaceous reservoir, eastern Persian Gulf Basin. Facies 66:24. https://doi.org/10.1007/s10347-020-00608-7

Fadhel MS, Al-Rahim AM (2019) 3D seismic model of faulting systems of a Jurassic - Cretaceous sedimentary packages in Merjan_West Kifl Oil fields - Central Iraq. Heliyon 5:. https://doi.org/10.1016/j.heliyon.2019.e02507

Fallatah MI, Alnazghah M, Kerans C, Al-Hussaini A (2024) Sedimentology and carbon isotope stratigraphy from the Late Jurassic – Early Cretaceous of the Arabian plate: The Weissert event and the VOICE in the Tethys Realm? Marine and Petroleum Geology 161:106670. https://doi.org/10.1016/j.marpetgeo.2023.106670

Flügel E (2010) Microfacies of carbonate rocks: analysis, interpretation and application. Springer

Fox JE, Ahlbrandt ThS (2002) Petroleum geology and total petroleum systems of the Widyan Basin and interior platform of Saudi Arabia and Iraq, Version 1.0. U.S. Dept. of the Interior, U.S. Geological Survey, Denver, Colo. :

Gezeeri TMN, Ebaid AM, Al Mutairi K, Mostafa M (2007) New Oil Entrapment in Lower Minagish Member-Minagish Field, Kuwait. OnePetro

Glennie KW, Boeuf MGA, Clarke MWH, et al (1973) Late Cretaceous Nappes in Oman Mountains and Their Geologic Evolution1. AAPG Bulletin 57:5–27. https://doi.org/10.1306/819A4240-16C5-11D7-8645000102C1865D

Goldstein RH, Reynolds TJ (1994) Systematics of Fluid Inclusions in Diagenetic Minerals. SEPM Society for Sedimentary Geology

Granier B (2008) Holostratigraphy of the Kahmah regional Series in Oman, Qatar, and the United Arab Emirates. In: CG2008_A07. http://paleopolis.rediris.es/cg/08/A07/index.html. Accessed 18 Aug 2025

Granier B, Bucur II (2011) Stratigraphic ranges of some Tithonian–Berriasian benthic foraminifers and Dasycladales. Re-evaluation of their use in identifying this stage boundary in carbonate platform settings. In: Grosheny D, Granier B, Sander N (eds) Platform to basin correlations in Cretaceous times. pp 9–10

Handhal AM, Chafeet HA, Dahham NA (2020) Microfacies, depositional environments and diagenetic processes of the Mishrif and Yamama formations at Faiha and Sindibad oilfields, south Iraq. Iraqi Bull Geol Min 16:51–74

Haq BU (2014) Cretaceous eustasy revisited. Global and Planetary Change 113:44–58. https://doi.org/10.1016/j.gloplacha.2013.12.007

Haq BU, Al-Qahtani AM (2005) Phanerozoic cycles of sea-level change on the Arabian Platform. GeoArabia 10:127–160. https://doi.org/10.2113/geoarabia1002127

Hardenbol J, Thierry J, Farley MB, et al (1999) Mesozoic and Cenozoic Sequence Chronostratigraphic Framework of European Basins. In: Graciansky P-C de, Hardenbol J, Jacquin T, Vail PR (eds) Mesozoic and Cenozoic Sequence Stratigraphy of European Basins. SEPM Society for Sedimentary Geology, p 0

Hillgartner H, Van Buchem FSP, Gaumet F, et al (2003) The Barremian-Aptian Evolution of The Eastern Arabian Carbonate Platform Margin (Northern Oman). J Sediment Res 73:756–773. https://doi.org/10.1306/030503730756

Hosseini S, Conrad MA, Clavel B, Carras N (2016) Berriasian-Aptian shallow water carbonates in the Zagros fold-thrust belt, SW Iran: Integrated Sr-isotope dating and biostratigraphy. Cretaceous Research 57:257–288. https://doi.org/10.1016/j.cretres.2015.09.007

Hosseiny E, Mohseni A (2023) Garau Formation as an unconventional hydrocarbon resource in southwestern Iran: a geochemical investigation. J Petrol Explor Prod Technol 13:1535–1549. https://doi.org/10.1007/s13202-023-01634-1

Hüßner H (1985) Jurassische Karbonate des westlichen Hohen Atlas (Marokko): Mikrofaziesanalyse und plattentektonischer Rahmen. Facies 12:141–217. https://doi.org/10.1007/BF02536979

Idan R, Amani L. M. Salih, Omar N. A. Al-Khazraji, Marwah H. Khudhair (2020) Depositional environments, facies distribution, and porosity analysis of yamama formation in majnoon oilfield. sequence stratigraphic approach. Iraqi Geol J 53:38–52. https://doi.org/10.46717/igj.53.1D.4Rw-2020-05-03

Irwin H, Curtis C, Coleman M (1977) Isotopic evidence for source of diagenetic carbonates formed during burial of organic-rich sediments. Nature 269:209–213. https://doi.org/10.1038/269209a0

Ivanova D (2000) Middle Callovian to Valanginian microfossil biostratigraphy in the West Balkan Mountain, Bulgaria (SE Europe). Acta Palaeontologica Romaniae 2:231–236

Ivanova D, Bonev N, Chatalov A (2015) Biostratigraphy and tectonic significance of lowermost Cretaceous carbonate rocks of the Circum-Rhodope Belt (Chalkidhiki Peninsula and Thrace region, NE Greece). Cretaceous Research 52:25–63. https://doi.org/10.1016/j.cretres.2014.08.003

Ivanova D, Kołodziej B (2010) Upper Jurassic-Lower Cretaceous Foraminifers from Štramberk type limestones of South Poland. Studia Universitatis Babes-Bolyai Geologia 55:3–31

Ivanova D, Kolodziej B (2010) Late Jurassic–Early Cretaceous Foraminifera from Štramberk-type Limestones, Polish Outer Carpathians. Studia UBB Geologia 55:3–31. http://dx.doi.org/10.5038/1937-8602.55.2.1

Jameel NK, Al-Zaidy AAH (2022) Microfacies Analysis and Stratigraphic Framework of Yamama Formation in Sindbad, Halfaya and Ad'daimah Oil Fields, Southern Iraq. Iraqi J Sci 63:4314–4327. https://doi.org/10.24996/ijs.2022.63.10.18

James NP, Choquette PW (1983) Limestones-the sea floor diagenetic environment. Geosci Can 10:162–179

Jenkyns HC (2010) Geochemistry of oceanic anoxic events. Geochem Geophys Geosyst 11:2009GC002788. https://doi.org/10.1029/2009GC002788

Jeong J, Al-Ali AA, Jung H, et al (2017) Controls on Reservoir Quality and Reservoir Architecture of Early Cretaceous carbonates in an Abu Dhabi Onshore Field Lekhwair, Kharaib and Lower Shuaiba Formations. SPE, Abu Dhabi, UAE, p D011S001R002

Kadkhodaie-Ilkhchi R, Rezaee R, Moussavi-Harami R, Kadkhodaie -Ilkhchi A (2013) Analysis of the reservoir electrofacies in the framework of hydraulic flow units in the Whicher Range Field, Perth Basin, Western Australia. Journal of Petroleum Science and Engineering 111:106–120. https://doi.org/10.1016/j.petrol.2013.10.014

Khadhaier AA, Ali KK (2024) Hydrocarbon Possibilities and Structural Setting in Ad'Daimah Oil Field, Southern Iraq. Iraqi Journal of Science 2490–2510. https://doi.org/10.24996/ijs.2024.65.5.13

Khalil R, Rahim H ur, Jan JA (2024) Facies analysis, depositional environment and diagenetic processes of the Lower Cretaceous Yamama Formation, Riyadh, Saudi Arabia. Carbonates and Evaporites 39:62. https://doi.org/10.1007/s13146-024-00973-2

Khazaal FA, Shakir LS (2022) Biostratigraphy of Yamama Formation at Luhais and Rifaee oilfields, Southern Iraq. Iraqi J Sci 63:2619–2629. https://doi.org/10.24996/ijs.2022.63.6.27

Khorshid SZ, Mohammed MF, Al –Taee AAJ (2021) Application of Neural Network Analysis for Seismic Data to Differentiate Reservoir Units of Yamama Formation in Nasiriya Oilfield A Case Study in Southern Iraq. Iraqi Journal of Science 2589–2602. https://doi.org/10.24996/ijs.2021.62.8.12

Kim, O'Neil (1997) Equilibrium and nonequilibrium oxygen isotope effects in synthetic carbonates. Geochimica et Cosmochimica Acta 61:3461–3475. https://doi.org/10.1016/S0016-7037(97)00169-5

Koch R, Moussavian E, Ogorelec B, et al (2002) Development of a Lithocodium (syn. Bacinella irregularis)-reef-mound- A patch reef within Middle Aptian lagoonal limestone sequence near Nova Gorica (Sabotin Mountain, W-Slovenia). Geologija 45:71–90. https://doi.org/10.5474/geologija.2002.006

Lawa FA, Mohammed I, Farouk S, et al (2023) Stratigraphic architecture of the Tethyan Cenomanian-Turonian succession and OAE2 in the Dokan Area, Kurdistan Region, northeast Iraq. Journal of African Earth Sciences 207:105064. https://doi.org/10.1016/j.jafrearsci.2023.105064

Lehmann C, Osleger DA, Montañez IP, et al (1999) Evolution of Cupido and Coahuila carbonate platforms, Early Cretaceous, northeastern Mexico. Geol Sco Am Bull 111:1010–1029. https://doi.org/10.1130/0016-7606(1999)111%253C1010:EOCACC%253E2.3.CO;2

Li F, Li L, Chen H, et al (2024) Heterogeneous Reservoir Petrophysical Property and Controlling Factors in Semi-Restricted Depositional Setting: A Case Study of Yamama Formation, X Oilfield, Middle East. Journal of Marine Science and Engineering 12:1011. https://doi.org/10.3390/jmse12061011

Longman MW (1980) Carbonate Diagenetic Textures from Near Surface Diagenetic Environments. Am Ass Pet Geol Bull 64:461–487. https://doi.org/10.1306/2F918A63-16CE-11D7-8645000102C1865D

Lucia, F Jerry (2007) Carbonate Reservoir Characterization. In: Carbonate Reservoir Characterization. Springer, Berlin, Heidelberg, pp 181–215

Lucia FJ (ed) (2007) Depositional Textures & Petrophysics. In: Carbonate Reservoir Characterization: An Integrated Approach. Springer, Berlin, Heidelberg, pp 111–141

Mahdi FA, Al-Zaidy AAH (2024) Microfacies Analysis and Stratigraphic Evolution of Garagu Formation in Selected Oil Fields, Northern Iraq. Iraqi Journal of Science 2521–2536. https://doi.org/10.24996/ijs.2024.65.5.15

Mancinelli A, Coccia B (1999) Le Trocholine dei sedimenti mesozoici di piattaforma carbonatica dell'Appennino centro-meridionale (Abruzzo e Lazio). Revue de Paléobiologie 18:147–171

Mansurbeg H, Alsuwaidi M, Morad D, et al (2024) Disconformity-controlled hydrothermal dolomitization and cementation during basin evolution: Upper Triassic carbonates, UAE. Geology 52:486–491. https://doi.org/10.1130/G51990.1

Mircescu CV, Bucur II, Săsăran E, et al (2019) Facies evolution of the Jurassic-Cretaceous transition in the Eastern Getic Carbonate Platform, Romania: Integration of sequence stratigraphy, biostratigraphy and isotope stratigraphy. Cretaceous Research 99:71–95. https://doi.org/10.1016/j.cretres.2019.01.015

Mohammed A, Dhaidan M, Al-Hazaa SH, et al (2022a) Reservoir characterization of the upper Turonian – lower Coniacian Khasib formation, South Iraq: Implications from electrofacies analysis and a sequence stratigraphic framework. Journal of African Earth Sciences 186:104431. https://doi.org/10.1016/j.jafrearsci.2021.104431

Mohammed A, Velledits F (2024a) Microfacies impacts on reservoir heterogeneity of early cretaceous Yamama carbonate reservoir in South Iraq. Sci Rep 14:24184. https://doi.org/10.1038/s41598-024-74640-w

Mohammed A, Velledits F (2024b) Facies-related reservoir heterogeneity of grain-supported limestones: insight from the Early Cretaceous Yamama Formation, southern Iraq. Carbonates Evaporites 39:118. https://doi.org/10.1007/s13146-024-01037-1

Mohammed AKA (2018) RESERVIOR CHARACTERISTICS OF KHASIB FORMATION IN AMARA FIELD, SOUTHERN IRAQ. The Iraqi Geological Journal 54–74. https://doi.org/10.46717/igj.51.2.4Ms-2018-12-26

Mohammed IQ, Farouk S, Mousa A, Lawa FA (2022b) Lithofacies types, mineralogical assemblages and depositional model of the Maastrichtian–Danian successions in the Western Desert of Iraq and eastern Jordan. Journal of African Earth Sciences 186:104397. https://doi.org/10.1016/j.jafrearsci.2021.104397

Moldovanyi EP, Lohmann KC (1984) Isotopic and Petrographic Record of Phreatic Diagenesis: Lower Cretaceous Sligo and Cupido Formations. Journal of Sedimentary Research 54:

Moore CH, Wade WJ (2013) Chapter 9 - Summary of Early Diagenesis and Porosity Modification of Carbonate Reservoirs in a Sequence Stratigraphic and Climatic Framework. In: Moore CH, Wade WJ (eds) Developments in Sedimentology. Elsevier, pp 207–238

Morad D, Nader FH, Gasparrini M, et al (2018a) Comparison of the diagenetic and reservoir quality evolution between the anticline crest and flank of an Upper Jurassic carbonate gas reservoir, Abu Dhabi, United Arab Emirates. Sedimentary Geology 367:96–113. https://doi.org/10.1016/j.sedgeo.2018.02.008

Morad D, Nader FH, Morad S, et al (2018b) Impact of Stylolitization On Fluid Flow and Diagenesis in Foreland Basins: Evidence from an Upper Jurassic Carbonate Gas Reservoir, Abu Dhabi, United Arab Emirates. Journal of Sedimentary Research 88:1345–1361. https://doi.org/10.2110/jsr.2018.70

Morad S, Al Suwaidi M, Mansurbeg H, et al (2019) Diagenesis of a limestone reservoir (Lower Cretaceous), Abu Dhabi, United Arab Emirates: Comparison between the anticline crest and flanks. Sedimentary Geology 380:127–142. https://doi.org/10.1016/j.sedgeo.2018.12.004

Morad S, Al-Aasm IS, Nader FH, et al (2012) Impact of diagenesis on the spatial and temporal distribution of reservoir quality in the Jurassic Arab D and C members, offshore Abu Dhabi oilfield, United Arab Emirates. GeoArabia 17:17–56. https://doi.org/10.2113/geoarabia170317

Morad S, Farooq U, Mansurbeg H, et al (2023) Variations in extent, distribution and impact of dolomitization on reservoir quality of Upper Cretaceous foreland-basin carbonates, Abu Dhabi, United Arab Emirates. Marine and Petroleum Geology 155:106357. https://doi.org/10.1016/j.marpetgeo.2023.106357

Morad S, Ketzer J m., De Ros L f. (2013) Linking Diagenesis to Sequence Stratigraphy: An Integrated Tool for Understanding and Predicting Reservoir Quality Distribution. In: Linking Diagenesis to Sequence Stratigraphy. John Wiley & Sons, Ltd, pp 1–36

Nagm E, Bamousa A, Memesh A, et al (2018) Relative sea-level changes and sedimentary facies development of the lowermost Cretaceous (Berriasian–Valanginian) cycles in the north of Ar Riyad city, Saudi Arabia. Journal of Asian Earth Sciences 163:163–176. https://doi.org/10.1016/j.jseaes.2018.05.036

Nazemi M, Valinasab H, Kadkhodaie-Ilkhchi A, et al (2024) Reservoir characterization of the Berriasian–Early Valanginian Lower Fahliyan Formation in Dorood Oilfield, Persian Gulf. Journal of Asian Earth Sciences 106393. https://doi.org/10.1016/j.jseaes.2024.106393

Neagu T (1975) Monographie de la faune des foraminiféres éocrétacés du couloir de Dâmbovicioara, de Codlea et des Monts Persani. Mémoires de l'Institut de Géologie et de Géophysique de la Roumanie 62:135–160

Neagu T, Cirnaru P (2004) Lower Aptian agglutinated Foraminifera from the southern Dobrogea and SE part of the Moesian Platform. Acta Palaeontologica Romaniae 4:277–297

Neuweiler F, Reitner J (1992) Karbonatbänke mit Lithocodium aggregatum Elliott, Bacinella irregularis Radoicic. Berl Geowiss Abh 3:273–293. https://doi.org/10.23689/FIDGEO-775

Paganoni M, Al Harthi A, Morad D, et al (2016) Impact of stylolitization on diagenesis of a Lower Cretaceous carbonate reservoir from a giant oilfield, Abu Dhabi, United Arab Emirates. Sedimentary Geology 335:70–92. https://doi.org/10.1016/j.sedgeo.2016.02.004

Pederson CL, McNeill DF, Klaus JS, Swart PK (2015) Deposition and Diagenesis of Marine Oncoids: Implications For Development of Carbonate Porosity. Journal of Sedimentary Research 85:1323–1333. https://doi.org/10.2110/jsr.2015.77

Peters KE, Walters CC, Moldowan JM (2004) The Biomarker Guide: Volume 1: Biomarkers and Isotopes in the Environment and Human History, 2nd edn. Cambridge University Press, Cambridge

Phillips ER, Waters CN, Ellison RA (2013) The Jurassic–Cretaceous depositional and tectonic evolution of the southernwestern margin of the Neotethys Ocean, Northern Oman and United Arab Emirates. In: Al Hosani K, Roure F, Ellison R, Lokier S (eds) Lithosphere Dynamics and Sedimentary Basins: The Arabian Plate and Analogues. Springer, Berlin, Heidelberg, pp 61–100

Pitman JK, Steinshouer D, Lewan MD (2004) Petroleum generation and migration in the Mesopotamian Basin and Zagros Fold Belt of Iraq: results from a basin-modeling study. GeoArabia 9:41–72. https://doi.org/10.2113/geoarabia090441

Pleş G, Bucur II, Păcurariu A (2015) Foraminiferal assemblages and facies associations in the Upper Jurassic carbonates from Ardeu Unit (Metaliferi Mountains, Romania). Acta Palaeontologica Romaniae 11:43–57

Pop G, Bucur I (2001) Upper Jurassic and Lower Cretaceous sedimentary formations from the Valcan Mountains (South Carpathians). Studia UBB Geologia 46:77–94. http://dx.doi.org/10.5038/1937-8602.46.2.7

Radoičić R (1959) Nekoliko problematičnih mikrofosila iz dinarske krede

Ramalho MM (1969) Quelques observations sur les Lituolidae (Foraminifera) du Malm portugais. Boletim Da Sociedade Geológica De Portugal 17:37–50

Rameil N (2008) Early diagenetic dolomitization and dedolomitization of Late Jurassic and earliest Cretaceous platform carbonates: A case study from the Jura Mountains (NW Switzerland, E France). Sedimentary Geology 212:70–85. https://doi.org/10.1016/j.sedgeo.2008.10.004

Rameil N, Immenhauser A, Warrlich G, et al (2010) Morphological patterns of Aptian Lithocodium-Bacinella geobodies: relation to environment and scale: Lithocodium-Bacinella, Aptian of Oman. Sedimentology 57:883–911. https://doi.org/10.1111/j.1365-3091.2009.01124.x

Read JF (1995) Overview of Carbonate Platform Sequences, Cycle Stratigraphy and Reservoirs in Greenhouse and Ice-House Worlds. In: Read JF, Kerans C, Weber LJ, et al. (eds) Milankovitch Sea-Level Changes, Cycles and Reservoirs on Carbonate Platforms in Greenhouse and Ice-House Worlds. SEPM Society for Sedimentary Geology, p 0

Redmond CD (1964) Lituolid Foraminifera from the Jurassic and Cretaceous of Saudi Arabia. Micropaleontology 10:405–414. https://doi.org/10.2307/1484650

Rider MH (1996) The Geological Interpretation of Well Logs. Whittles Publishing

Sabouhi M, Moussavi-Harami R, Kadkhodaie A, et al (2022) A qualitative-quantitative approach for studying the impact of facies and diagenesis control on the rudist biostrome of the Sarvak formation, Abadan plain, SW Iran. Journal of Petroleum Science and Engineering 212:110245. https://doi.org/10.1016/j.petrol.2022.110245

Sadooni F (1993) Stratigraphic Sequence, Microfacies, and Petroleum Prospects of the Yamama Formation, Lower Cretaceous, Southern Iraq. Am Ass Pet Geol Bull 77:. https://doi.org/10.1306/BDFF8F92-1718-11D7-8645000102C1865D

Sadooni FN, Aqrawi AAM (2000) Cretaceous Sequence Stratigraphy and Petroleum Potential of the Mesopotamian Basin, Iraq. In: Alsharhan AS, Scott RW (eds) Middle East Models of Jurassic/Cretaceous Carbonate Systems. SEPM Society for Sedimentary Geology, p 0

Saleh AH (2014) Microfacies and environmental study of the lower cretaceous yamama formation in Ratawi field. Arab J Geosci 7:3175–3190. https://doi.org/10.1007/s12517-013-0991-5

Salvini-Bonnard G, Zaninetti L, Charollais J (1984) Les foraminifères dans le Crétacé inférieur (Berriasien moyen–Valanginien inférieur) dans la région de la Corraterie, Grand Salève (Haute-Savoie, France): inventaire préliminaire et remarques biostratigraphiques. Revue de Paléobiologie 3:75–184

Sarraj RHA, Mohialdeen IMJ (2020) Sedimentology, palynofacies and hydrocarbon generation potential of the Cretaceous Balambo Formation from Zagros Fold-Thrust Belt, Kurdistan, NE Iraq. Arab J Geosci 13:552. https://doi.org/10.1007/s12517-020-05577-3

Schlagintweit F, Bover-Arnal T, Salas R (2010) New insights into Lithocodium aggregatum Elliott 1956 and Bacinella irregularis Radoičić 1959 (Late Jurassic–Lower Cretaceous): two ulvophycean green algae (?Order Ulotrichales) with a heteromorphic life cycle (epilithic/euendolithic). Facies 56:509–547. https://doi.org/10.1007/s10347-010-0222-4

Schlagintweit F, Enos P (2013) Uppermost Jurassic?–Neocomian shallow-water carbonates of the Blake Nose, USA: DsDp site 392a revisited. Acta Palaeontologica Romaniae 9:39–56

Schlumberger LI (1974) II-Applications. New York

Schmid DU, Leinfelder RR (1996) The Jurassic Lithocodium aggregatum-Troglotella incrustans foraminiferal consortium. Palaeontology 39:21–52

Scholle PA, Ulmer-Scholle DS (eds) (2003) GRAINS: Non-skeletal Grains: Pellets and Peloids. In: A Color Guide to the Petrography of Carbonate Rocks: Grains, textures, porosity, diagenesis. American Association of Petroleum Geologists, p 0

Seibel MJ, James NP (2017) Diagenesis of Miocene, incised valley-filling limestones; Provence, Southern France. Sedimentary Geology 347:21–35. https://doi.org/10.1016/j.sedgeo.2016.09.006

Sequero C, Aurell M, Bádenas B (2020) Oncoid distribution in the shallow domains of a Kimmeridgian carbonate ramp (Late Jurassic, NE Spain). Sedimentary Geology 398:105585. https://doi.org/10.1016/j.sedgeo.2019.105585

Sequero C, Bádenas B, Aurell M (2019) Factors Controlling Oncoid Distribution in the Inner Areas of a Late Kimmeridgian Carbonate Ramp (Northeast Spain). In: Boughdiri M, Bádenas B, Selden P, et al. (eds) Paleobiodiversity and Tectono-Sedimentary Records in the Mediterranean Tethys and Related Eastern Areas. Springer International Publishing, Cham, pp 171–174

Sharland PR, Casey DM, Davies RB, et al (2004) Arabian Plate Sequence Stratigraphy – revisions to SP2. GeoArabia 9:199–214. https://doi.org/10.2113/geoarabia0901199

Singh SK, Nath PK, Al-Ajmi AS, et al (2017) New Sedimentological Data within the Minagish Formation: Insights from Undeveloped Area, Onshore Kuwait. OnePetro

Tiab D, Donaldson EC (2016) Chapter 3 - Porosity and Permeability. In: Tiab D, Donaldson EC (eds) Petrophysics (Fourth Edition). Gulf Professional Publishing, Boston, pp 67–186

Tucker ME, Wright VP (2009) Carbonate sedimentology. John Wiley & Sons

Vahrenkamp VC, Van Laer P, Franco B, et al (2015) Late Jurassic to Cretaceous Source Rock Prone Intra-Shelf Basins of the Eastern Arabian Plate – Interplay between Tectonism, Global Anoxic Events and Carbonate Platform Dynamics. OnePetro

Valinasab H, Soltani B, Hassanzadeh H, et al (2023) Seismic sequence stratigraphy and depositional modelling of the Lower Fahliyan Formation in the northwestern Persian Gulf, SW Iran. Mar Pet Geol 152:106251. https://doi.org/10.1016/j.marpetgeo.2023.106251

Van Bellen RC, Dunnington HV, Wetzel R, Morton DM (1959) Lexique Stratigraphic International Asia, Iraq, Congress Geol. International Commission de Stratigraphique 3:

Wagoner JCV, Posamentier HW, Mitchum RM, et al (1988) An Overview of the Fundamentals of Sequence Stratigraphy and Key Definitions. In: Wilgus CK, Hastings BS, Posamentier H, et al. (eds) Sea-Level Changes: An Integrated Approach. Society of Economic Paleontologists and Mineralogists, p 0

Wang H, Xiao E, Latif K (2023) A Case Study on the Co-Occurrence of Oncoids and Ooids in the Cambrian Miaolingian Series, North China Platform. Arab J Sci Eng 48:7905–7924. https://doi.org/10.1007/s13369-022-07589-5

Wang Y, Huang W, Cheng T, et al (2025) Facies-Controlled Sedimentary Distribution and Hydrocarbon Control of Lower Cretaceous Source Rocks in the Northern Persian Gulf. Journal of Marine Science and Engineering 13:576. https://doi.org/10.3390/jmse13030576

Wilson JL (1975) The Stratigraphy of Carbonate Deposits. In: Carbonate Facies in Geologic History. Springer New York, New York, pp 20–55

Worden RH, Carrigan WJ (2005) Oil-anhydrite TSR reactions in the Permian Khuff Fm, Saudi Arabia. Geochimica et Cosmochimica Acta

Worden RH, Smalley PC, Oxtoby NH (1995) Gas Souring by Thermochemical Sulfate Reduction at 140°C1. AAPG Bulletin 79:854–863. https://doi.org/10.1306/8D2B1BCE-171E-11D7-8645000102C1865D

Wyllie MRJ, Gregory AR, Gardner GHF (1958) An experimental investigation of factors affecting elastic wave velocities in porous media. Geophysics 23:459–493. https://doi.org/10.1190/1.1438493

Ye S-J, Rabiller P (2000) A New Tool For Electro-Facies Analysis: Multi-Resolution Graph-Based Clustering. OnePetro

Yousef I, P Morozov V, N Kolchugin A, et al (2023) Microfacies analysis and depositional environment of the Upper Devonian Dankovo-Lebedyansky sediments, Tatarstan, Volga-Ural Basin, Russia. Petroleum Research 8:244–255. https://doi.org/10.1016/j.ptlrs.2022.07.003

Zaninetti L, SAKVUBU-BIBBARD G, Charollais J, Decrouez D (1987) Montsalevia, n. gen.(Montsaleviidae, n. fam., foraminifère), dans le Crétacé inférieur (Berriasien moyen-Valanginien) du Mont Salève et du Jura méridional (Haute-savoie, France); Note préliminaire. Revue de Paléobiologie 6:165–168

Ziegler AM (2001) Late Permian to Holocene Paleofacies Evolution of the Arabian Plate and its Hydrocarbon Occurrences. GeoArabia 6:445–504. https://doi.org/10.2113/geoarabia0603445